REALIZATION OF A SCANNING PHOTOACOUSTIC TECHNIQUE : THERMAL PROPERTIES OF BULK AND FILM SAMPLES
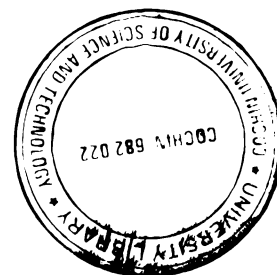
Thesis submitted to

COCHIN UNIVERSITY OF SCIENCE AND TECHNOLOGY

in partial fulfillment of the requirements for the award of the degree of

DOCTOR OF PHILOSOPHY

By

RAGHU.O

Department of Instrumentation

Cochin University of Science and Technology

Cochin – 682 022

February 2007

Dedicated to...

My late father,

My mother &

My supervising teacher

CERTIFICATE

Certified that the work presented in this thesis is based on the bona fide

work done by Mr. Raghu. O, under my guidance in the Department of

Instrumentation, Cochin University of Science and Technology, and has

not been included in any other thesis submitted previously for the award

of any degree.
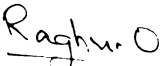
Cochin-682 022

21st February, 2007

Dr. Jacob Philip

Supervising Guide
Dr. Jacob Philip
DIRECTOR
Sophisticated Test and Instrumentation Centre
Cochin University of Science & Technology, Cochin-682 022

DECLARATION

Certified that the work presented in this thesis is based on the original work done by me under the guidance of Dr. Jacob Philip, Director, Sophisticated Test and Instrumentation Centre (STIC), Cochin University of Science and Technology, and has not been included in any other thesis submitted previously for the award of any degree.

Raghu.O

Cochin-682 022   Raghu.O

21st February, 2007

Contents

Chapter 1: Photoacoustics and photoacoustic microscopy : A Review   1

Chapter 2: Instrumentation developed for photoacoustic microscopy   40

Chapter 3: Photoacoustic imaging of selected solid sample configurations   87

Chapter 4: Thermal properties of commercial paint coatings using scanning photoacoustic technique   107

Chapter 5: Determination of thermal effusivity of selected solid samples by scanning photoacoustic technique 136

Chapter 6: Summary and conclusions 160

Preface

Photothermal science encompasses a wide range of techniques and phenomena based on the conversion of absorbed optical energy into heat. Optical energy is absorbed and eventually converted into thermal energy in all light absorbing materials irrespective of whether they are solids, liquids or gases. It is common for excited electronic states in atoms or molecules to loose their excitation energy by a series of non-radiative transitions that result in the heating of the material. Such processes form the basis of photothermal effects and techniques.

Among the large number of photothermal techniques available, photoacoustics assumes a very significant place because of its essential simplicity and the variety of applications it finds in science and technology. The photoacoustic (PA) effect is the generation of an acoustic signal when a sample, kept inside an enclosed volume, is irradiated by an intensity modulated beam of radiation. The radiation absorbed by the sample is converted into thermal waves by nonradiative de-excitation processes. The propagating thermal waves cause a corresponding expansion and contraction of the gas medium surrounding the sample, which in turn can be detected as sound waves by a sensitive microphone. These sound waves have the same frequency as the initial modulation frequency of light. Lock-in detection method enables one to have a sufficiently high signal to noise ratio for the detected signal. The PA signal amplitude depends on the optical absorption coefficient of the sample and its thermal properties. The PA signal phase is a function of the thermal diffusivity of the sample.

Measurement of the PA amplitude and phase enables one to get valuable information about the thermal and optical properties of the sample.

Since the PA signal depends on the optical and thermal properties of the sample, their variation will get reflected in the PA signal. Therefore, if the PA signal is collected from various points on a sample surface it will give a profile of the variations in the optical/thermal properties across the sample surface. Since the optical and thermal properties are affected by the presence of defects, interfaces, change of material etc. these will get reflected in the PA signal. By varying the modulation frequency, we can get information about the subsurface features also. This is the basic principle of PA imaging or PA depth profiling. It is a quickly expanding field with potential applications in thin film technology, chemical engineering, biology, medical diagnosis etc. Since it is a non-destructive method, PA imaging has added advantages over some of the other imaging techniques. A major part of the work presented in this thesis is concerned with the development of a PA imaging setup that can be used to detect the presence of surface and subsurface defects in solid samples.

Determination of thermal transport properties such as thermal diffusivity, effusivity, conductivity and heat capacity of materials is another application of photothermal effect. There are various methods, depending on the nature of the sample, to determine these properties. However, there are only a few methods developed to determine all these properties simultaneously. Even though a few techniques to determine the above thermal properties individually for a coating can be found in literature, no technique is available for the simultaneous measurement of these parameters for a coating. We have developed a scanning photoacoustic

technique that can be used to determine all the above thermal transport properties simultaneously in the case of opaque coatings such as paints. Another work that we have presented in this thesis is the determination of thermal effusivity of many bulk solids by a scanning photoacoustic technique. This is one of the very few methods developed to determine thermal effusivity directly.

In the following paragraphs, we give a chapter wise description of the contents of the thesis.

Chapter 1 is a review of the phenomenon of photoacoustics with special emphasis on photoacoustic microscopy. The position of photoacoustics in the field of photothermal phenomena is put in proper perspective. The basic principles of PA effect and a brief outline of the Rosencwaig-Gersho theory along with the special cases, which are of interest to us, are discussed. The instrumentation requirements for performing PA experiments are described mentioning the advantages and disadvantages of some of the components. A somewhat comprehensive survey of the applications of PA effect is described in one of the sections. Developments in PA microscopy which is one of the main themes of the work presented in this thesis is discussed along with the instrumentation requirements and applications of the technique for nondestructive evaluation of solids.

Design, fabrication and calibration details of a photoacoustic microscope (PAM) are described in Chapter 2 of the thesis. Any PA microscope should have the following four units. 1) PA cell 2) Scanning Unit 3) Signal Processing system 4) Movement control and data acquisition. We have designed and fabricated each of these units to overcome some of the problems encountered in previous designs. In

order to improve the signal to noise ratio a new type of PA cell having two identical microphones has been designed. Its calibration is discussed in this chapter. The signals from the two microphones of the PA cell are added electronically after a stage of preamplification. The circuit design of the summing amplifier is discussed. We have designed a scanning unit which has two translation stages driven by stepper motors under computer control. The design of this unit along with the design of stepper motor driver circuit is described. The stepper motors are driven by signals from the parallel port of a personal computer (PC). The PA amplitude and phase data are acquired at regular intervals from various points on the sample. This is also done under computer control. The software developed for this purpose in Visual Basic programming language is given as an appendix to this chapter.

The testing and calibration of the instrument using standard samples is a very important stage in any instrumentation development. The PAM developed by us has been tested on some standard sample configurations. These include samples having surface and subsurface defects, samples which have an interface of two different materials, samples in which other materials are inserted below the surface etc. The details of these samples and the PA images obtained for them using the instrument developed by us are given in the third chapter of the thesis. Some of the samples studied by us are a copper disc with pits on the surface, a section of a PCB, a copper disc with a subsurface groove, a steel pin inserted inside a Teflon disc etc. The results of the imaging experiments are presented and the merits and demerits of the system are discussed.

Determination of thermal properties of thin opaque coatings such as paints by a scanning photoacoustic technique forms the subject matter of Chapter 4. After a brief review of the literature in this field, we give a detailed account of the theory of PA effect using thermal wave interference approach developed by Bennett and Patty. From an explicit expression for phase difference between PA signals from a sample and that from a thick reference of the same material, we can determine the thermal effusivity and diffusivity of the sample. The only parameters to be known for this are the effusivity of the backing material and the modulation frequency used. Once effusivity and diffusivity of the sample are known, thermal conductivity and heat capacity can be determined, if the density of the sample is also known. We have performed the measurements on four samples of commercially available black paint on a copper substrate. One of the paints is coated on substrates having different thermal properties varying from good conductors to insulators and the thermal properties of the paint are determined in each case. The results of these measurements are given and discussed in this chapter.

Chapter 5 of the thesis is devoted to the measurement of the thermal effusivity of PTFE samples doped with various amounts of $Sr_2Te_2Ce_5O_{16}$ ceramics. We have used a scanning PA technique for this purpose. The sample along with a suitably chosen reference material is kept side by side with their top surfaces at the same horizontal level. The laser beam scans these samples over which a very thin uniform coating of carbon black is given. The change in amplitude and phase values of the PA signal when the material beneath the coating changes is used to determine the thermal effusivity of the sample. The results of these measurements are given and discussed.

Finally, chapter 6 gives a summary and conclusion of the work done in the thesis. Scope for further improvement of the works presented in the thesis is discussed.

The work in this thesis has been presented in the following conferences/ symposia proceedings

1. A dual channel photoacoustic cell for photoacoustic microscopy of solid samples

    Proceedings of the National symposium on instrumentation (NSI-27), 27-29th , November,2002 Bharathiar University, Coimbatore

2   A dual channel photoacoustic microscope for nondestructive evaluation of solid samples

    Proceedings of the National symposium on Instrumentation (NSI-30), 30th Nov, 1-2nd Dec 2005 Cochin University of Science and Technology, Kochi.

3   Development of a scanning photoacoustic technique for the quality evaluation of coatings, such as paints.

    Proceedings of the XIX Kerala Science Congress, Kannur, 29-31stJanuary 2007

The following papers have been published during the course of this work.

1. A dual channel photoacoustic cell for photoacoustic microscopy of solid samples

    O.Raghu and J.Philip, *J.Instrum.Soc.India* 33, (2003) 155-158

2. Thermal properties of paint coatings on different backings using a scanning photoacoustic technique

O.Raghu and J.Philip, *Meas.Sci.Technol.* **17**, (2006) 2945-2949

3. A dual channel photoacoustic microscope for nondestructive evaluation of solid samples

O.Raghu and J.Philip, *J.Instrum.Soc.India* **36(4)**, (2006) 279-283

Acknowledgements ...

Looking back, I feel that this thesis is the result of my association with a lot of persons during the past seven years of my life at CUSAT. The erudite and scholarly persons I met here, the knowledge and insights I gained here, and the extremely nice friends I got here, make this period one of the very best in my life. I am trying to put in words my deep sense of gratitude towards a few of these persons.

First and foremost, I express my heartfelt gratitude for the able guidance of my supervising teacher Prof Jacob Philip, Director, Sophisticated Test and Instrumentation Centre, CUSAT. He introduced me into the problem, monitored my progress at every stage and made very valuable suggestions at critical junctures. There have been times when my self-confidence touched the lowest ebb during the course of this work. It was his patient appreciation of my problems, constant encouragement and morale boosting that helped me get over those phases. I shall always cherish my days as a student under him.

I am extremely grateful to Dr. K.N.Madhusoodanan, Head, Dept. of Instrumentation, for allowing me to use the facilities of the department. Thanks are due to the present and former Heads of Dept. of Physics for granting me the permission to use the library facilities for my research work.

My research work involved a lot of instrumentation development. I have got immense help from the technical staff of the department of instrumentation. I would like to express my sincere thanks to Mr. Murali, Mr.Gopi Menon, Mr. Sukumaran, Mr.K.V.Jose, Mr. Jose Jacob, Mr.Casimir and Mr.Joshy for their timely help. I express my gratitude towards the office and library staff of the department of instrumentation also for their help and cooperation.

CHAPTER 1

Photoacoustics and Photoacoustic Microscopy: A Review

1.1: Introduction

The photoacoustic (PA) or optoacoustic effect is an energy conversion process. The absorption of incident modulated electromagnetic radiation by a medium (sample) contained within a cell of constant volume produces an intermittent temperature change inside the sample, leading to a corresponding fluctuation in the pressure of the gas in the cell, which can be monitored by means of a sensitive acoustic microphone [1]. The PA effect was discovered by Alexander Graham Bell way back in 1880, who observed that audible sound is produced when chopped sunlight is incident on a light absorbing material [2]. In a series of experiments, Bell demonstrated that the PA effect in solids was dependent on how strongly the incident light was absorbed by the material in the cell. Bell and his co-workers observed that only weak signals are produced when the cell is filled with a light absorbing liquid, but when filled with light absorbing gases the signals are quite strong. Several attempts were made by the nineteenth century investigators like Bell, Lord Rayleigh, Mercadier and Preece to explain the production of PA signal in solids. None of them could give a satisfactory explanation and a quantitative theory [3]. After the initial flurry of interest generated by Alexander Graham Bell's original work, experimentation with PA effect was considered as being "no more than an interesting

curiosity of no great scientific or practical value". Furthermore, experiments were difficult to perform quantitatively for want of sensitive sound detectors.

After lying dormant for nearly 50 years photoacoustics resurfaced in the late 1930s with the advent of sensitive microphones. However, during this period the use of the phenomenon was almost entirely limited to gas analysis. Major players in the field at that time like Viengerov, Pfund and Luft [3] got reasonably good sensitivities in gas concentration analysis using photoacoustics. To some extent their work has contributed to our present day knowledge regarding photoacoustic cell design, noise isolation etc.

Allen Rosencwaig deserves much of the credit for the 'rediscovery' of the photoacoustic effect, for the development of photoacoustic spectroscopy in solids and for much of our understanding of the principles of this technique and several others that now form a part of photothermal science. The Rosencwaig-Gersho theory [4] of the photoacoustic effect for a sample in a photoacoustic cell provided a comprehensive theoretical framework that led to the rapid development and application of the effect. This led to the invention of numerous other detection schemes and to the current widespread interest in photothermal science.

In this context it is worthwhile to view this phenomenon in a broader perspective. Photothermal effects are caused by the heating of a sample after the absorption of optical energy (or, in general the absorption of an energetic beam). After the optical absorption, other de-excitation channels besides heating can also occur [5]. These other 'de-excitation branches' compliment the heating branch in such a way that the branching ratios must add up to 1. Some of these branches are photochemistry, luminescence, photoelectricity etc. Photothermal heating can result

in many different effects, which in turn, provide the detection mechanisms. Some of these effects are

1. Change in temperature of the sample.

2. A modulated infrared emission from the surface

3. A modulated thermal expansion resulting in a distortion of the surface.

4. The generation and propagation of an acoustic wave

5. A modulation of the optical properties of the surface such as reflectivity

6. A modulated refractive index gradient in any gas or other transparent medium in contact with the heated surface.
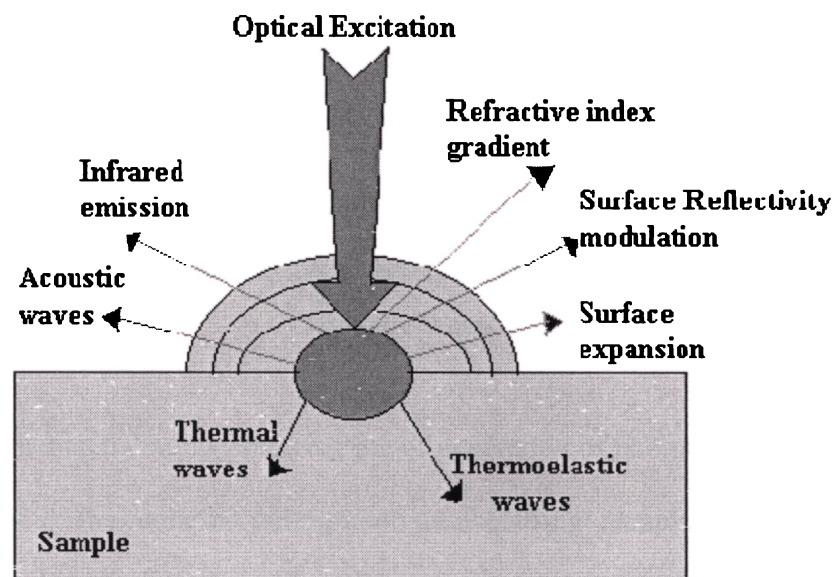
Fig 1.1: Photothermal phenomena caused by illumination of a surface by a modulated beam of light.

Some of these effects are schematically represented in Fig 1.1. All of these effects have been used to probe the photothermal response of a medium [6]. The generation and propagation of the acoustic wave and its detection by means of sensitive transducers such as microphones is the subject of study in "photoacoustic effect" [PA effect]. In our work, we have concentrated on this effect.

1.2: PA effects in solids: Principles

In the photoacoustic effect as applied to solids, a light absorbing substance is exposed to modulated incident radiation as shown in Fig 1.2.
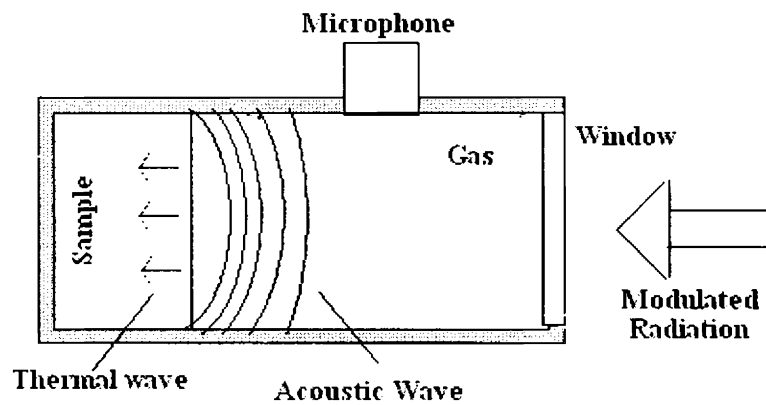
Fig 1.2 : A schematic diagram showing the of generation of photoacoustic signal

A portion of the radiation falling upon an absorbing sample is absorbed and results in optical excitation. Non-radiative de-excitation processes, which normally occur, give rise to the generation of thermal energy within the sample. If the incident radiation is modulated then the generation of thermal energy within the sample will also be periodic and a thermal wave will be produced having the same frequency as

4

this modulation. Energy is transferred by the thermal wave towards the sample boundary, where a periodic temperature change is generated.

The photoacoustic cell is a small gas-tight enclosure with a sensitive microphone built into one wall. The periodic variations in the temperature at the surface of the sample results in the generation of an acoustic wave in the gas immediately adjacent and this wave propagates through the volume of the gas to the microphone which converts it into electrical signals.

Therefore the photoacoustic signal is the result of two types of processes occurring in the sample: the absorption of electromagnetic radiation specified by the absorption coefficient β and the thermal propagation in the sample specified by the thermal diffusivity, α. For absorbing samples the optical absorption length $l_\beta = 1/\beta$, is an important parameter and may be taken as the depth into the sample at which essentially all of the incident radiation has been absorbed. The thermal wave produced in the sample is heavily damped and may be considered to be fully damped out within a distance $2\pi\mu_s$ where μ_s is the thermal diffusion length. It is normally assumed that only those thermal waves originating from a depth less than or equal to μ_s will make an appreciable contribution to the photoacoustic signal measured. The thermal diffusion length is a function of thermal diffusivity and the modulation frequency ω of the incident radiation. These are connected through the relation

$$\mu_s = \sqrt{\frac{2\alpha}{\omega}} \qquad (1.1)$$

This important relationship means that for a sample of given thermal diffusivity, the depth examined μ_s may be varied by adjusting the modulation frequency ω.

5

The observed photoacoustic signal is a complex quantity having a magnitude and phase relative to the modulation of incident radiation. Being a function of the absorption coefficient, modulation frequency and thermal characteristics of the sample as well, the photoacoustic signal is directly proportional to the incident power of the radiation and also depends upon the characteristics of the gas in contact with the sample surface and the properties of the backing material upon which the sample is positioned.

The first attempt at a modern quantitative theory of photoacoustics was made by Parker [7]. Some years later a more general theory for the photoacoustic effect in condensed media was formulated by Rosencwaig and Gersho [4]. This theory, now commonly referred to as the RG theory, derived exact expressions for the periodic temperature at the sample - gas interface while treating the transport of the disturbance in the gas in an approximate heuristic manner. However, this is valid for most experimental conditions. Subsequently further improvements were made to the theory. Bennet and Foreman [8], Aamodt et al [9], and Westel and McDonald [10] refined the theory by treating the transport of the acoustic disturbance in the gas more exactly. Although these refinements did not change the basic results of the RG theory for most experimental conditions, they were able to account for the observed deviations from the RG theory at very low frequencies and at frequencies near cell resonances. There has been a further refinement to the theory by McDonald and Wetsel who have included contributions to the signal from thermally induced vibrations in the sample [11]. A three dimensional theory of photoacoustic effect in solids developed by H.C.Chow also shows that for a sample with large lateral dimensions the signal is similar to its one dimensional counterpart developed by

Rosencwaig and Gersho [12]. In the next section we describe the Rosencwaig-Gersho theory in detail.

1.3: Rosencwaig – Gersho theory of photoacoustic effect

Rosencwaig – Gersho theory (RG theory) is a one dimensional analysis of the production of photoacoustic signal in a simple cylindrical cell as shown in Fig 1.3
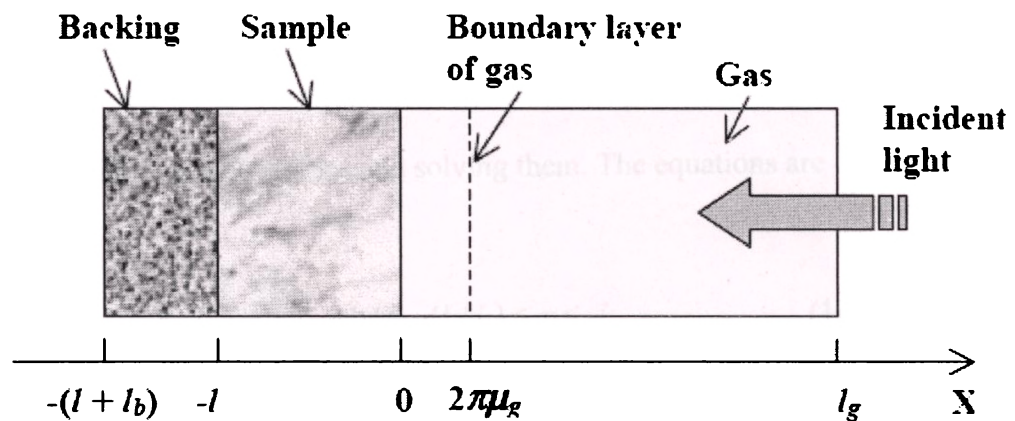
Fig 1.3 : Cross-sectional view of a simple cylindrical PA cell

The diameter of the cell is D and length of the cell is L. In this analysis we make use of the following symbols.

k : thermal conductivity

ρ : density

c : specific heat capacity

$\alpha = \dfrac{k}{\rho c}$: thermal diffusivity

$a = \left(\dfrac{\omega}{2\alpha} \right)^{1/2}$: thermal diffusion coefficient

$\omega = 2\pi\upsilon$, where υ is the frequency of modulation of the light beam

$\mu = \dfrac{1}{a}$: thermal diffusion length

β : optical absorption coefficient of the sample

$l_\beta = 1/\beta$: optical absorption length

The subscripts b, s and g are used with the above symbols to represent these parameters for the backing, sample and gas regions respectively.

1.3.1 : Expression for temperature at the sample gas boundary.

The first step of the analysis is to write the heat diffusion equations in the backing, gas and the sample regions and solving them. The equations are

$$\frac{d^2U}{dx^2} = \frac{1}{\alpha_b}\frac{dU}{dt} \quad \text{where} -(l_s+l_b) \le x \le -l \tag{1.2}$$

$$\frac{d^2U}{dx^2} = \frac{1}{\alpha_g}\frac{dU}{dt} \quad \text{where } 0 \le x \le l_g \tag{1.3}$$

$$\frac{d^2U}{dx^2} = \frac{1}{\alpha_s}\frac{dU}{dt} - Ae^{\beta x}(1+e^{i\omega t}) \quad \text{where} -l_s \le x \le 0 \tag{1.4}$$

where U is the temperature and $A = \dfrac{\beta I_0 \eta}{2k_s}$. I_0 is the maximum intensity of the incident light, η is the efficiency with which the absorbed light is converted to heat (We assume $\eta = 1$). Solving the above differential equations and applying the conditions for continuity of heat flux and temperature at the boundaries of the three different regions we can obtain the complex amplitude of the periodic temperature at the solid gas boundary (x = 0). It is given by

$$U_0 = \frac{\beta I_0 \eta}{2k_s(\beta^2 - o_s^2)} \left[\frac{(b+1)(r-1)e^{\sigma_s l_s} - (r+1)(b-1)e^{-\sigma_s l_s} + 2(b-r)e^{-\beta_s}}{(g+1)(b+1)e^{\sigma_s l_s} - (g-1)(b-1)e^{-\sigma_s l_s}} \right] \qquad (1.5)$$

The new symbols used in this equation are

$$\sigma = (1+i)a \qquad (1.6)$$

$$b = \frac{k_b \sigma_b}{k_s \sigma_s} = \frac{e_b}{e_s} \qquad (1.7)$$

where $e = \sqrt{k\rho c}$ is the thermal effusivity

$$g = \frac{k_g \sigma_g}{k_s \sigma_s} = \frac{e_g}{e_s} \qquad (1.8)$$

$$r = \frac{\beta}{\sigma_s} = \frac{1}{\sqrt{2}} e^{-i\frac{\pi}{4}(\frac{\mu_s}{l_\beta})} \qquad (1.9)$$

When specific values of the parameters are known we can evaluate equation (1.5). The magnitude and phase of U_0 yield the magnitude and phase of the periodic temperature variation at the surface of the sample.

1.3.2 : Production of the acoustic signal

The acoustic signal arises due to the periodic heat flow from the solid sample to the surrounding gas medium. This periodic heat flow causes a periodic temperature fluctuation in the gas medium as given by the sinusoidal component of U in the solution of equations 1.2 to 1.4

$$U_g(x,t) = U_0 e^{-\sigma_g x} e^{i\omega t} \quad \text{for } 0 \le x \le l_g \qquad (1.10)$$

The actual periodic physical temperature variation in the gas T_g is the real part of this equation

$$T_g(x,t) = e^{-a_g x} \left[U_1 Cos(\omega t - a_g x) - U_2 Sin(\omega t - a_g x) \right] \qquad (1.11)$$

9

where U_1 and U_2 are the real and imaginary parts of U_0. As the distance from the surface of the sample increases the time dependent component of the temperature in the gas rapidly attenuates to zero and at a distance of just one thermal wavelength or $2\pi\mu_g$ the periodic temperature variation of the gas is effectively fully damped out. Only this boundary layer of the gas of thickness $2\pi\mu_g$ is capable of thermally responding to the periodic temperature at the surface of the sample. The spatially averaged temperature of the gas within the boundary layer as a function of time is obtained as

$$\overline{U_g}(t) = \frac{1}{2\pi\sqrt{2}} U_0 e^{i(\omega t - \frac{\pi}{4})} \tag{1.12}$$

Because of the periodic heating of the boundary layer, it expands and contracts periodically and thus acts as an acoustic piston on the rest of the gas column. It produces an acoustic pressure signal that travels through the entire gas column. Assuming that the rest of the gas responds adiabatically to the action of this piston, the incremental pressure is

$$\delta P(t) = Q e^{i(\omega t - \frac{\pi}{4})} \tag{1.13}$$

where
$$Q = \frac{\gamma P_0 U_0 \mu_g}{\sqrt{2} l_g T_0} \tag{1.14}$$

Here, γ is the ratio of specific heats of the gas, P_0 is the ambient pressure in the cell, and T_0 is the ambient temperature. The actual pressure variation is the real part of $\delta P(t)$. Thus the complex amplitude of the sinusoidal pressure variation in the gas is given by

$$U_0 = \frac{\beta I_0 \gamma P_0 \mu_g}{2\sqrt{2} T_0 k_s l_g (\beta^2 - o_s^2)} \left[\frac{(b+1)(r-1)e^{\sigma_s l_s} - (r+1)(b-1)e^{-\sigma_s l_s} + 2(b-r)e^{-\beta_s}}{(g+1)(b+1)e^{\sigma_s l_s} - (g-1)(b-1)e^{-\sigma_s l_s}} \right] \quad (1.15)$$

1.3.3 : Special cases

The difficulty in interpreting eq. (1.15) can be reduced by examining various special cases. The special cases are determined by the relative magnitudes of the optical absorption length $l_\beta = 1/\beta$, the thermal diffusion length μ_s and thickness l_s of the sample respectively. Also, it is convenient to define

$$Y = \frac{\gamma P_0 I_0}{2\sqrt{2} T_0 l_g} \quad (1.16)$$

which always appears as a constant factor in the expression for Q.

We consider the case of optically opaque solids, which is relevant in our case. In this case, most of the light is absorbed within a distance that is small compared to l_s and essentially no light is transmitted to the backing.

Case (a) : Thermally thin solids ($\mu_s \gg l_s$, $\mu_s \gg l_\beta$)

Using the approximations $e^{-\beta_s l_s} \approx 0$, $e^{\pm \sigma_s l_s} \approx 1$ and $|r| \gg 1$, we get

$$Q \approx \frac{(1-i)}{2a_g} \left(\frac{\mu_b}{k_b} \right) Y \quad (1.17)$$

In this case, the signal is independent of β_s. This would be the case for a very black absorber such as carbon black. The signal is quite strong, depends on the thermal properties of the backing material and varies as ω^{-1}.

Case (b): Thermally thick solids ($\mu_s < l_s$, $\mu_s > l_\beta$)

Setting $e^{-\beta_s l_s} \approx 0$, $e^{-\sigma_s l_s} \approx 0$ and $|r| > 1$,

$$Q = \frac{(1-i)}{2a_g}\left(\frac{\mu_s}{k_s}\right)Y \tag{1.18}$$

Eq. (2.8) is similar to Eq. (2.7), except that the thermal parameters of the backing material are now replaced by those of the sample. Here also, the signal is independent of β and varies as ω^{-1}.

Case (c): Thermally thick solids ($\mu_s \ll l_s$, $\mu_s < l_\beta$)

Setting $e^{-\beta_s l_s} \approx 0$, $e^{-\sigma_s l_s} \approx 0$ and $|r| < 1$

$$Q \approx \frac{i\beta\mu_s}{2a_g}\left(\frac{\mu_s}{k_s}\right)Y \tag{1.19}$$

This is a very interesting and important case because even though the sample is optically opaque, it is not photoacoustically opaque, as long as $\mu_s < l_\beta$, i.e., acoustic signal is proportional to β. The signal is also dependent on the thermal properties of the sample and varies as $\omega^{-3/2}$.

1.4 : Instrumentation requirements

A photoacoustic setup used for studies on solid samples should have the following units (1) an excitation light source (2) a modulator (3) PA cell (4) a detector and (5) a signal processing system. The block diagram of a basic PA spectrometer is shown in Fig 1.4
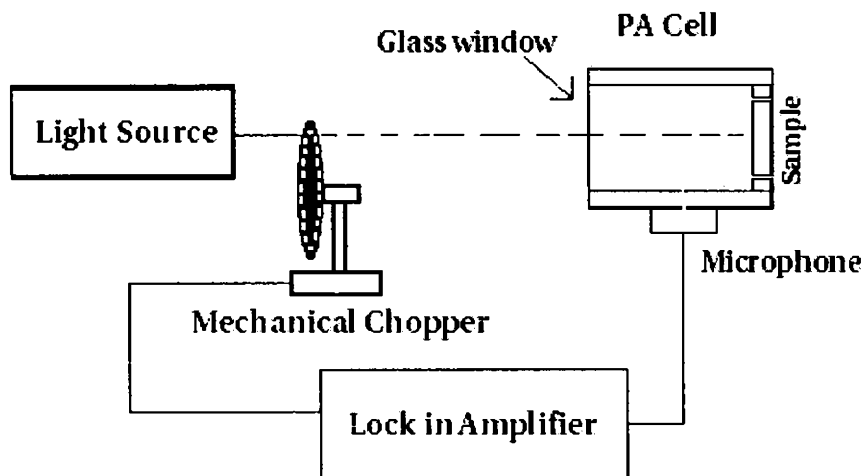
Fig 1.4 : Parts of a basic photoacoustic setup

1.4.1 : Excitation sources

These fall into two categories 1) Broad spectral range sources for spectroscopic applications 2) Lasers. High pressure Xe arc lamps, high pressure Hg lamps, tungsten lamps, Nernst glower etc. are the commonly used incoherent sources. Any of these lamps and monochromator combination can provide tunability over a wide wavelength range from the infrared to the ultraviolet. Lasers are widely used because they provide a well-defined localized region of heating required for thermal wave probing techniques. Their extremely narrow line width provides high spectral radiance. The limited tunability is a main drawback of laser sources.

1.4.2 : Modulator

The incident light beam has to be intensity modulated for the generation of PA signals. Several methods have been used to impose a temporal variation on the optical energy applied to a sample. A rotating sectored blade wheel (mechanical chopper) provides an inexpensive and efficient way to modulate a light beam. They provide a square wave modulation with a 100% modulation depth, covering a

frequency range from about 1 Hz to 20kHz. The main limitations of a mechanical chopper are its frequency range and its restriction to square wave modulation. While using mechanical choppers precaution should be taken to minimize the vibration noise transmitting directly from the chopper to the microphone detector. For some sources such as CO and CO_2 gas lasers and semiconductor laser diodes the optical output can be directly modulated by varying the electrical drive current of the source. The depth of modulation is not in all cases 100%. However, there are the advantages of eliminating the need for a separate modulator, the environmental acoustic noise, the low frequency jitter problems which are present with mechanical choppers etc. Electro optic modulation involves changing the plane of polarisation of an incoming polarized light beam in a non-linear optical crystal (ADP or KDP) by the application of a modulated electric field across the crystal. The acousto-optic method involves the spatial modulation of a laser beam by an acoustically formed diffraction grating.

1.4.3 : Photoacoustic Cell

The experimental chamber or cell for a gas microphone PA sytem is the section containing the sample and the microphone. Designing the cell properly is an important prerequisite for the successful working of PA experiments. Some of the criteria governing the design of a PA cell are given below.

1) The cell should be acoustically isolated from the surroundings. For this the cell should be designed with good acoustic seals and with walls of sufficient thickness to form a good acoustic barrier. The thermal mass of the cell walls should be large.

2) The PA signal that may arise from the interaction of the light beam with the walls and windows of the cell should be minimized. For this, the windows should

14

be as optically transparent as possible and the interior walls of the cell should be well polished. Although the cell walls will absorb some of the incident and scattered light, the resulting PA signal will be quite feeble as the thermal mass of the walls is quite large. The cell geometry should be such that the scattered and reflected light towards the walls and microphone are as minimum as possible.

3) The signal in a PA cell for solid samples varies inversely with gas volume [4]. Hence gas volume in the cell should be minimized. However, the volume should not be minimized to such an extent that the acoustic signal produced at the sample suffers dissipation at the cell window and walls before reaching the microphone. Moreover, for all chopping frequencies of interest, the length of the gas column l_g in the cell should be greater than the thermal diffusion length μ_g since it is this boundary layer of gas that acts as an acoustic piston generating the signal inside the cell. Tam has suggested an optimum gas column length of 1.8 μ_g [13]. Another important parameter to be considered in the design of a PA cell is the thermo viscous damping, because this could be a source of signal damping at the cell boundaries. Thermoviscous damping coefficient varies as $\omega^{1/2}$ and becomes important at high frequencies whereas thermal diffusion length, which varies as $\omega^{-1/2}$, is predominant at low frequencies. Considering all these effects, the distance between the sample and the window can be chosen to be 1-3 mm [3].

Depending on the type of the experimental studies, different types of cell designs have appeared in literature [14-15]. The most common cell design adopts cylindrical geometry in which the light beam is centered along the axis. Such a cell can be operated either in the resonant mode or in the non-resonant mode. Cell

resonances amplify the acoustic power at the resonant frequency. Geometries other than cylindrical have also been used in PA cell design [3,16-19].

There is considerable interest in the use of cells that employ Helmholtz resonance [20-22]. In this design we have a sample chamber of volume V_1 and a separate microphone chamber of volume V_2. These chambers are connected by a channel of length l_c and cross sectional area A. The resonant frequency is given by

$$f_{res} = \frac{C_0}{2\pi} \sqrt{\frac{A}{l_c V_r}}$$
(1.20)

where $V_r = \frac{V_1 V_2}{V_1 + V_2}$ and C_0 is the velocity of sound in air. This configuration can avoid the generation of spurious acoustic signals due to interaction of the scattered light from the sample, sample holder and window with the microphone surface. Since the sample chamber can be kept away from the microphone chamber by a sufficiently long connecting tube, temperature variation studies can be performed where the sample has to be kept at very high or very low temperature [23-24].

1.4.4 : Acoustic Detectors

The PA signal generated in the cell can be detected by any sensitive microphone. A condenser microphone produces electrical signal when a pressure wave impinges on the diaphragm. Such microphones have flat frequency response in the audible frequency range, low distortion and are not sensitive to mechanical vibrations. Electret microphones can also be used for detecting PA signals. No bias voltage is required for electret microphones and due to the large capacitance area possible from electret materials they can be made into miniaturized microphones. Piezoelectric devices can also be used to sense the elastic waves generated in radiation absorbing solids and liquids.

1.4.5 : Signal processing

A pervasive problem in all experimental disciplines is the extraction of good quality data from noisy signals. This is particularly so in the case of PA signals. In general, the following methods can be applied to enhance the signal to noise ratio: low pass filtering, ensemble averaging, phase sensitive detection, box car integration and mathematical methods (curve fitting, digital filtering etc.). Usually a phase sensitive lock-in amplifier is used to measure the amplitude as well as the phase of the PA signal. A lock-in amplifier can also eliminate noise from other sources.

1.5: Applications of Photoacoustic Effect

Much experimental and theoretical work has been reported in literature to demonstrate the applications of PA effect in various branches of science, technology and medicine [5,25-26]. There are four general classes of applications of PA effect, as outlined below.

1.5.1 : PA Spectroscopy (PAS)

In this class of applications, the PA signal amplitude is measured for a range of optical excitation wavelengths producing a PA spectrum; other factors are usually kept or assumed fixed. This is actually an excitation spectrum based on acoustic detection. PAS is the most fundamental and earliest application of the PA effect. Some of the attractive features of PAS are : 1) It requires minimal sample preparation 2) It enables measurements of highly absorbing and scattering media 3) It can be used on a broad range of materials (gases, liquids, solids, powders, gels, thin films etc.) 4) It can be used to determine a very wide range of absorption

coefficient magnitudes in the range 10^{-3} to 10^5 m^{-1} 5) It is a non contact, nondestructive method and has the potential for remote sensing.6) It can be used in spectral depth profiling 7) It can be used with a range of photothermal detection mechanisms 8) It provides an increase in signal to ratio with increase in input light power.

Two important optical properties of a solid that can be determined from PA spectrum are surface reflectivity and optical absorption coefficient. To obtain reflectivity, a normalisation of the signal must be performed using a spectrally flat absorber such as carbon black. Dividing the sample signal by that from the reference (carbon black) allows the source intensity variations to be eliminated, resulting in a normalized signal which is dependent solely on reflectivity. Here we assume that the nonradiative recombination efficiency is nearly 1.

Optical absorption coefficient can be determined by measuring PA signal at a single wavelength or measurement over a broad spectral region. Measurements on different types of samples such as metallic, semiconducting, dielectric and organic materials have been reported in literature [27-32]. It is capable of dealing with samples of very low optical density, very high optical density, light scattering samples and specularly reflecting samples [33-41]. Several investigators have exploited the PA technique to study the variation of optical band gap with composition in semiconducting chalcogenide glasses [42-57].

PA monitoring of weak absorption in solids with high detection sensitivity of the order of 10 cm^{-1} using piezoelectric detection has been reported on highly transparent solids like CaFe, SrFe etc [58]. Because of the high sensitivity, this technique is suitable for absorptions in thin films also. This method has found a

high degree of application in thin film optical coatings like laser mirrors, absorption by glass surfaces, thin layer chromatography, surface chemistry, surface catalysis etc [59]. PAS can be used effectively for studying adsorbed or chemisorbed molecular species and compounds as well as surface passivation, surface oxidation or reduction on metals, semiconductors and insulators.

PA spectroscopy on opaque and highly absorbing samples gives the power spectrum of the excitation source. Following this principle, we can fabricate a power meter with a wide wavelength range. It can also be used to study Urbach tail, excitations and other fine structures in crystalline, powder and amorphous semiconductors which in turn helps us to study the effect of impurities dopants, electromagnetic fields etc. on the material [60-63].

Biological materials present conventional spectroscopic techniques with many difficulties. Their inherent highly light scattering properties, depth varying structures etc are some of them. Photoacoustic and photothermal spectroscopic techniques provide immense possibilities here. In dermatology the optical and thermal properties of skin have been studied in vivo using specially designed PA cells. The use of sunscreens to protect skin from UV damage has also been studied photoacoustically [64]. In hematology PAS of blood from patients having different illnesses show changes from that of normal people [65]. PA technique has also been used to study the sedimentation process in blood because any change in the amount of erythrocytes (red cells) in a region of blood due to sedimentation will affect the PA signal from that region [66]. PA technique has found application in the study of effects of environmental stresses on the photosynthetic activity in plants [67].

1.5.2 : PA monitoring of de-excitation mechanisms.

De-excitation mechanisms after optical absorption in a medium frequently involve heat evolution (thermal de-excitation). There are other de-excitation channels such a fluorescence, photochemistry, photoelectricity, energy transfer etc. If S is the photoacoustic signal originating from a material which has many de-excitation branches, then

$$S = S_0(1-\Sigma\phi_i f_i) \qquad (1.21)$$

where S_0 is the PA signal if only heat is produced, ϕ_i is the branching ratio for the ith state, which decays with a fraction f_i of its energy not producing heat and a fraction $(1-f_i)$ producing heat. This equation is the basis of PA monitoring of different types of de-excitation mechanisms.

The measurement of fluorescent quantum efficiency by PA method is very useful for studying laser materials. For example, the fluorescence quantum yield of laser dyes in various solvents at various concentrations can be measured to understand the effect of solvent quenching and concentration quenching. New laser solid materials in the form of powders can be tested without the necessity of growing macroscopic crystals as conventional methods of measuring luminescent quantum efficiency would require. There are several publications which report their measurement by PA effect and related applications [68-75].

Photoacoustics offers a unique tool for the study of photochemical processes in solids. The simplest mechanism by which photochemistry influences the magnitude of the PA signal is that of complimentarity. When the two branches are complimentary, the increase of one branch leads to the decrease of the other. By varying the modulation frequency and analyzing the phase of the PA signal,

information can be obtained on the kinetic parameters and on the energy content of the intermediates. Works done by Cohen et al, Ort and Parson etc. provide ample examples of the power of PA technique for monitoring photochemical reactions [76-79]. Diebold, Gray and Bard have studied the photochemical induced gas evolution and consumption by PA methods [80-81].

When part of the light energy absorbed is converted into electrical energy (eg. in a photovoltaic or photoconductive device) the thermal energy produced in the optical excitation will be less than the absorbed light energy. That means the observed PA signal from the sample is smaller when the sample is photoelectrically active than when it is inactive. Cohen and Tam have used PA technique to measure the photoelectric quantum efficiencies of Si solar cell and organic dye films [82-83].There are several other published works on the use of PA monitoring of photoelectrical carrier generation and related effects in semiconductors and organic dyes [84-88].

When molecules in excited state collide among themselves or with molecules in the ground state or with foreign molecules, energy transfer takes place. There is also the possibility of stimulated transition of molecules to different energy states by light. PA effect can be used to monitor such energy transfers. Useful information regarding production of various singlet and triplet excited states in organic vapors, the relaxation times involved in such energy transfers, pressure broadening etc. are obtained in this way. There are several papers describing this use of PA effect in literature [89-95].

1.5.3 : PA measurement of thermo physical properties.

The optical generation of thermal and acoustic waves can be used to gather information such as sound velocity, elasticity, flow velocity, thermal diffusivity, thermal effusivity, specific heat, thermal conductivity, thickness of thin films, subsurface defects and so on. The technique has proved particularly attractive for thermal property measurement because it combines non-contact application of well-defined amounts of thermal energy with non-contact method for the determination of the resulting temperature changes. Because of the very high sensitivity of the detection technique the temperature changes employed in a property determination can be very small. This is significant in the case of materials whose thermal properties vary sharply with temperature. Monitoring the variations in the PA signal as a function of temperature provides information about the occurrence of phase transitions.

Adams and Kirkbright were the first to use PA technique to obtain thermal diffusivity values of solids [1]. Front surface illumination can lead to an accurate determination of both thermal diffusivity and effusivity from which conductivity and specific heat can be extracted [96-97]. Several methods to measure thermal diffusivity of solids using PA effect have been developed. They include the phase lag, dual phase heating and thermal wave inference. PA measurements of diffusivity and effusivity of thin coatings has been reported [98-99]. PA method has the capability of giving spatial information regarding thermal properties [100-103]. Starting with Florian et al a number of papers have appeared utilizing PA technique for studying phase transitions in solids [104-109].

1.5.4 : PA Imaging

The technique of PA imaging is concerned with the detection of variations in surface and subsurface thermoelastic properties in a sample. In particular, if little lateral resolution is desired and PA imaging is mainly concerned with the property variations in the thickness direction, the technique is usually called 'PA depth profiling'. On the other hand, if high lateral resolution is required, the technique is called 'PA microscopy'. PA imaging rely on the detection of variations in magnitude or phase of the PA signal as the sample surface is scanned with the modulated beam of light. Since this application has special relevance in respect of the work presented in this thesis, a detailed account of this topic is given in the next few sections.

1.6: Photoacoustic Microscopy (PAM): Principles

PA microscopy (PAM) is a quickly expanding field actively investigated by many research groups because of its potential applications in thin film technology, chemical engineering, biology, medical diagnosis etc. It provides a unique method for obtaining surface and subsurface imaging of irregularities, flaws, doping concentrations etc. that cannot be obtained by other nondestructive methods. All variations of PA imaging rely on the detection of the magnitude or phase of the PA signal depending on the modulation frequency of the excitation beam or depending on the location on the sample. Rosencwaig has pointed out that all the three primary physical processes that occur during photoacoustic process can contribute to microscopic visualization of the sample [110]. These processes are

A) Absorption of the intensity modulated incident energy

23

B) Subsequent generation and propagation of thermal waves that result from the energy absorption process

C) The generation and propagation of elastic waves resulting from the heating process B

Process A provides information about the local absorption or reflection/scattering properties of the sample. It is the same process that provides visualization in an optical microscope or electron microscope. The ultimate resolution in process A is determined by the wavelength of the light beam. Depth profiling ie, visualization at selected and variable depths is not readily possible with this process.

Process C provides information about the local elastic properties of the sample. This is the same process that permits both surface and subsurface visualization in a conventional ultrasonic flaw detector and in an acoustic microscope. Here resolution is determined by the wavelength of the acoustic waves. Depth profiling is not possible in conventional transmission ultrasonics, although it can be done in the reflection mode using pulse time techniques.

Process B is unique to photoacoustic microscopy. This process provides information about local thermal properties such as the thermal diffusivity and thermal expansion coefficient of the sample. Visualization results from the interaction of the thermal waves with features in the sample that exhibit differences in these thermal properties. The resolution is determined by the wavelength of the thermal waves or the thermal diffusion length as shown by Thomas et al [111]. The depth of penetration is limited to one or two thermal diffusion lengths in the sample which in turn depend on the modulation frequency and properties of the sample.

24

In general, a PA microscope will provide information about the sample from all three of the physical process A, B and C although in many cases one or more of them can be neglected. So care must be taken to correctly interpret the results.

Von Gutfeld and Melcher were the first to demonstrate that subsurface holes in an aluminium cylinder could affect the PA signal detected by a piezoelectric transducer [112]. Wong et al. first reported actual PA images of subsurface structures in solids [113-114]. They found that any surface microstructures observable with an optical microscope on a silicon carbide sample (used in the manufacture of turbine blades) could also be detected by changes in the PA signal. Further, subsurface inhomogeneities not visible with an optical microscope could also be determined. PA microscopy by ultrasonic scattering has been done by Wickramasinghe et. al, and Tam and Coufal [115-116]. Freese and Teegarden have used nondestructive PA imaging to locate the inhomogeneities in a layerd sample [117]. A pulsed PA microscope that minimises the possibility of sample damage by the focused laser beam has been developed by Petts and Wickramasinghe [118]. Several groups such as Thomas et. al, Ash et al, Busse and Rosencwaig have done investigations on scanning PAM and used it to map surface and subsurface features of integrated circuits, ceramic substrates etc [119-125]. In these studies they found that the PA phase image is usually more valuable than the PA amplitude image because the former is much less affected by the variations in optical absorption, but mainly depends on the variation of thermal properties. PA imaging of compositional variation of $Hg_{1-x}Cd_xTe$ semiconductors, which are useful for mid IR detection by Mc Clelland et.al. is a good example of an application of PA

microscopy for industrial quality control [126]. PA mapping of damages due to ion implantation has been demonstrated by Macfarlane et.al [127].

In all these experiments PA imaging experiments have been performed with point-by-point laser excitation and data collection. Coufal et.al have shown that PA imaging can be performed by a spatial multiplexed technique using Hadmard transform and Fourier transform [128-129]. This method has the advantages of lowering the risk of sample damage due to heating and improved signal to noise ratio. Time domain PA microscopy techniques have also been developed [130]. R.S.Quimby has demonstrated a PAM technique in which beam position is modulated rather than beam intensity [131]. This method is shown to provide greater detail and contrast than conventional PAM. Another group that has made several investigations on PAM is that of Inglehart et.al [132-133]. They have made theoretical and experimental studies regarding the spatial resolution of PA microscopy.

Along with these developments on the instrumentation and application side, successful theoretical models have been worked out regarding PA microscopy and depth profiling [134-138].

1.7: Photoacoustic Microscopy : Instrumentation

In general a photoacoustic microscope has the following units. 1) Light source 2) Modulator 3) PA cell 4) Scanning unit 5) Signal processing system. These are shown schematically in Fig 1.5. Every other unit, except the scanning unit is similar to that in a PA spectrometer.
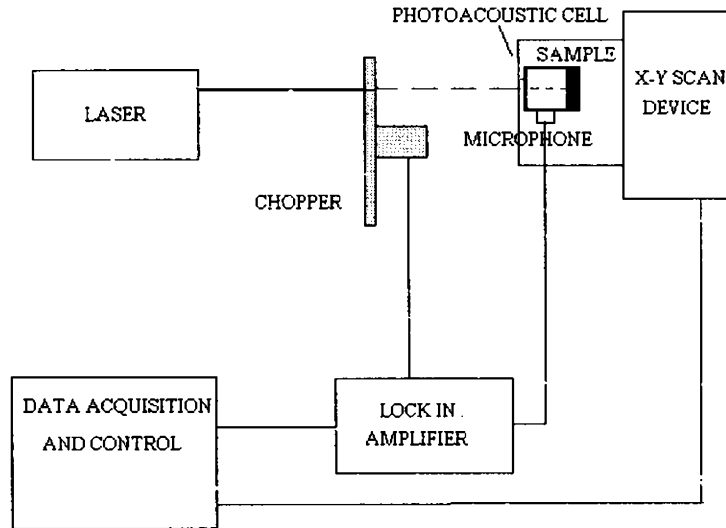
Fig 1.5 : Schematic digram of a photoacoustic microscope

Scanning the sample with modulated beam of light can be done in different ways. In the PA microscope developed by Sudhakaran and Philip the light beam is fixed and focused on to the sample in the PA cell. Scanning is done by moving the PA cell using two translation stages (for motion in X and Y directions) driven by stepper motors [139]. As the cell moves, the light beam will be focused on to different points on the sample. The cell is kept at each position for a few seconds and the amplitude and phase of the PA signal from each position is measured. After completing the scan over the entire sample in this way the data obtained is processed to produce a photoacoustic amplitude/phase image of the sample. Instead of moving the sample/PA cell, some other groups have used the technique of moving the intensity modulated light beam. This is done either by moving the light source or using rotating mirrors for reflecting focused light on to the sample.

The PA signal from each point on the sample needs some time to settle down to a steady value. Hence a time delay is usually given between successive steps. The readings are noted only after this settling time. Since the data to be collected is very large, the scanning and data collection is usually automated using a microprocessor or computer.

1.8: Applications of Photoacoustic Microscopy: Nondestructive Evaluation (NDE) of Solids

Non-destructive evaluation (NDE) is dominated by the problem of detecting, imaging and sizing structural defects such as cracks, which might lead to a component failure. It also includes non-destructive methods that provide information about the characteristics of the materials utilized in the manufacture of components. The most widely used NDE techniques are: ultrasonics; X-ray radiography; eddy current, dye-penetrant and visual inspection. Thermal techniques are yet to make a major impact in the NDE field but recently they are being used to solve an increasing number of industrial inspection problems. They have significant advantages over the traditional NDE methods in a number of new important areas, notably for the inspection of new materials, ceramics, composites and coatings that are becoming essential to modern industry. The salient features of thermal techniques are the following:

1) ability to detect interfaces between media of differing thermal properties

2) well developed non-contact generation and detection techniques

3) potential for rapid large area scanning for defects.

28
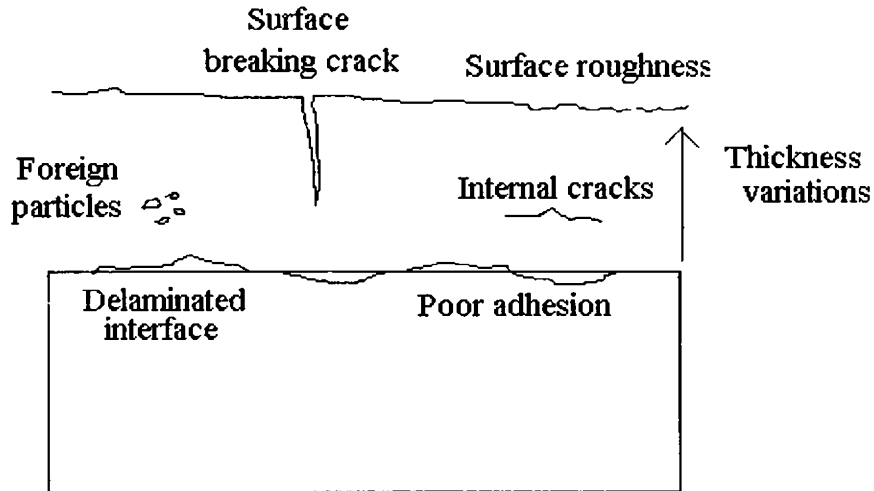
Fig 1.6 : Schematic diagram of defects in a coating

Fig 1.6 is a schematic diagram of some of the main structural imperfections that may be present in a coating on an engineering component. A poor bond between the coating and the substrate may lead to the failure of such a component. The bond may be partially or completely absent (i.e. a delamination). The coating structure may vary because of local sites of high porosity or the presence of foreign particles. The coating thickness may vary and its surface may be rough. Internal stresses in the coating layer may be produced during the deposition process leading to the development of cracks. Some similar defects may be found in composite material components at or near the surface. For each of these important groups of materials thermal NDE techniques are of unique importance

PA microscopy which is one tool of thermal wave NDE has the following applications.

1)   PAM gives visual information on a microscopic scale

2)   By changing the wavelength of the incident focused light beam PAM can give optical absorption data on a microscopic scale.

3)   PAM gives information about the local thermal and elastic properties on a microscopic scale.

4)   PAM gives information about de-excitation processes on a microscopic scale. Thus the presence of fluorescent species, photochemical processes etc in a small region can be investigated. In semiconductor device materials the presence of electrical shorts or leaks during bipolar device manufacture will lead to photovoltaic processes which will get reflected in the PAM signal.

5)   PAM allows for depth profiling on a microscopic scale. This can be used for thin film thickness measurements in a localized manner.

Some of the other fields which have made use of PAM recently are: photoacoustic evaluation of stratified materials, imaging of hydrogen in metals and alloys, CdTe surface characterization, imaging of voids in direct wafer bonding, evaluation of defects and thermal conductivity in the surface layer of ion implanted semiconductor, analysis of ultra shallow junctions and imaging of biological samples [140-157].

References

[1] M.J.Adams and G.F.Kirkbright, *Analyst* (1977) **102**, 281

[2] A.G.Bell, *Am J Sci* (1880) **20**, 305

[3] A.Rosencwaig, *Photoacoustics and Photoacoustic spectroscopy* Wiley,

New york (1980)

[4] A.Rosencwaig and A.Gersho, *J Appl Phys* (1976) **47**, 64

[5] A.C.Tam, *Rev of Mod Phys* (1986) **58(2)**, 381

[6] D.P.Almond and P.M.Patel, *Photothermal Science and Techniques,* (1996)

Chapman and Hall, London

[7] J.G.Parker, *Appl Optics* (1973) **12**, 2974

[8] M S Bennett and R A Foreman, *Appl Optics* (1976) **15**, 2405

[9] L.C.Aamodt, J C Murphy and J G Parker, *J.Appl.Phys* (1977) **48**, 927

[10] G C Wetsel and F A McDonald, *Appl.Phys.Lett* (1977) **30**, 252

[11] F A McDonald and G C Wetsel, *J.Appl.Phys* (1978) **49**, 2313

[12] H.C.Chow, *J.Appl.Phys* (1980) **51(8)**, 4053

[13] A.C.Tam Ultrasensitive Laser spectroscopy P-1 Ed Klinger Academic Press

New York

[14] C.F.Dewey, Optoacoustic spectroscopy and detection, ed.Y.H.Pao

Academic Press, New York (1977) 47

[15] L.G.Rosengren, *Appl.Opt.* (1975) **14**, 1960

[16] P.M.Morse, Vibration and Sound, Mc Grow Hill, New York, (1948)

[17] L.A.Farrow and R.F.Richton, *J.Appl.Phys* (1977) **48**, 4962

[18] C.F.Dewey Jr, R.D.Kamm and C.E.Hackett, *Appl.Phys.Lett.* (1978) **23**, 633

[19] E.Kritchman, S.S.Shtrikman and M.Statkine, *J.Opt.Soc.Amer.* (1978) **68**, 1257

[20] N.C.Femelius and T.W.Hass, *Appl.Opt.* (1978) **17**, 3348

[21] N.C.Femelius, *Appl.Opt,* (1979) **18**, 1784

[22] R.S.Quimby, P.M.Selzer and W.M.Yen, *Appl.Opt.* (1977) **16**, 2630

[23] J.C.Murphy and L.C.Aamodt, *J.Appl.Phys.* (1977) **48**, 3502

[24] P.A.Bechthold, M.Campagna and J.Chatzipetros, *Opt.Commun.* (1981) **36**, 369

[25] C.K.N.Patel and A.C.Tam, *Rev Mod Phys* (1981) **53(3)**, 517

[26] G.A.West, J.J.Barrett, D.R.Siebert and K.V.Reddy, *Rev.Sci.Instrum.* (1983) **54(7)**, 797

[27] M.Futamata, A.Fuji, I.Atsuya and C.Sata, *Trans.Jap.Welding Soc.* (1992) **23**, 3

[28].J.R.Schoonover, Y.L.Lee, S.N.Su, S.H.Lin and Eyring, *Appl.Spectroscopy* (1984) **38**, 154

[29] D.M.Todorovic, P.M.Nikolic, Z.D.Ristovski, *Physical Acoustics* Eds O.Leroy and M.A.Breazeale, Plenum Press,New York (1991) 641

[30] H.Tokumoto, M.Tokumoto and T.Ishiguro, *J.Phys.Soc.Jpn* (1981) **50**, 602

[31] P.G.Varlashkin and M.J.D.Low,*Appl.Spectrosc* (1986) **40**, 507

[32] D.W.Vidrine, *Appl.Spectros.* (1980) **34**, 314

[33] A.Rosencwaig and A.Gersho, *Science* (1975) **190**, 556

[34] M.J.Adams, G.F.Krikbright and K.R.Menon, *Anal. Chem.*(1979) **51**, 508

[35] F.A.Mc Clelland and R.N.Kniseley, *Appl.Phys.Lett.* (1976) **28**, 467

[36] E.M.Monahan Jr and A.W.Nolle, *J.Appl.Phys.* (1977) **48**, 3519

[37] A.Rosencwaig, *Advances in Electronics and Electron Physics* (1978) **46**, 207

[38] A.Hordvik and H.Schlossberg, *Appl. Opt.* (1976) **16**, 101

[39] A.Rosencwaig, *Rev.Sci.Instrum.* (1977) **48**, 113

[40] G.C.Wetsel Jr. and F.A.Mc Donald, *Bull.Am.Phys.Soc.* (1977) **22**, 252

[41] A.Rosencwaig, *Opt.Commun.* (1973) **7**, 305

[42] K.N.Madhusoodanan and J.Philip, *Pramana-J.Phys.* (1989) **33**, 705

[43] K.N.Madhusoodanan, J.Philip, G.Parthasarathy, S.Asokan and E.S R.Gopal,

    Phil.Mag. (1988) **B58**, 123

[44] K.Nandakumar and J.Philp, *Indian J.Phys.* (1995) **69A**, 595

[45] K.Nandakumar and J.Philp, *J.Non-cryst Solids* (1992) **144**, 247

[46] K.N.Madhusoodanan, A.Srinivasan, E.S.R.Gopal, K.Nandakumar and J.Philip,

    Indian J.Phys. (1991) **65A(4)**, 306

[47] K.N.Madhusoodanan, J.Philip, S.Asokan, G.Parthasarathy and E.S.R.Gopal,

    J.Non-Cryst.Solids (1989) **109**, 225

[48] K.N.Madhusoodanan and J.Philip, *Phys.Stat.Sol.(a)* (1988) **108**, 775

[49] K.Nandakumar and J.Philp, *Bull.Mater.Sci.* (1988) **11**, 297

[50] J.H.Harris and M.A.Tenhover, *J.Non-cryst Solids* (1986) **83**, 272

[51] T.Ikari, S.Shigetoni and Y.Koga, *J.Phys. C: Solid state Phys.* (1984) **17**, L969

[52] R.S.Ram, O.Prakash and A.N.Pandey, *Pramana – J.Phys.* (1987) **28**, 293

[53] A.Srinivasan, K.N.Madhusoodanan, E.S.R.Gopal and J.Philip,

    J.Non-cryst Solids (1993) **155**, 267

[54] A.Srinivasan, K.N.Madhusoodanan, E.S.R.Gopal and J.Philip, *Phil.Mag.*

    (1992) **B65**, 99

[55] T.Somasundaram, P.Ganguly and K.J.Rao, *Proc.Indian Acad. Sci.(Chem.Sci.)*

    (1983) **92**, 65

[56] Zegadi, M.A.Silifkin, M.Danin, A.E.Hill and R.D.Tomilinson,

    Phys.Stat.Sol.(a) (1992) **133**, 533

[57] C.S.Sunandana and A.K.Bhatnagar, *Solid State Commun.* (1984) **51**, 143

[58] A.Hordvik and H.Schlossberg, *Appl.Opt*, (1976) **16**, 101

[59] P.Hess and J.Pelze (eds) *Photoacoustics and Photothermal Phenomena*

Springer-Verlag, (1988) **58(2)**

[60] P.C.Claspy, C.Ha and Y.H.Pao, *Appl. Opt*, (1977) **16**, 2972

[61] P.Rochon and T.J.Racey, J.Photoacoustics (1983) 1, 475

[62] L.Baldassarre and A.Cingolani, *Solid State Commun.* (1982) **44**, 705

[63] M.Fathallah and M.Zouaghi, *Solid State Commun*, (1985) **54**, 317

[64] K.Giese, A.Nicolaus, B.Sennhenn and K.Kolmel, Can.J.Phys. (1986) **64**, 1139

[65] Q.Pan, S.Qin, s.zhong, J.Zhong S.Zhu *Springer series in optical sciences*

(1987) **58**, 542

[66] J.P.Jarrinen,V.Risto et.al., *IEEE Transactions on Sonics and Ultrasonics*

(1985) **32(2)**, 375

[67] A.C.Pereira, G.O.Neto, H.Vargas, N.Cella and L.C.M.Miranda,

Rev.Sci. Instrum. (1994) **65**, 1512

[68] R.G.Stearne and G.S.Kino, *Appl.Phys.Lett.* (1985) **47**, 1048

[69] W.G.Adams, J.G.Highfield and G.F.Kirkbright, *Anal.Chem.* (1977) **49**, 1850

[70] R.S.Quimby and W.N.Yen, *Opt.Lett.* (1978) **3**, 181

[71] W.Lahaman and H.J.Ludwing, *Chem.Phys.Lett.* (1977) **45**, 177

[72] A.Rosencwaig and E.A.Hildum, *Phys.Rev.B* (1981) **23**, 3301

[73] C.D.Merkle and R.C.Powell, *Chem.Phys.Lett.* (1977) **46**, 303

[74] R.G.Peterson and R.C.Powell, *Chem.Phys.Lett.* (1978) **53**, 366

[75] J.Etxebarria and J.Fernadez, *J.Phys.C: Solid state Phys.* (1983) **16**, 3803

[76] D.Cahen, H.Garty and S.R.Caplen, *FEBS Lett.* (1978) **91**, 131

[77] D.Cahen, S.Malkin and E.J.Lerner, *FEBS Lett.* (1978) **91**, 339

[78] D.R.Ort and W.W.Parson, *J.Biol.Chem.* (1978) **253**, 6158

[79] D.R.Ort and W.W.Parson, *Biophys,* (1979) *J.***25**, 355

[80] G.J.Diebold, *J.Phys.Chem.* (1980) **84**, 2213

[81] R.C.Gray and A.J.Bard, *Anal.Chem.* (1978) **50**, 1262

[82] D.Cahen, *Appl.Phys.Lett.* (1978) **33**, 810

[83] A.C.Tam, *Appl.Phys.Lett.* (1980) **37**, 978

[84] W.Thielemann and H.Neumann, *Phys.Stat.Solidi.* (1980) *A* **61**, K123

[85] K.Wasa K.Tsubouchi and N.Mikoshiba, *Jpn.J.Appl.Phys.* (1980) **19**, L653

[86] H.Tokumoto, M.Tokumoto and T.Ishiuro, *J.Phys.Soc.Jpn,* (1981) **50**, 602

[87] T.Iwasaki, T.Sawada, H.Kamada, A.Fujishima, and K.Honda, *J.Phys.Chem.*
(1979) **83**, 2142

[88] T.Iwasaki, S.Oda, T.Sawada and K.Honda, *Photogra.Sci.Eng.* (1981) **25**, 6

[89] K.Kaya, C.L.Chatelain, M.B.Robin and N.A.Kuebler, *J.Am.Chem.Soc.*
(1975) **97**, 2153

[90] M.B.Robin and N.A.Kuebler, *J.Am.Chem.Soc.* (1975) **97**, 4822

[91] M.B.Robin, *J.Lumin.* (1976) **13**, 131

[92] M.B.Robin,N.A.Kuebler,K.Kaya and G.J.Diebold, *Chem.Phys.Lett.*
(1980) **70**, 93

[93] J.Gelfand, W.Hermina and W.H.Smith, *Chem.Phys.Lett.* (1979) **65**, 201

[94] E.A.Rohlfing, J.Gelfand, R.B.Miles and H.Rabitz, *J.Chem.Phys.*
(1981) **75**, 4893

[95] A.Karbach, J.Roper and P.Hess, *Rev.Sci.Instrum.* (1984) **55**, 892

[96] A.Lachaine, *J.Appl.Phys.* (1985) **57(2)**, 5075

[97] U.Zammet, M.Marinelli,R.Pezzoferrato, F.Scudiere and S.Martellucci,

J.Phys.E Sci.Instrum. (1988) **21**, 935

[98] T.Swimm, *Appl.Phys.Lett.* (1983) **42**, 955

[99] A.Lachaine and P.Poulet, *Appl.Phys.Lett,* (1984) **45(9)**, 953

[100] P.Charpentier, F.Lepoutre and L.Bertrand, *J.Appl..Phys.* (1982) **51**, 608

[101] O.Pessoa, C.L.Ceasar, N.A.Patel, H.Vargas, C.C.Ghizone and

L.C.M.Miranda, *J.Appl.Phys,* (1986) **59**, 1316

[102] P.Korpium, R.Tilgner and D.Schmidt, *J.Phys. Colloq.* (1983) **44**, C6 43

[103] A.Torres-Filho, L.F.Perondi, L.C.M.Miranda, *J.Polym.Sci.* (1988) **35**, 103

[104] R.Florian, J.Pelzel, M.Rosenberg, H.Vargas and R.Wernhardt,

Phys.Stat.Sol. (a) (1978) **48**, 35

[105] P.Korpiun and R.Tilgner, *J.Appl.Phys.* (1980) **51**, 6115

[106] K.Junge, B.Bein, J.Pelzel, *J.Phys.* (1983) **44**, C_6-55

[107] J Issac, J.Philip and B.K.Chaudhari, *Pramana-J.Phys.* (1988) **31**, L153

[108] J Issac, J.Philip and B.K.Chaudhari, *Pramana-J.Phys,* (1989) **32**, L167

[109] J.Issac and J.Philip, J.Appl.Phys. (1991) **69**, 7765

[110] A.Rosencwaig, *J.Appl.Phys.* (1980) **51(4)**, 2210

[111] R.L.Thomas, J.J.Pouch, Y.H.Wong, L.D.Favro, P.K.Kuo and A.Rosencwaig

J.Appl.Phys. (1980) **51**, 1152

[112] R.J.von Gutfeld and R.L.Melcher, *Appl.Phys.Lett.* (1977) **30**, 257

[113] Y.H.Wong, R.L.Thomas and G.F.Hawkins , *Appl.Phys.Lett.* (1978) **32**, 538

[114] Y.H.Wong, R.L.Thomas and J.J.Pouch, *Appl.Phys.Lett.* (1979) **35**, 368

[115] H.K.Wickramasinghe, R.C.Bray, V.Jipson, C.F.Quate and J.R.Salcedo,

Appl.Phys.Lett. (1978) **33**, 923

[116] A.C.Tam and H.Coufal, *Appl.Phys.Lett.* (1983a) **42**, 33

[117] R.P.Freese and K.J.Teegarden *NBS Spec.Publ.(U.S)* (1979) **568**, 313

[118] C.R.Petts and H.K.Wickramasinghe, *Proceedings of IEEE Symposium on Ultrasonics* Ed.B.R.McAvoy, (1980) **1**, 636

[119] L.D.Favro, P.K.Kuo, J.J.Pouch and R.L.Thomas, *Appl.Phys.Lett.* (1980) **36**, 953

[120] J.J.Pouch, R.L.Thomas, Y.H.Wong, J.Schuldies and J.Srinivasan, *J.Opt.Soc.Am.* (1980) **70**, 562

[121] E.A.Ash, E.Dieulsaint and H.Rakouth, *Electron.Lett.* (1980) **16**, 470

[122] G.Busse and A.Rosencwaig , *Appl.Phys.Lett.* (1980) **36**, 815

[123] G.Busse and A.Ograbeck, *J.Appl.Phys.* (1980) **51**, 3576

[124] S.Perkowitz and G.Busse, *Opt.Lett,* (1980) **5**, 228

[125] A.Rosencwaig and G.Busse, *Appl.Phys.Lett.* (1980) **36**, 725

[126] J.F.McClelland, R.N.Kniseley and J.L Schmit, *Scanned Image Microscopy* Ed.E.A.Ash (Academic,New York) (1980) 353

[127] R.A.Macfarlane, L.D.Hess and G.L.Olson, *Proceedings of IEEE Symposium on Ultrasonics* Ed.B.R.McAvoy (1980) **1**, 628

[128] H.Coufal, H.Moller and S.Schneider, *Appl.Opt.*, (1982a) **21**, 116

[129] H.Coufal, H.Moller and S.Schneider, *Appl.Opt.*, (1982b) **21**, 2339

[130] R.S.Quimby, *Appl.Phys.Lett.*, (1984) **45(10)**, 1037

[131] R.S.Quimby, *Appl.Phys.Lett.*, (1981) **39(11)**, 880

[132] L.J.Inglehart, K.R.Grice, L.D.Favro, P.K.Kuo and R.L.Thomas, *Appl.Phys.Lett,* (1983), **43(5)**, 446

[133] P.K.Kuo, L.D.Favro, L.J.Inglehart, R.L.Thomas and Srinivasan , *J.Appl.Phys.*,(1982), **53(2)**, 1258

[134] P.K.Kuo and L.D.Favro, *Appl.Phys.Lett.* (1982) **40(12)**, 1012

[135] J.Ospal and A.Rosencwaig, *J.Appl.Phys.* (1982) **53(6)**, 4240

[136] R.S.Quimby and Z.M.Liu, *Can.J.Phys.* (1986) **64**, 1276

[137] L.R.de Freitas, A.M.Mansnares and E.C.de Silva, *Rev.Sci.Instrum.* (2003) **74(1)**,

[138] K.R.Grice, L.J.Inglehart, L.D.Favro, P.K.Kuo and R.L.Thomas, *J.Appl.Phys.* (1983) **54(11)**, 6245

[139] A.A.Sudhakaran, Ph.D.Thesis, Cochin University of Science and Technology (1996)

[140] R.Takuaue, H.Tobimatsu, M.Matsunaga and K. Hosokawa, *J.Appl.Phys* (1986) **59(12)**, 3975

[141] P.Cielo, G.Rousset and L.Bertrand, *Appl.Opt.*, (1986) **25(8)**, 1327

[142] S.Aithal, G,Rousset, L.Bertrand, P.Cielo and S.Dallaire, *Thin Solid Films* (1984) **119**, 153

[143] G.Mussati, E.Sala, S.Maffi, G.Razzini and L.P.Bicelli, *Appl.Phys.Lett.* (1995) **66(22)**, 2966

[144] M.Belgadillo et.al, *Appl.Phys.B* (1997) **64**, 97

[145] A.C.Gracias, C.Kuranga, J.R.Senna and M.D.Silva, *Rev.Sci. Instrum.* (2000) **71(4)**, 1869

[146] N.Taka batake, T.Kabayashi, Y.Show and T.Izumi, *Mat. Sci and Engg.* (2002) **B 91-92**, 186

[147] N.Nicolaides, A.Salnick J.Ospal, *Rev.Sci.Instrum.* (2003) **74(1)**, 586

[148] M.C.Pilatou, N.J.Voogd et al, *Rev.Sci.Instrum.* (2003) **74(10)**, 4495

[149] P.K.Khandelwal, P.W.Heitman,A.J.Silversmith and T.D.Wakefield,

Appl.Phys Lett (1980) **37(9)**, 779

[150] T.Hoshimiya, H.Endoh and Y.Hiwatashi, *Jpn.J.Appl.Phys.* (1996) **35**, 2916

[151] H.Endoh, Y.Hiwatashi and T.Hoshimiya, *Jpn.J.Appl.Phys,* (1997) **36**, 3312

[152] H.Endoh, R.Mukai Y.Hiwatashi, T.Kumabayashi, T.Hoshimiya,

Proceedings of IEEE Ultrasonics Symposium (1997) 685

[153] T.Hoshimiya, H.Endoh and Y.Hiwatashi, *Proceedings of IEEE Ultrasonics*

Symposium, (1996) 789

[154] H.Endoh, Y.Hiwatashi T.Hoshiyama, *Proceedings of IEEE Ultrasonics*

Symposium, (1999), 850

[155] R.M.Burbelo, I.Y.Kucherov and A.G.Kuzmich, *Proceedings of IEEE*

Ultrasonics Symposium, (1995) 829

[156] U.Bernini, P.Mormile,A.Novellino and P.Russo, *J.Mater.Process.Tech,*

(1995) **54**, 181

[157] T.Hoshimiya, *NDT&E International* (1999) **32**, 133

CHAPTER 2

Instrumentation Developed for Photoacoustic Microscopy

2.1: Introduction

As discussed in the first chapter photoacoustic microscope (PAM) is a useful tool for detecting surface and subsurface features of a solid sample non-destructively. Various groups working in this area have used different models in the design of this device. Essentially all these designs involve the following units. 1) Light source 2) Focusing mechanism 3) PA cell 4) Scanning mechanism 5) System electronics and 6) Computer interface. The specific details of each of these subunits and the techniques used for the realization of the various functions involved in the process vary from group to group[1-4].

In most of the PA imaging systems described in literature, lasers are the preferred excitation sources. For focusing light to various points of the sample ordinary lenses and microscope objectives are used. The spot size of the focused beam has a direct bearing on the resolution of the PA images obtained. Conventional designs of PA cells can be used for PA microscopy. Unlike in the case of signals from PA spectrometers, signals in a PAM are noisier because of the mechanical movements required in the system. Hence, if methods to increase signal to noise ratio are used in the design of PA cells, we get better results. One important requirement in a PA microscope is the designing of a mechanism to illuminate various points on the sample successively point by point and to obtain the signal

from those points. Certain designs of PAM involve moving the beam of light on the sample surface while the sample itself is kept fixed [5]. On the other hand, there are designs in which the beam is kept fixed while the sample or the PA cell as a whole is moved to obtain the same effect [6]. The movements should be very smooth and the distance moved in each step should be very small to ensure high enough resolution. There should be provision for scanning in two perpendicular directions in a plane (X-Y plane). Usually a time delay is provided between the positioning of the beam at two spots on the sample. It helps to make the signal steady before measurement. The PAM also requires the usual measuring devices such as lock-in amplifier, preamplifier etc. In fact they are much more important in a PAM than in a PA spectrometer because of the greater noise and smaller signal in the former. It also requires the electronic circuitry that generates the signals controlling the movements of the scanning system. The movements are controlled by microprocessor or PC. The software also takes care of the data acquisition, storing and processing.

Sudhakaran and Philip developed a PAM for surface and subsurface imaging of solid samples [7]. This setup has a laser source, the light from which is intensity modulated using a mechanical chopper and is focused on to a sample kept in the PA cell using a convex lens. The PA cell containing the sample is moved in a step by step manner so that the modulated and focused beam of light can fall on different points on the sample successively. The scanning unit consists of two translation stages (for X and Y motions) on which the PA cell is fixed. The translation stages are driven by stepper motors. The stepper motors are controlled by a microprocessor (Intel 8085). The data acquisition is done manually using a lock in amplifier. This

41

PAM was able to give images of defects created artificially on solid samples such as cracks on silicon wafers, holes in a nylon disc, pits in a brass disc etc. The set up was also used to perform depth profiling and could detect subsurface features with reasonably good resolution.

One of the important problems encountered in this setup was the noise signals generated during the motion of the PA cell. Since the PA cell used was a conventional one, similar to that used in PA spectrometers, the signal to noise ratio was rather low. Besides manual data acquisition from a large number of points was a difficult task.

We have tried to modify the above setup so as to reduce the problems encountered in it and also to automate the setup by interfacing to a PC. In the following sections we describe the design and fabrication of our photoacoustic microscope.

2.2: Dual Microphone PA Cell: Design and Fabrication

2.2.1 : Principle

It is a well known fact that the PA signals obtained are always embedded in a lot of spurious signals called noise. There are many causes for the origin of these noise signals. A few of them can be eliminated or at least minimized by proper designing of PA cells. Some other noises such as Johnson noise, Brownian motion noise etc. are always present in the system upto a certain degree [8]. The frequency dependence of different types of noise signals is not similar. Some types of noises are predominant at lower frequencies while some others predominate at higher

frequencies. Generally speaking, the noise signals in a PA system at low frequencies are quite large.

To quantify signal quality, signal to noise ratio (S/N) is used. This is defined as [9]

$$\frac{S}{N} = \frac{\text{Signal amplitude}}{\text{Standard deviation of signal}}$$

For periodic modulation, phase detection technique (lock in amplification) is extremely efficient for extracting very weak harmonic signals contaminated with noise. Here synchronous detection is accomplished by a multiplier followed by a low pass filter. The signal is multiplied with the reference and only the low frequency components of the multiplication are filtered to the output by the low pass filter, giving a response only to signals in the vicinity of the reference frequency. All other signals and noise of the rest of the spectrum are rejected. The result is an effective narrowing of the noise band width yielding an improvement in the signal to noise ratio.

It is found that the noise signals are having a wide range of frequencies. The amplitude of each frequency component is different and it may vary with time also. The noise level of a PA signal is an average of these and more or less remains the same at a given modulating frequency in a given environment. When we amplify the signal, the noise also gets amplified keeping signal to noise ratio unchanged.

To improve the signal to noise ratio of the PA signal we have designed a two channel PA cell. The idea is to pick up the PA signals using two identical symmetrically placed microphones. These two signals are added electronically using a summing amplifier. The signal gets doubled but the noise level more or less

remains the same. This is because the interference of noise signals from the two channels may cancel out some signals and may increase some other signals. The overall result is that the noise level almost remains the same. The PA signal, being at a particular frequency gets doubled. We have designed the cell in such a way that the dimensions of the cell are very small compared to the wavelength of the PA signals. This eliminates the possibility of destructive interference between the PA signals from the two channels. The overall result is that S/N ratio gets almost doubled. The output from the summing amplifier is sent to the lock-in amplifier for measurement.

In most of our experiments we are interested in the relative PA signal level compared to a reference sample/region rather than the absolute value of the PA signal. Hence this method of increasing the signal to noise ratio will not cause any problem in the interpretation of the results of our experiments.

2.2.2   : Construction details

Fig 2.1 shows a schematic diagram of the PA cell. It is made from a rectangular block of brass of dimensions 7.5cmx5cmx5cm. It has two pairs of mutually perpendicular holes, so that holders for sample, microphones and glass window can be plugged into it. The sample holder is a cylindrical rod (diameter 2.5 cm, length 4 cm), with a notch of depth 0.25 cm at one end. Another cylindrical rod of the same dimensions, but with a hole of diameter 1.6 cm drilled along its axis and a circular glass plate attached at one end, forms the window holder. The sample holder and the window holder have rubber O–rings so that they can be fitted tightly into the cell body. The holes in the rectangular block are designed in such a way that when the sample and window holders are completely pushed inside, there is an air

column of length 0.2 cm and diameter 1.8 cm between the top of the sample holder and the bottom of the glass window.
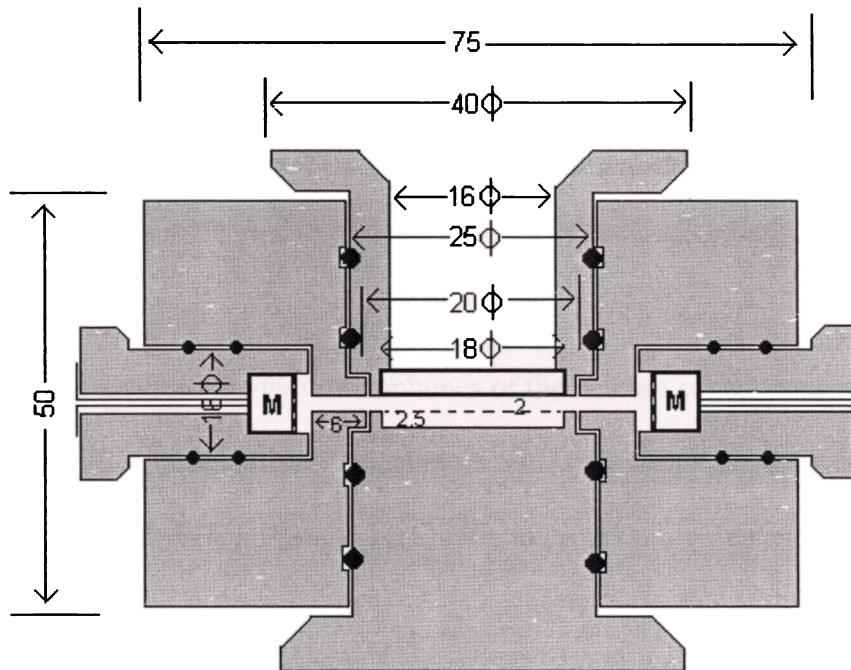
Sectional sideview
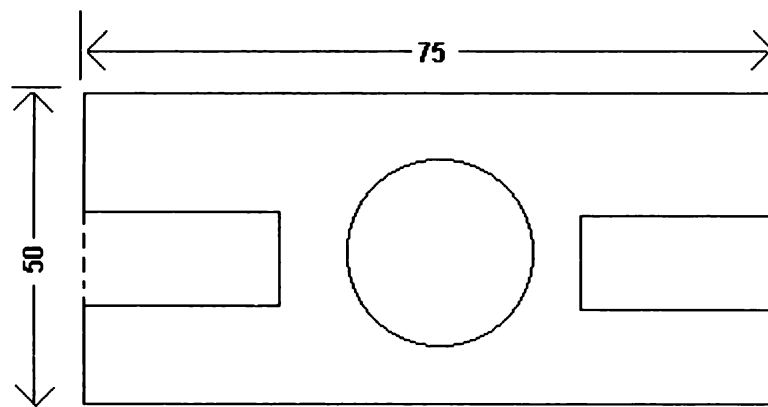
Top view

Fig 2.1 : Dual channel PA cell. (All dimensions are in millimeters. ϕ represents cylindrical shape)

The microphone chambers are similarly made from cylindrical rods of diameter 1.6 cm and length 3.5 cm. We have made use of locally available electret

microphones having a diameter 1 cm and length 0.6 cm. Their sensitivity in the frequency range of our interest is about 12mV/Pa, which is comparable to that of imported ones. For some of the sensitive measurements we have made use of the imported electret microphone Knowles BT 1759 which has a better noise isolation [10]. The microphones are fitted into appropriate holes made in the cylindrical rods mentioned above.

2.2.3 : Amplifier design

The signals from the two microphones of the cell are added using a low noise summing amplifier designed for this purpose [11]. Its circuit consists of identical preamplification stages for signals from each microphone, a buffer stage and the summing stage. The amplifier circuit is as shown in Fig 2.2

IC1 and IC2 are low noise FET input OPAMPs (LF356). The 1kΩ resistor and 100kΩ potentiometer together with the 1MΩ feedback resistor provide a voltage gain which can be varied. In our experiments we have usually kept the gain fixed at 10. The voltage divider arrangement of 1MΩ and 3.3MΩ provide a base level to the signal at the same time ensuring that the output wave does not get clipped. IC3 and IC4 are used as buffer stages to match the impedance with the summing amplifier input. IC5 which is the summing amplifier adds the signals from the two channels. We have not provided any voltage amplification at this stage. Thus the overall gain of the amplifier is the sum of gains at the two preamplifier stages which are kept exactly equal. We have tested the frequency response of this amplifier. It gives the same constant gain at all frequencies which are used in our PA experiments.
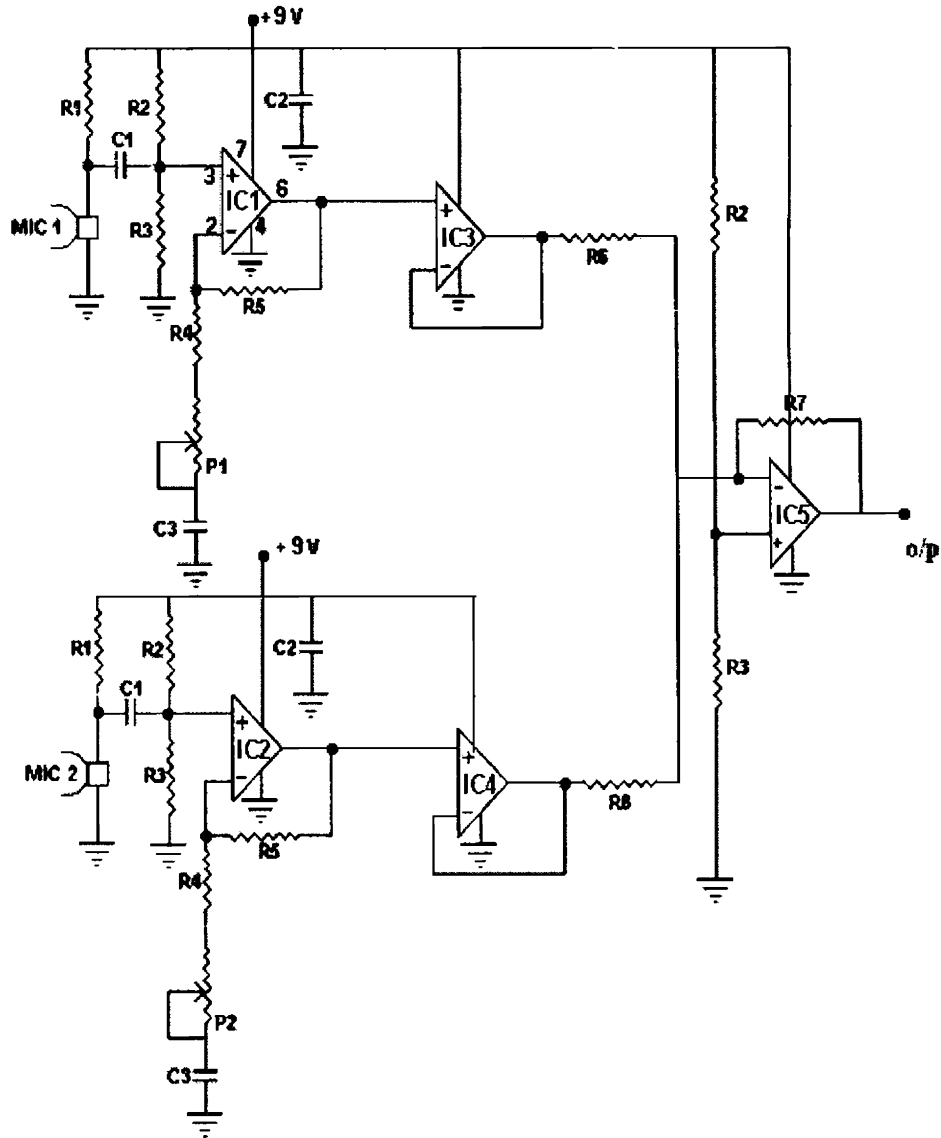
46

Fig 2.2 : Circuit of summing amplifier (IC1-IC5 -IC LF356, R1 -2.2kΩ, R2-3.3MΩ, R3-1MΩ, R4 -1kΩ, R5,R6,R7 -10kΩ P1,P2 -100kΩ pot,C1,C2 -4.7μF,C3 -0.01μF)

2.3: Two microphone PA cell : Calibration

In order to know the variation of amplitude and phase of the PA signal from the cell with modulation frequency, the experimental setup shown in Fig 2.3 has been used. It consists of a 120 mW He-Cd laser, a mechanical chopper for intensity modulation and the PA cell. The sample region in the cell is filled with a thick dense packing of fine carbon black powder.

The variation of photoacoustic signal amplitude with incident light modulation frequency is shown in Fig 2.4. The plots for the individual
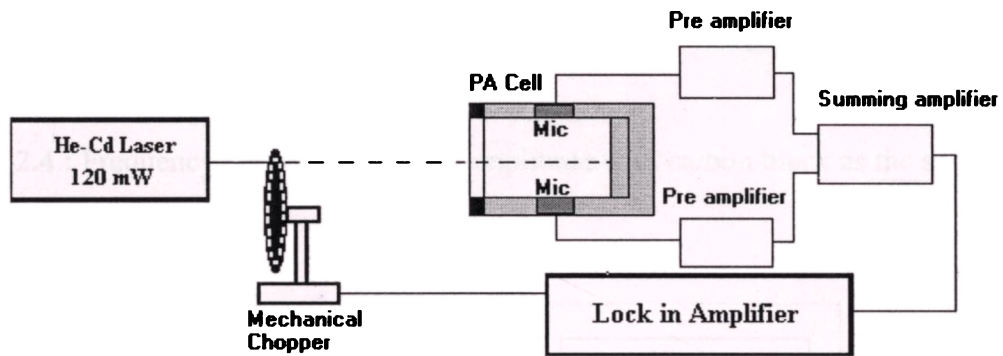
Fig 2.3 : Block diagram of the set up for calibration of the PA cell

microphones and also for the dual microphone system are shown in these figures. The variations of PA amplitude in the two cases are identical and obviously the signal is much stronger in the latter case. Besides PA signal amplitude variation exhibits the f^{-1} dependence (f being the modulation frequency) as predicted by the Rosencwaig-Gersho (R-G) theory [12].
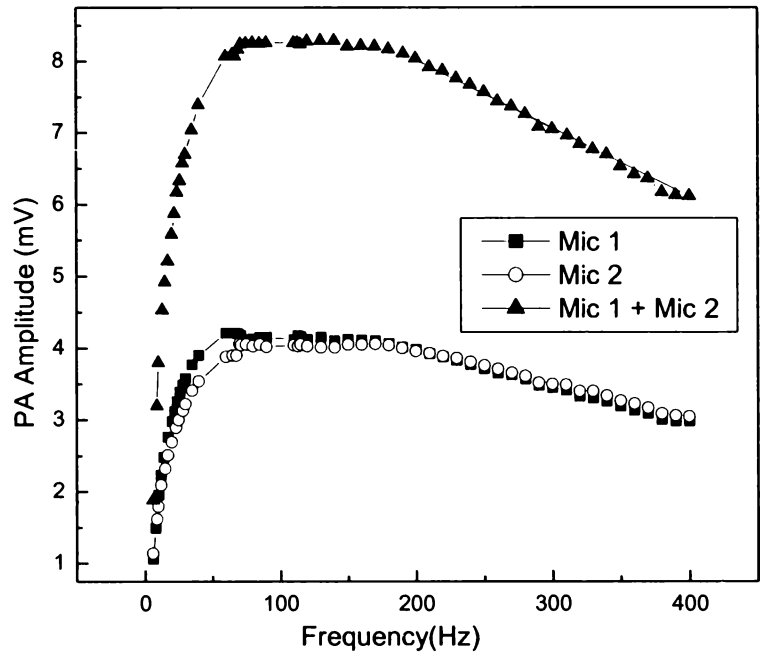
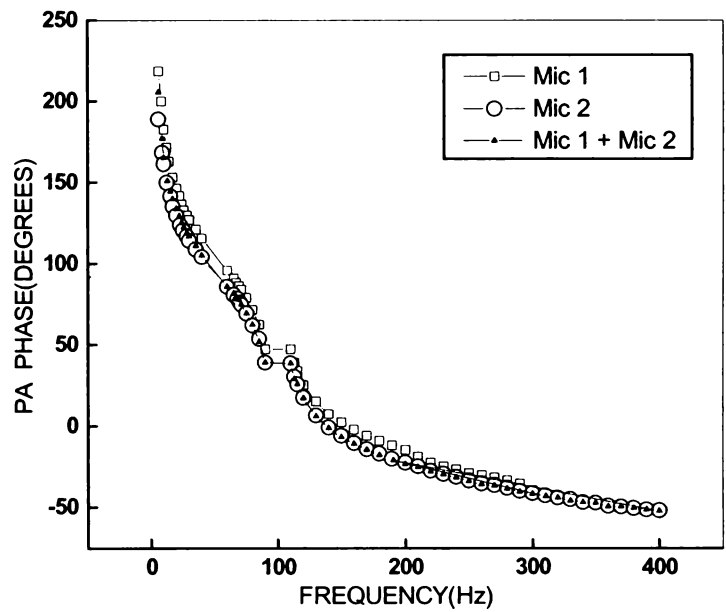**Fig. 2.4** : Frequency dependence of PA amplitude with carbon black as the sample

Fig. 2.5 : Frequency dependence of PA phase with carbon black as the sample

The corresponding variation of the phase of the PA signal is shown in Fig 2.5. For a saturated PA signal, R-G theory predicts that the phase shift at the sample surface should be constant, and that the PA phase decreases exponentially with frequency. The experimental results shown in Fig 2.5 agree with this prediction. So the cell can be used to measure thermal diffusivity of solid samples. Our calibration shows that a dual channel PA cell, of the type fabricated in this work, provides the same frequency response as a conventional one, at the same time providing a much higher signal amplitude and S/N ratio [13].

In order to study the effect of the position of the spot of light on the frequency response of the cell we have focused the beam at different points on the carbon black sample such as the centre of the sample, points away from the centre etc. Frequency variation of amplitude and phase of the PA signal are similar from all these points.

2.4: Design and fabrication of the scanning unit
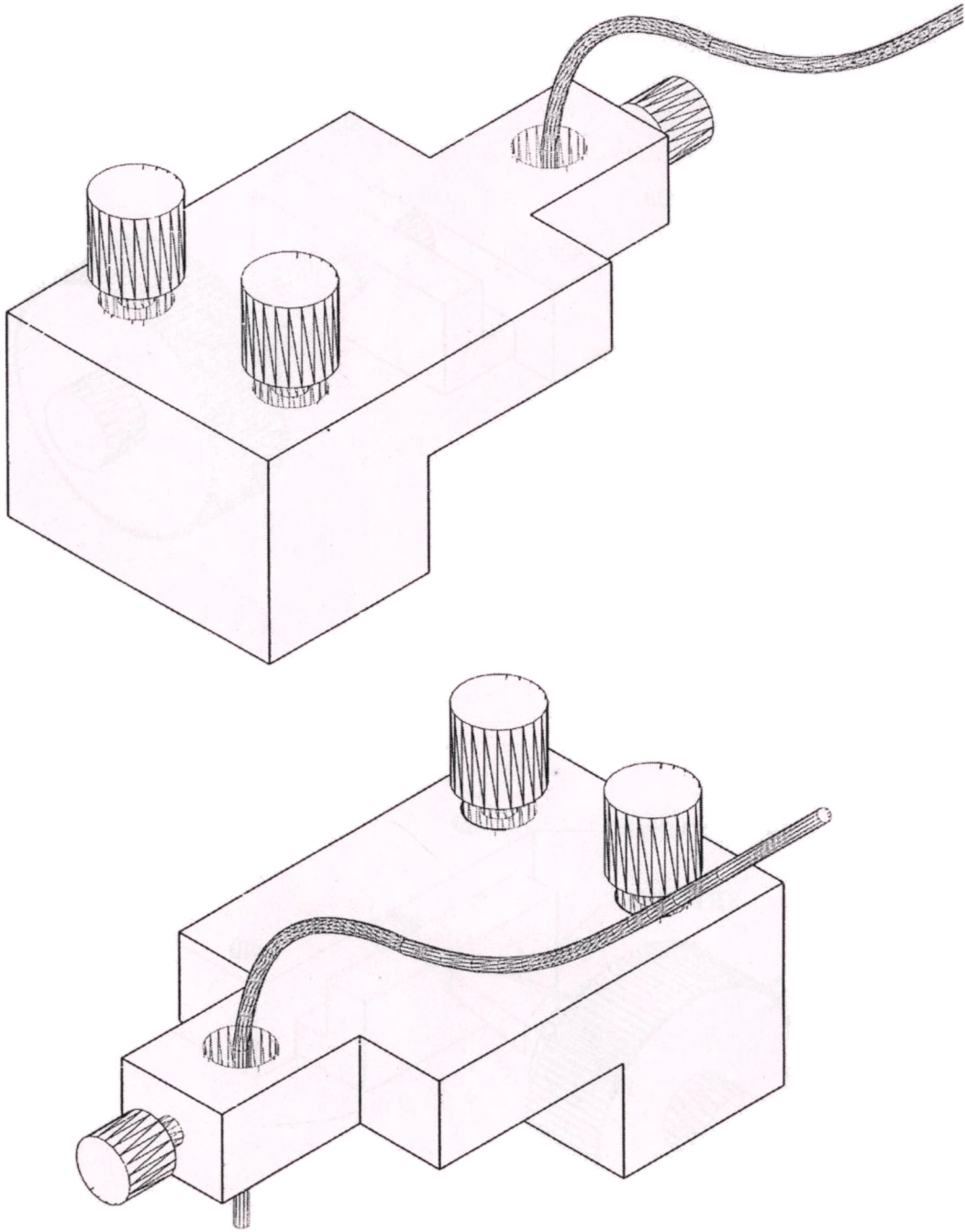
2.4.1: Translation stages and gear system

The successful operation of the PAM depends on the design and and fabrication of the scanning unit. We have used a design in which the sample is kept fixed in the PA cell while the intensity modulated beam of light is moved over the sample surface. The most important parts of our scanning unit are the optic fiber holder, a platform, translation stages and stepper motors. One tip of the optic fiber is attached to a fiber positioner which is held steady on a horizontal platform. Intensity modulated light is launched into the fiber using a short focus convex lens. The other end of the fiber is held vertically downwards using a fiber holder made of perspex

(Fig 2.6 (a)). This fiber holder is attached to a horizontal platform made of nickel plated cast iron. The platform can be moved in two mutually perpendicular directions in the horizontal plane (X-Y directions). This is made possible using translation stages. Each translation stage is made of aluminium with a micrometer of pitch 0.5 mm attached to it. The micrometers are attached to stepper motors using a gear system of spikes ratio 1:1. The gears are made of delrin. When the stepper motor shaft rotates, the gear system transfers the rotation to the micrometer sleeves and hence the translation stages move forward or backward. The stepper motors takes 200 steps to complete one rotation of the shaft. During one complete rotation the micrometer moves through 0.5 mm. Hence, the translation stages move through of 0.5/200 mm or 25 μm when the motor shaft rotates one step. The translation stages, stepper motors and PA cell are mounted on a heavy base plate made of cast iron. The various parts of the system and the stages of assembling it are shown in figures 2.6(a)-2.6(f). Figures 2.7(a) and 2.7(b) show the photographs of the system.
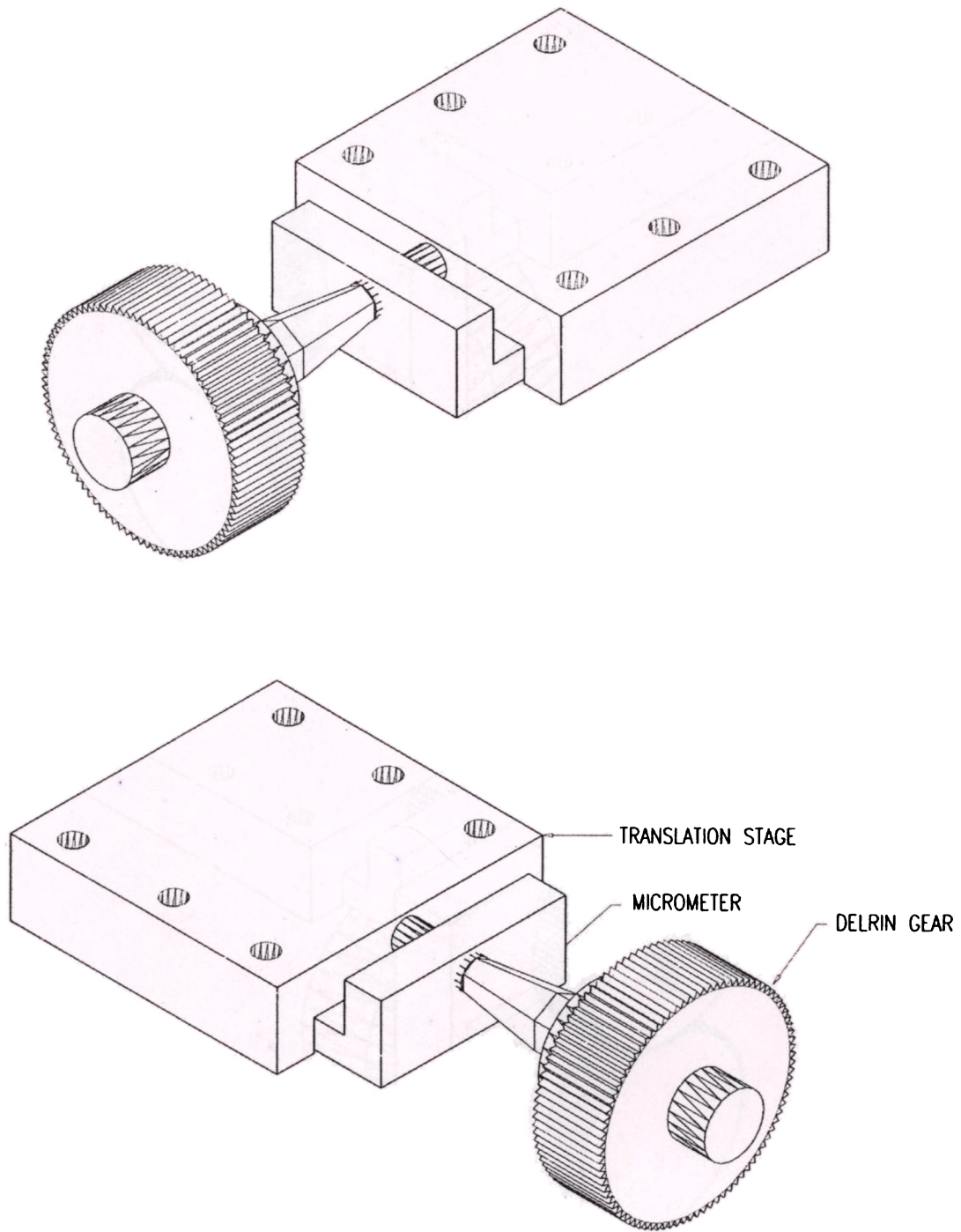
2.4.2: Stepper motors

The stepping motor is an electromagnetic device which converts digital pulses into discrete mechanical rotational movements [14-16]. In rotary stepper motors, the output shaft of motor rotates in equal increments, in response to a train of input pulses. The stepping action is caused by sequential switching of supply to the two phases of motor as per a switching logic table

The basic two phase stepper motor consists of two pairs of stator poles. Each of the four poles has its own winding. The excitation of any one winding generates a north pole (N) and a south pole (S') which gets induced at the diametrically opposite ends [Fig 2.8].

51

Fig 2.6(a): Optic fiber with holder

TRANSLATION STAGE

MICROMETER

DELRIN GEAR

Fig 2.6(b): Translation stages with micrometer
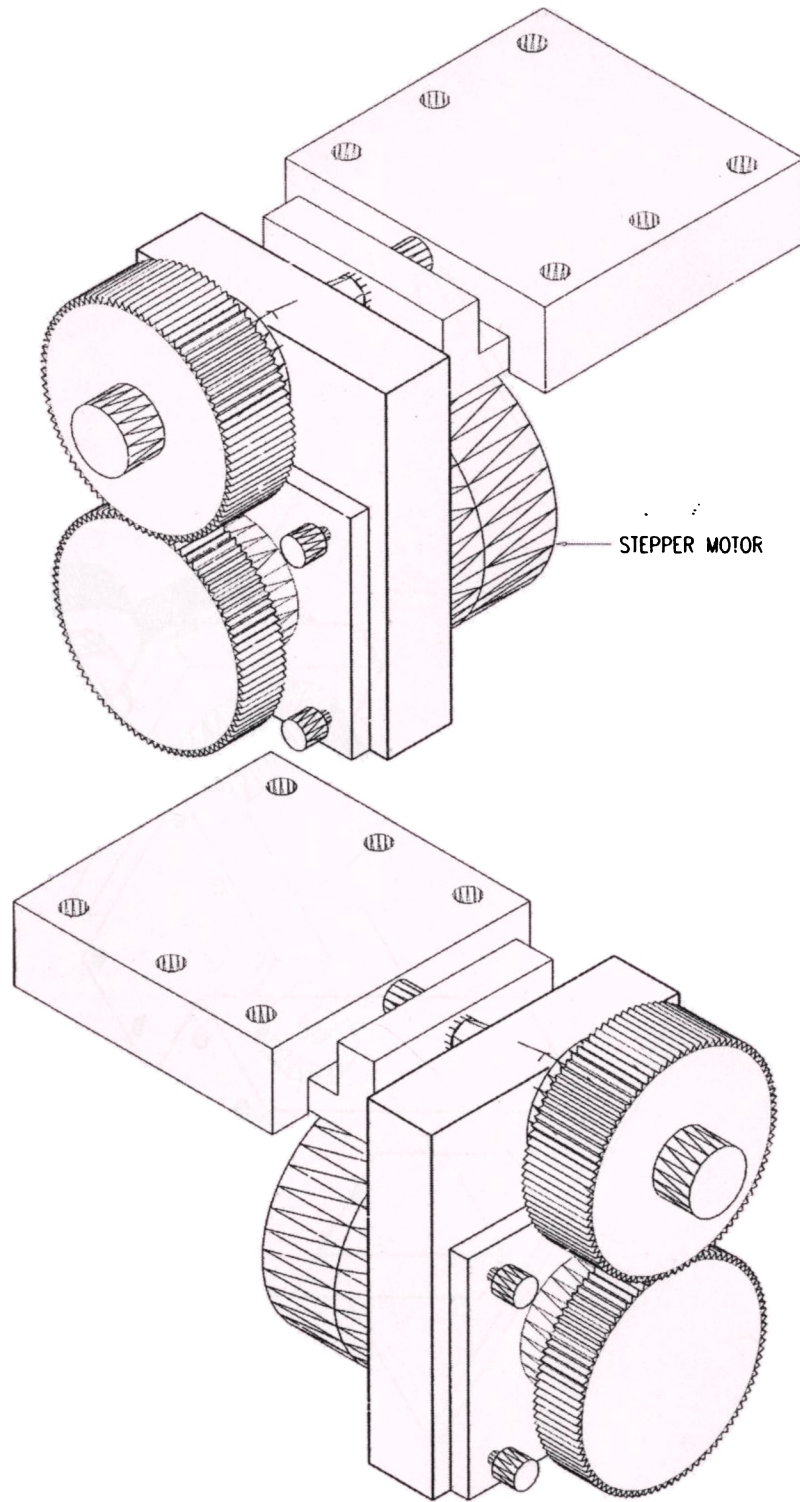
STEPPER MOTOR

Fig 2.6(c): Translation stages with stepper motors and gear

PHOTO ACOUSTIC CELL
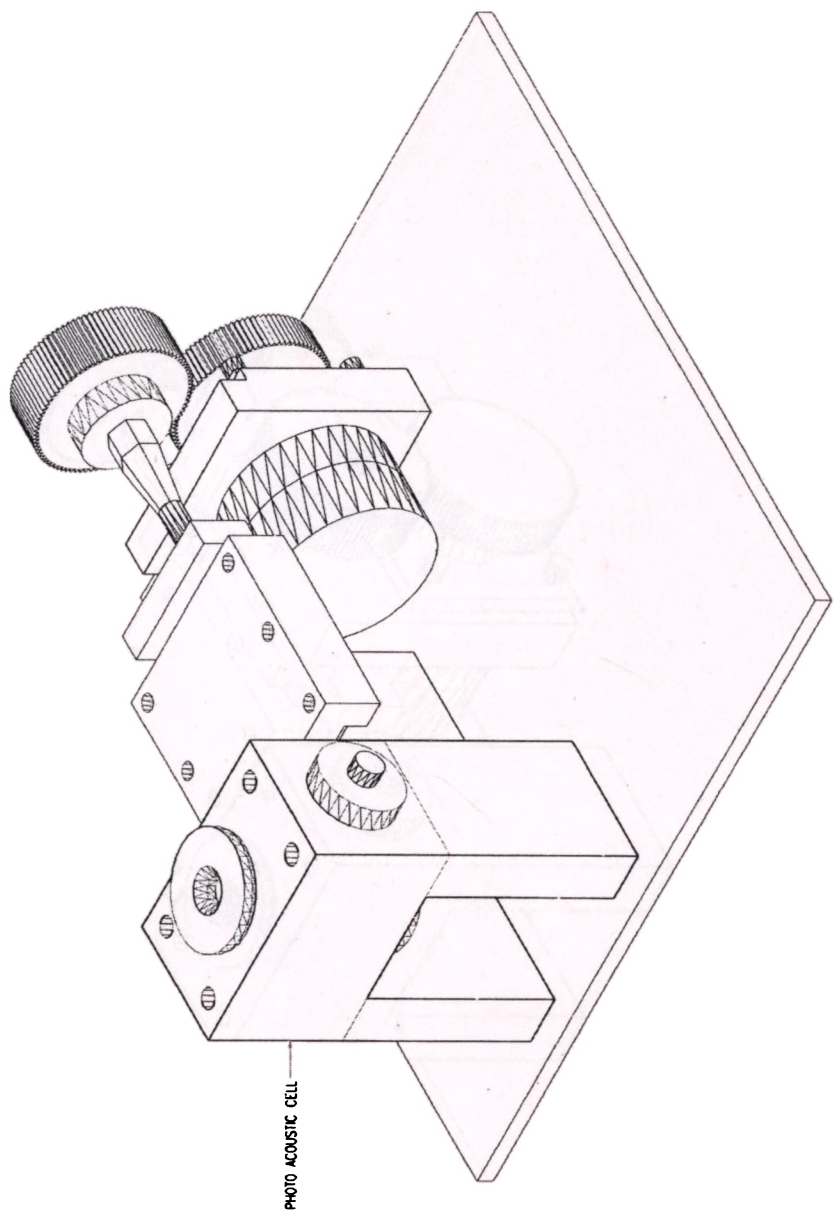
Fig 2.6(d): Assembling the system

55
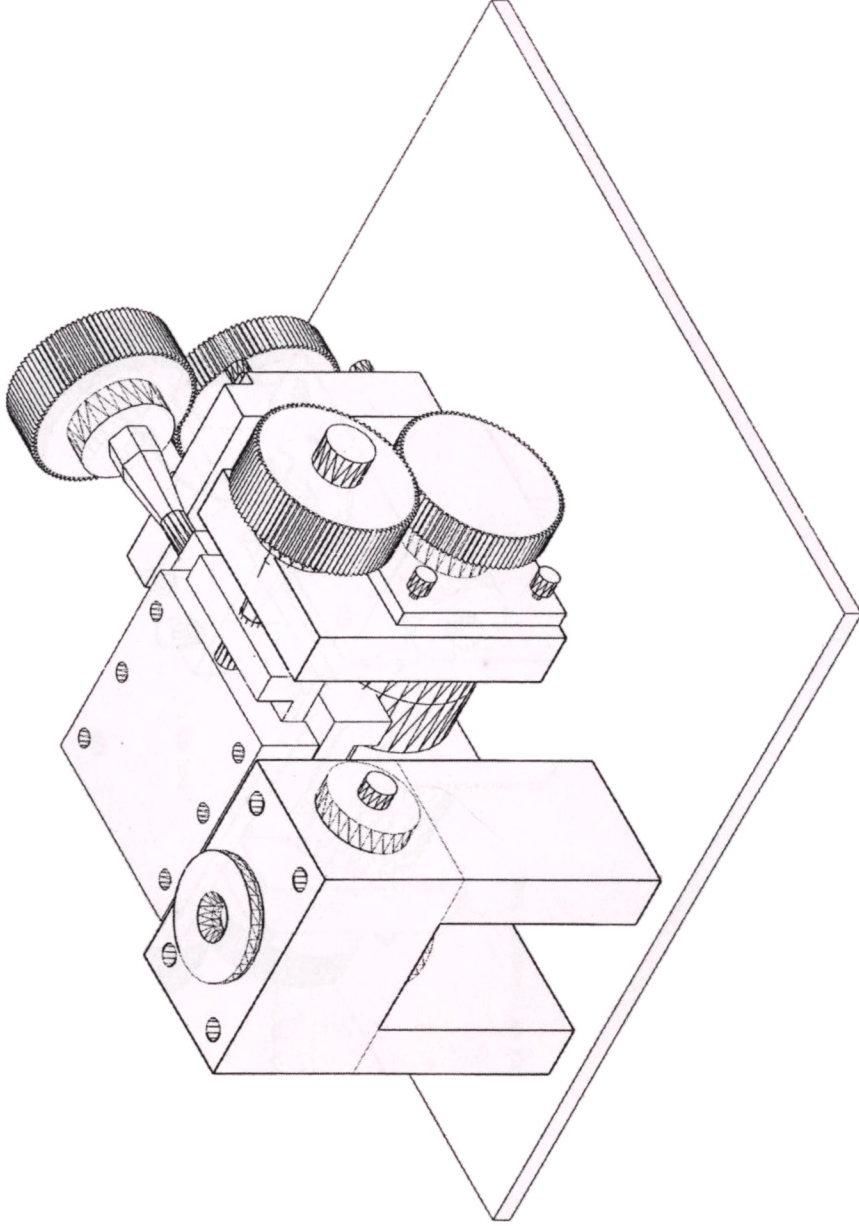
Fig 2.6(e): Photoacoustic cell with X,Y translation stages and stepper motors

56
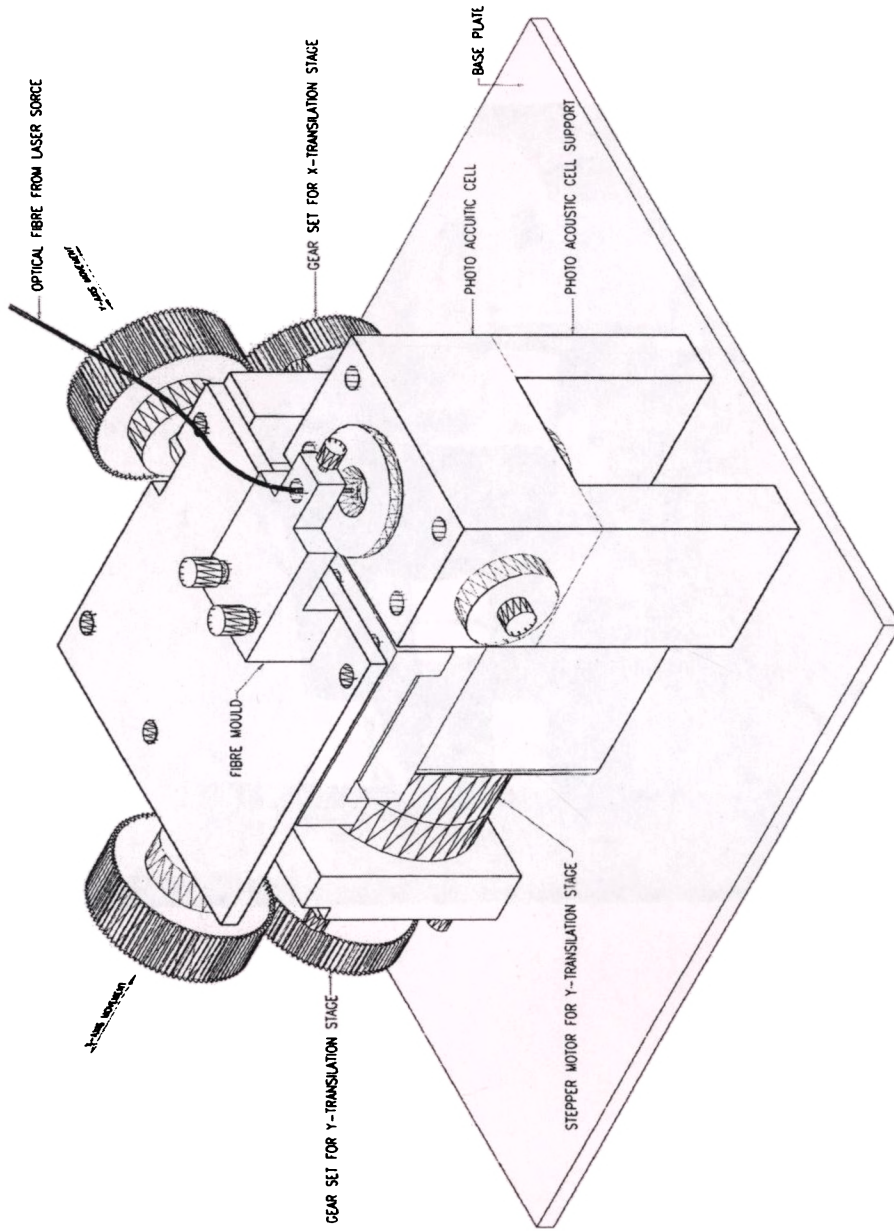
Fig 2.6(f): Complete design of photoacoustic microscope

OPTICAL FIBRE FROM LASER SORCE

GEAR SET FOR X-TRANSLATION STAGE

BASE PLATE

PHOTO ACCUTIC CELL

PHOTO ACOUSTIC CELL SUPPORT

FIBRE MOULD

GEAR SET FOR Y-TRANSLATION STAGE

STEPPER MOTOR FOR Y-TRANSLATION STAGE

57
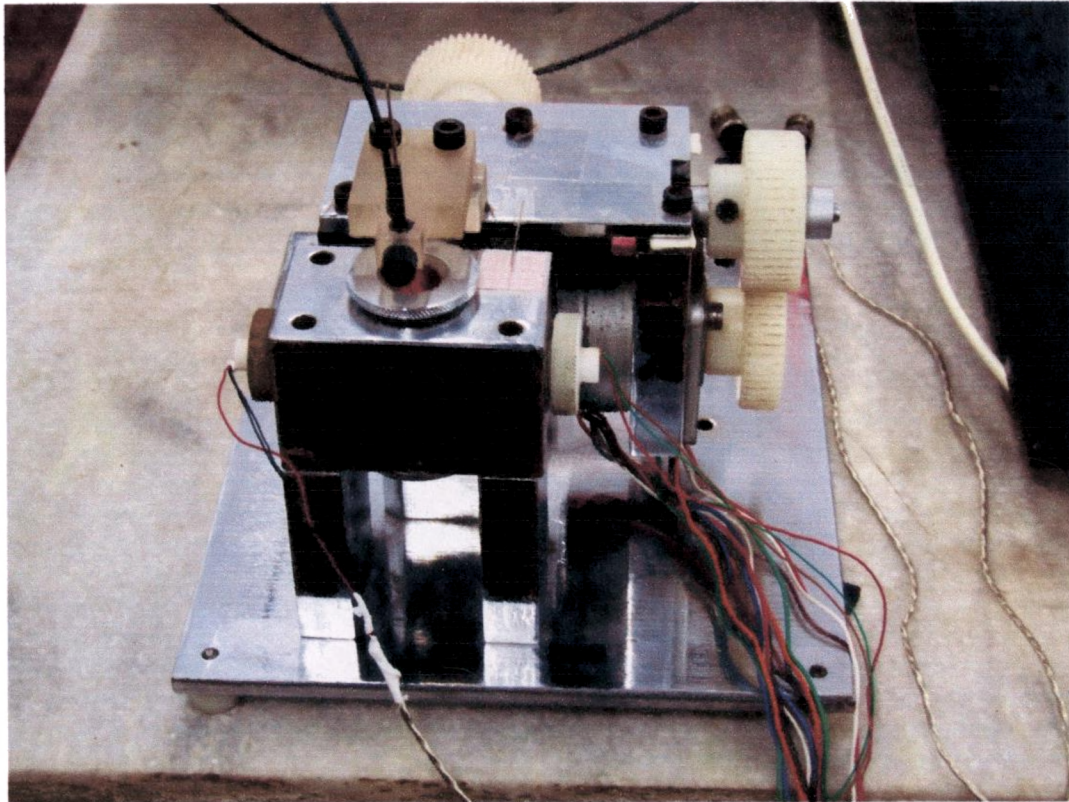
Fig 2.7(a): Photograph of the PA cell and scanning unit
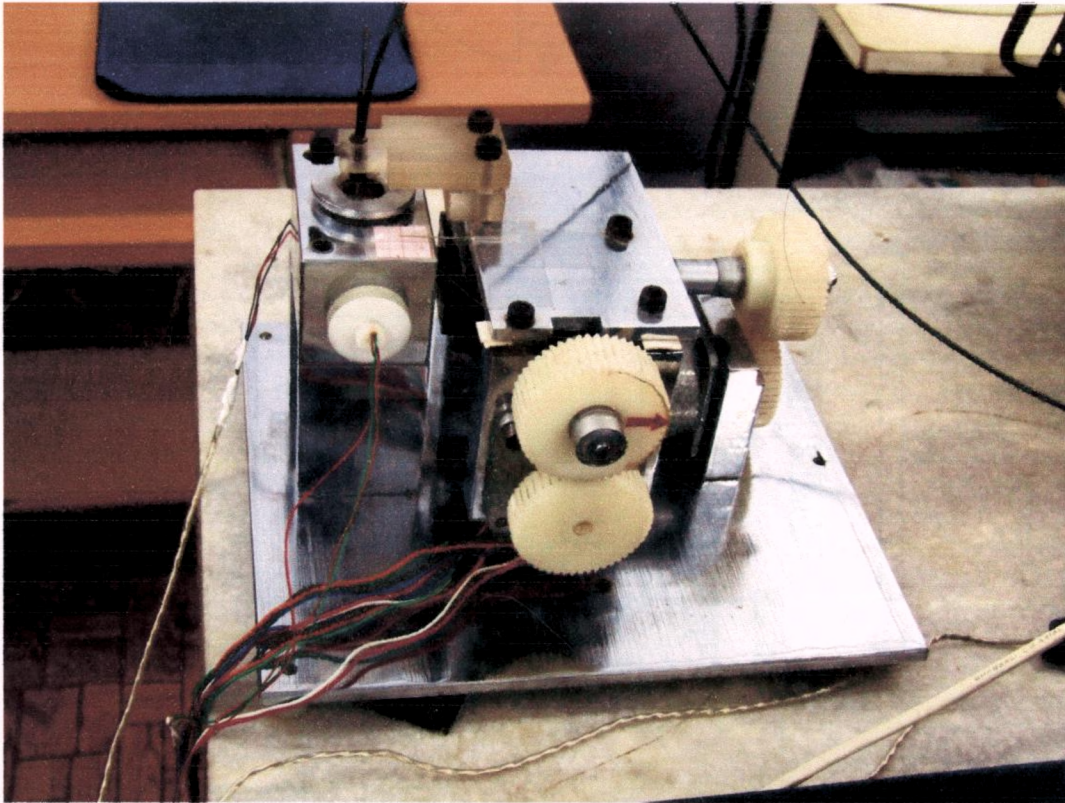
Fig 2.7(b): Another view of the setup
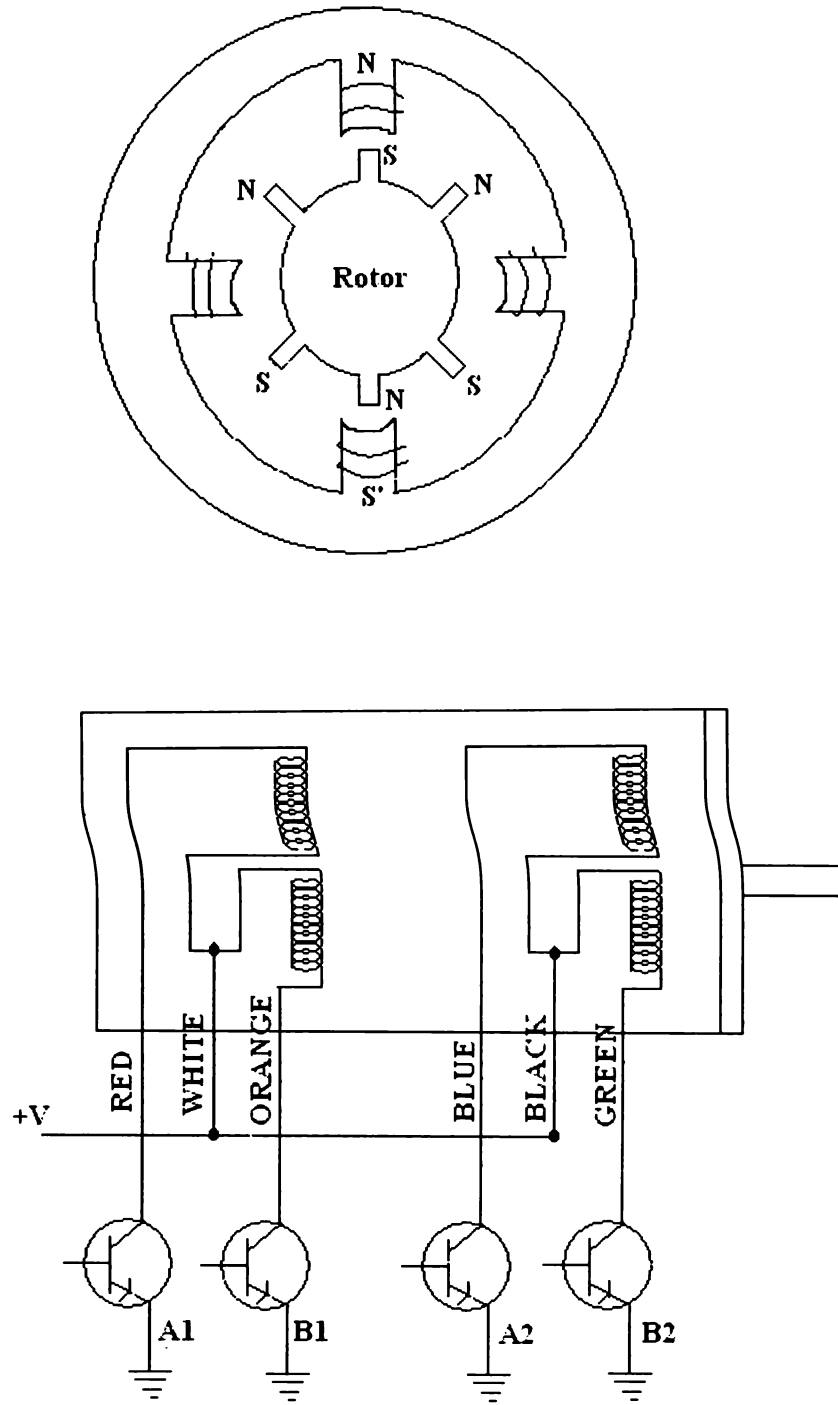
Fig 2.8: Sectional view of a stepper motor showing the coils

In the two phase switching scheme any two adjacent stator winding are energized. There are two magnetic poles active in perpendicular directions and none of the rotor pole faces can be in direct alignment with the stator poles, but a partial symmetric alignment of rotor poles is possible. In order to use the stepper motor continuously we have to energize repeatedly the four combination of phases following the sequence shown in tables 2.1 and 2.2

STEP	A1	B1	A2	B2
1	1	0	1	0
2	1	0	0	1
3	0	1	0	1
4	0	1	1	0

Table 2.1 Switching logic sequence for Clockwise rotation

STEP	A1	B1	A2	B2
1	0	1	1	0
2	0	1	0	1
3	1	0	0	1
4	1	0	1	0

Table 2.2 Switching logic sequence for Counter Clockwise rotation

We have used two stepper motors of torque 1kg-cm each (Type STM 600, Srijan Control Drives) to drive the platform in X and Y directions. They operate at a DC voltage of 6V and consume approximately 2.4W power. The speed of the motor can be controlled by varying the intervals between each pulse sequence applied to the motor. Both motors used in our scanning unit can rotate $1.8°$ for each step. This means that the motors require 200 steps motion for a complete rotation. Since pitch of the shafts of the translation stages which are coupled to the stepper motors is 0.5mm, the spatial shift of the platform for every step is 0.5/200 mm or 25μm.

2.4.3: Driving circuit

The switching logic pulses are sent to the stepper motors from a PC. The parallel port of the PC (LPT1) is the most flexible way of getting the computer to communicate with the outside world. We have used the parallel port which is generally used to interface printers to interface the stepper motor [17]. The parallel port consists of 25 pins, but it can transmit only 8 bits of data (through pins 2-9). Pins 18-25 are ground pins while the remaining pins are for various control signals.

If an electrical device is directly connected to the parallel port of PC it will damage the parallel port because it cannot handle currents larger than a few milliamperes. Thus we need a current amplifier in between the parallel port and the electrical device (stepper motor in this case). The ULN2003 integrated circuit which comes as a 16 pin DIP is precisely suited for this purpose. It has an array of 7 Darlington pairs each of which amplify the current to many times the input current value. Two such ICs are used in our driving circuit shown in Fig 2.9. The power supply fabricated for the ICs is given in Fig 2.10
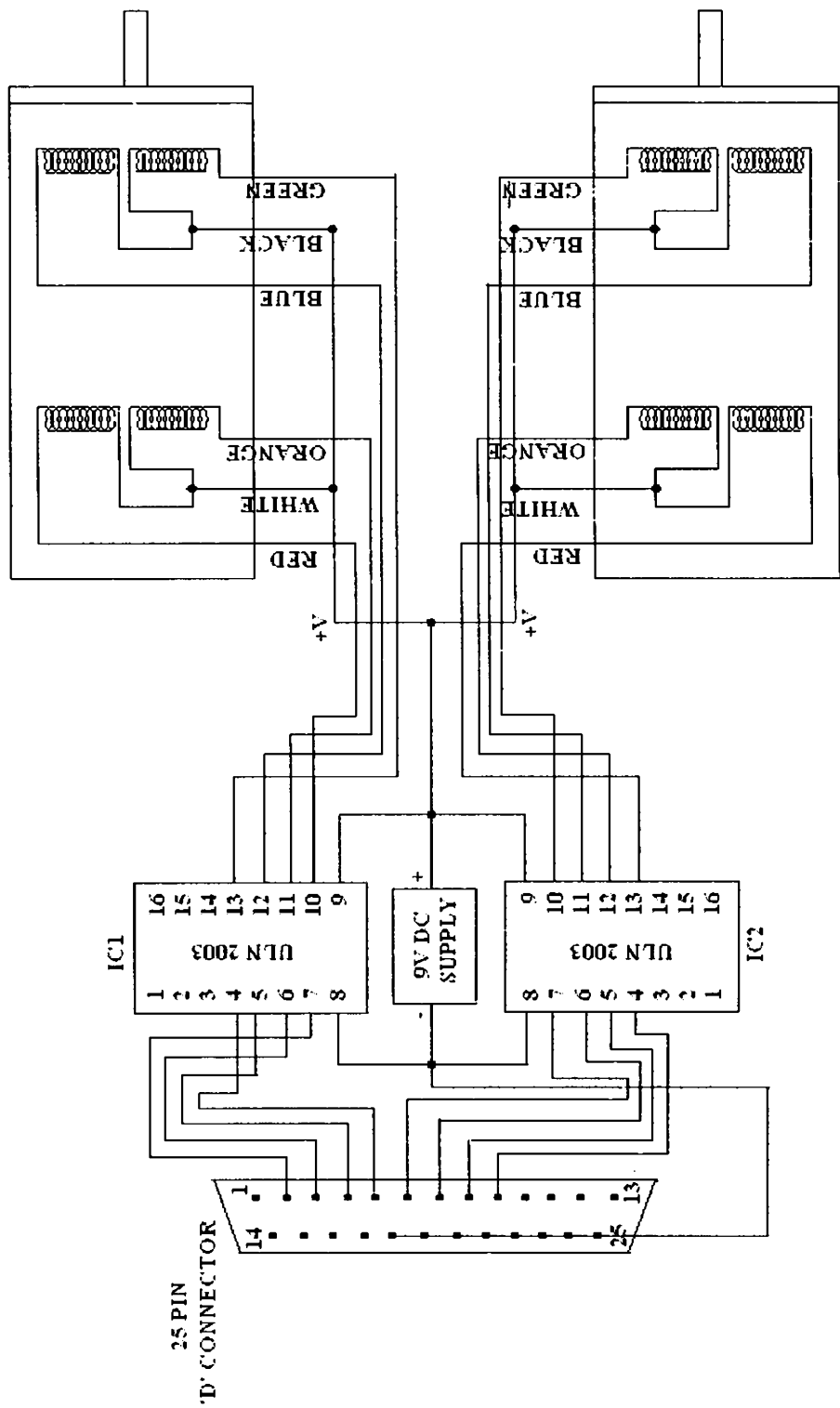
Fig 2.9 Driver circuit for stepper motors and interfacing with parallel port of PC

63
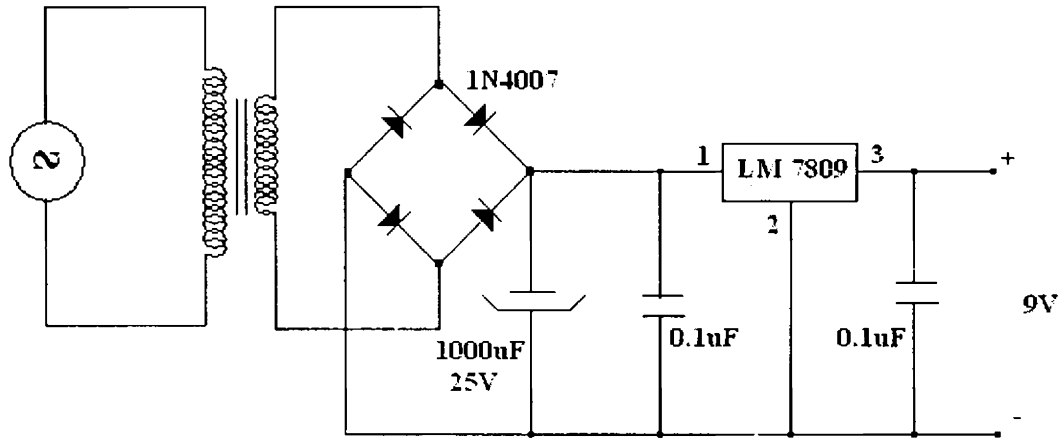
Fig 2.10: Power supply for stepper motor driving circuit and summing amplifier

2.5: Computer interfacing

Since we have to collect amplitude and phase of the PA signal from a large number of spots on the sample, manual data acquisition is almost impossible. Besides, the operation of the PAM involves sending pulses to stepper motors which drive the X and Y translation stages, waiting for a fixed time interval between successive steps etc. All these functions are taken care of by computer programs in modern PAMs.

We have developed a software in visual Basic (VB) computer programming language which controls all of the above mentioned operations. Visual Basic is a very user friendly programming language which works in windows platform [18]. It gives a wide range options while designing the front end or user interface. It is an object oriented event driven programming language which any one familiar with Windows applications like MS Word or Excel can operate. It gives almost all the

64
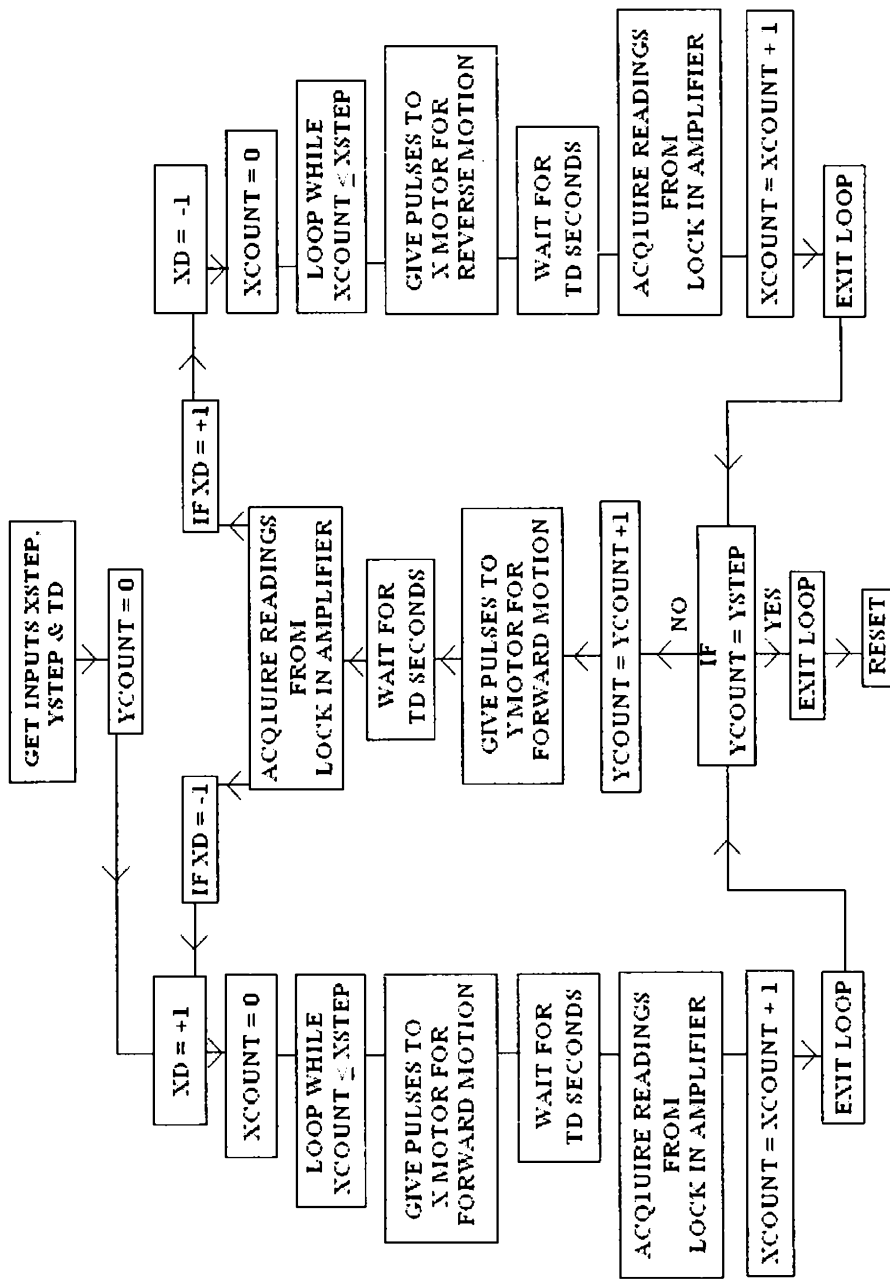
Figure 2.11 Flow chart of computer program for scanning and data acquisition

facilities given by programming languages like C which are more commonly used for technical applications[19]. Fig 2.11 shows a flow chart of the software developed by us. The complete program is given as an Appendix to this chapter (Appendix 2.1). At the start of the program the user gives the number of steps to be taken in X direction, Y direction and the time delay required between two successive steps (TD). The user can also fix the size of each step starting from 25µm upwards. On clicking the start scan button, the user is prompted to give a file name to store the data. The scanning starts immediately after this.

The spot of light from the optical fiber usually starts from a point near the top left corner on the sample whose coordinates are taken as (0,0). The control then enters two loops – an outer loop for Y motion and inner loops for X motion. For a given value of y all x values from 0 to xstep (maximum number of steps to be moved in x direction) are taken. Then y advances through one step and x values are taken from 0 to xstep in the reverse direction. The process gets repeated till y value reaches ystep (maximum number of steps to be moved in y direction). After each step the program waits for a time interval previously set by the user. Then it sends a query to the lock in amplifier demanding the amplitude and phase values to be measured.

The lock-in amplifier is interfaced using the serial port of the PC (RS 232 interface). In this scheme of interface, the PC is a DTE device and has a 9 pin D type connector (DB 9). The lock in amplifier has a 25 pin D type connector (DB 25). Out of these only 8 pins are used in this connection. The lock in SR830 (Stanford Research Systems) specifies a group of commands for setting various parameters such as sensitivity, time constant etc and also for sending data to the

computer on request. The VB program sends these commands to the lock in using its MS Comm control and acquires data. The data is stored as an ASCII file as well as displayed on the computer monitor.

Pulses to the stepper motor are sent from the PC through parallel port (LPT1-address H378) The program uses a dynamic link library function inpout32.dll specially written for this purpose. It sends the binary codes corresponding to the pulses required to drive the motors.

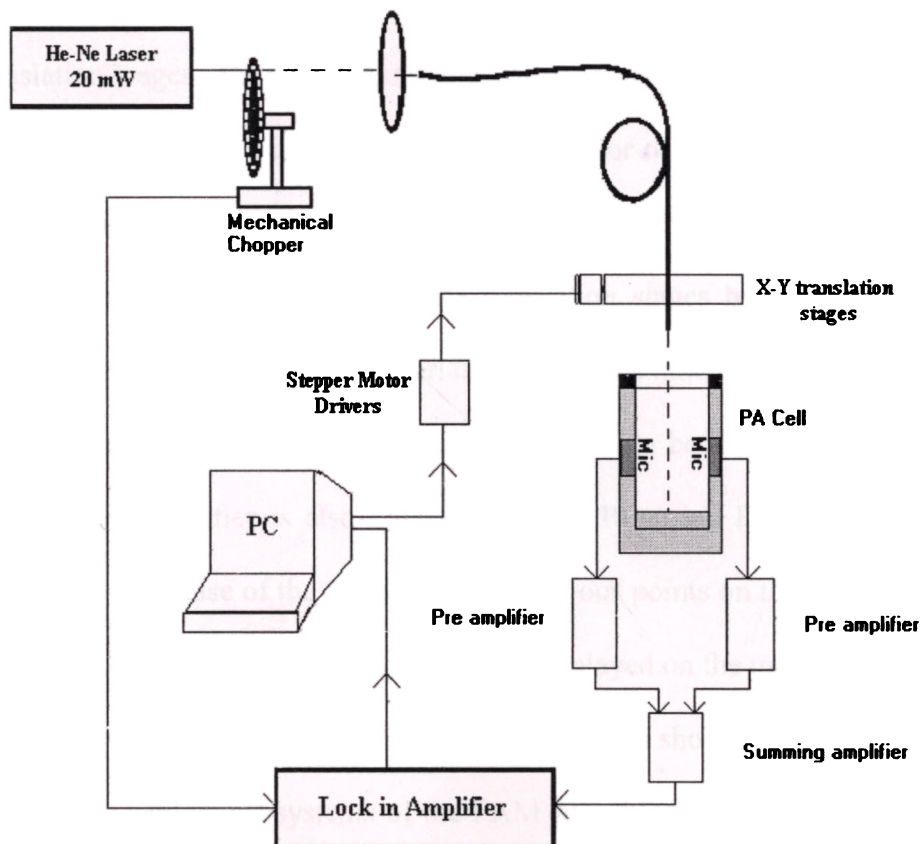## 2.6: Organization of the system as a PA microscope

Fig 2.12 The complete set up of PA microscope

Fig 2.12 shows the complete setup of the photoacoustic microscope. As explained in the various sections above, the light from the He-Ne laser is intensity modulated using a mechanical chopper. It is then guided into an optical fiber. The light coming out of the fiber is focused on to the sample placed in the dual channel PA cell. The electrical signals from the two electret microphones of the cell are added using the summing amplifier after a stage of preamplification. The resultant signal is then fed to the lock in amplifier for measurement. The tip of the optic fiber bringing light onto the sample can be moved so that the light beam can scan the entire sample surface point by point. This is achieved by fixing the fiber tip to a platform which moves in accordance with the movement of a pair of X and Y translation stages. The movements of the translation stages are in turn controlled by means of stepper motors. The driver circuit for the motors converts the weak pulses produced by computer into strong pulses. The computer program developed in VB controls the movement of the translation stages by sending the driving pulses to the stepper motors appropriately. It gives a time delay between two steps of movement, which helps the signal to settle down before taking measurement. The lock in amplifier is also interfaced to the PC using RS 232 interface. The amplitude and phase of the PA signal from various points on the sample are stored as an ASCII file on the PC. The data is also displayed on the monitor and refreshed periodically. The photograph of the complete setup is shown in Fig 2.13.

The various subsystems of the PAM have been tested repeatedly to check the correctness of the proposed mode of operation. The entire system has also been tested to ensure that the various units are working in tandem to produce a smooth

functioning of the device. Finally, measurements have been performed on a number of samples, the results of which are discussed in the next chapter.
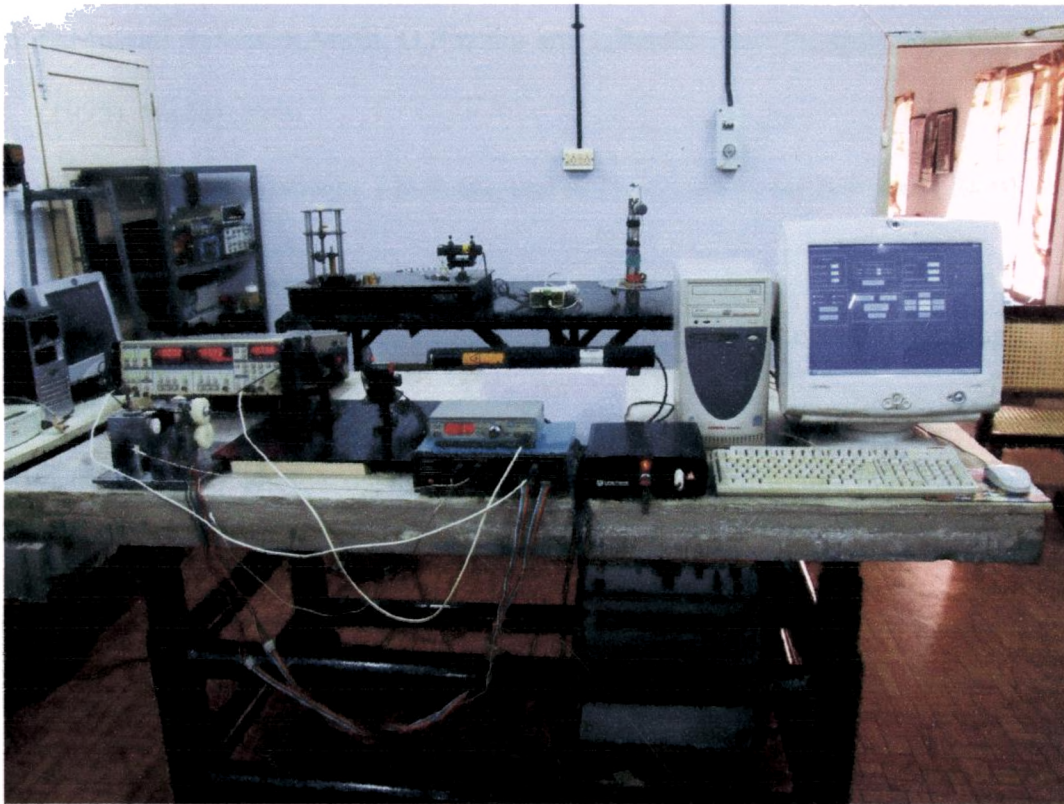
Fig 2.13: Complete experimental setup

References

1. G.Busse , IEEE Trans. Sonics & Ultrasonics (1985) **SU-32 (2)**, 355

2. A.Rosencwaig, *Anu. Rev. Matter.Sci.* (1985) **15**,103

3. G.Birnabaum and G.S.White, Research techniques in nondestructive testing (Acdem Press Inc London England) (1984) **7**, 259

4. J.C.Murphy, J.W.Maclachlan and L.C.Aamodt, *IEEE Trans UFFC*-(1986) **33 (5)**, 529

5. G.Mussati, E.Sala, S.Maffi, G.Razzini and L.Peraldo Bicelli, *Appl.Phys.Lett.* (1995) **66(22)**, 2966

6. A.C. Gracias, C.Kuranga, J.R.Senna and M.D.Silva, *Rev.Sci.Instrum.* (2000) **71(4)**, 1869

7. A.A.Sudhakaran, *Ph.D Thesis* Cochin University of Science and Technology, (1996)

8. A.Rosencwaig, Photoacoustics and Photoacoustic spectroscopy (Wiley New York, 1980)

9. D.P.Almond and P.M.Patel, Photothermal science and techniques, Chapman and Hall London (1996)

10. Knowles electronics, U.K , Tecnnical Manual, www.knowlesacoustics.com

11. Horowitz and Hill, The Art of Electronics, Cambridge Low Price Edition (II)

12. A.Rosencwaig and A.Gersho, *J.Appl.Phys.* (1976) **47**, 64

13. O.Raghu and J.Philip, *J. Instrum. Soc. of India* (2003) **33** , 155

14. S.Boada , M.P.Srinivasan and A.Pittet, Stepping motors (Centre for electronic design and technology,IISc., Bangalore)

15. S.W.Fardo and D.R.Patrick, Electrical Power Systems Technology,

(Prentice Hall Inc.Englewood)

16. Srijan Control Drives Pvt.Ltd, Operation manual for D.C.Stepping motors

17. Shobhan Kumar Dutta, *Electronics for You* ,Dec 2000, 89

18. Programming with Visual Basic, Jose Mojica, O'Reilly Media I edition (2001)

19. Steven Holzner, C Programming, Prentice Hall India

Appendix 2.1

Source program in VB for the operation of the PAM

```
Option Explicit
'All the variables used in this program are defined in advance in this section

Public xstep As Integer  'User specified no of steps in x direction
Public ystep As Integer  'User specified no of steps in y direction
Public xcount As Integer 'counter index
Public ycount As Integer 'counter index

Public td               'Time Delay between steps specified by the user
Public tdelay
Dim xcode As Integer    'Represents the current state of the x stepper motor
Dim ycode As Integer    'Represents the current state of the y stepper motor

Public sign As Integer  'Represents the direction of motion of the motors
'+1 for forward -1 for reverse
Dim i As Variant        'a variable required by shell function

Dim xsizecount As Integer 'counter index '
Public xsize As Integer  'user specified size of x steps
Dim ysizecount As Integer 'counter index
Public ysize As Integer  'user specified size of y steps

Dim xmanual As Integer   'user specified no of x steps to be run manually
Dim ymanual As Integer   'user specified no of y steps to be run manually
Dim xmcount As Integer
Dim ymcount As Integer
Dim xmanualsize As Integer
Dim ymanualsize As Integer

Dim Rx As Integer       'For resetting
Dim Rxcount As Integer
Dim Ry As Integer
Dim Rycount As Integer

Dim start
Dim Amplitude
Dim phase
Dim frequency
Dim fAmplitude 'variables to store data written into file
Dim fphase
Dim ffrequency
Dim Givefilename
Dim filename
```

```
Dim Message
Public reverse As Integer

Private Sub cmdstartscan_Click()

'If the user has not supplied the input data the program asks for it.
If (txtxstep.Text = "" Or txtystep.Text = "" Or txttimedelay.Text = "") Then
MsgBox "Give the necessary Input Data"
GoTo restart
End If

'The text box contents are converted to integers and stored in variables
xstep = Int(txtxstep.Text)
ystep = Int(txtystep.Text)
td = Val(txttimedelay.Text)

Givefilename = "Give the name of the  text file in which this set of readings are to
be stored"
filename = InputBox(Givefilename, "Save as ", "C:\Raghu\Readings\data.txt")
If (filename = "") Then
Message   =   MsgBox("Data   will   be   stored   into   the   file
C:\Raghu\Readings\data.txt.You can remove it if you don't want", vbOKOnly)
filename = "C:\Raghu\Readings\data.txt"
End If

'Now signals are sent to start the forward motion of the motors
ycount = 0          'Counter index-y
sign = 1            'initiates the direction indicator -1 reverse 1 forward
Do While (ycount < ystep)   'loop 1 begins

xforward:

xcount = 0       'Counter index-x
If (sign = 1) Then
Do While (xcount < xstep)  'loop 2 begins
xsizecount = 0
Do While (xsizecount < xsize) 'loop 3 begins

If (xcode = 5) Then
Call xnine
xsizecount = xsizecount + 1
microdelay
If (xsizecount = xsize) Then
Call Delay(td)
Call Lockin(sign)
xcount = xcount + 1
Exit Do
End If
```

73

End If

If (xcode = 6) Then
Call xfive
xsizecount = xsizecount + 1
microdelay
If (xsizecount = xsize) Then
Call Delay(td)
Call Lockin(sign)
xcount = xcount + 1
Exit Do
End If
End If

If (xcode = 10) Then
Call xsix
xsizecount = xsizecount + 1
microdelay
If (xsizecount = xsize) Then
Call Delay(td)
Call Lockin(sign)
xcount = xcount + 1
Exit Do
End If
End If

If (xcode = 9) Then
Call xten
xsizecount = xsizecount + 1
microdelay
If (xsizecount = xsize) Then
Call Delay(td)
Call Lockin(sign)
xcount = xcount + 1
Exit Do
End If
End If

Loop 'loop 3 ends
Loop 'loop 2 ends
sign = -1

End If
'**
'After completing one line along x axis the y motor moves through one step

yincriment:

```
If (ycount = ystep) Then
Exit Do
End If
ysizecount = 0
Do While (ysizecount < ysize) '  Loop 5 begins


If (ycode = 5) Then
Call ynine
ysizecount = ysizecount + 1
microdelay
If (ysizecount = ysize) Then
Call Delay(td)
Call Lockin(sign)
ycount = ycount + 1
GoTo nextline
End If
End If

If (ycode = 6) Then
Call yfive
ysizecount = ysizecount + 1
microdelay
If (ysizecount = ysize) Then
Call Delay(td)
Call Lockin(sign)
ycount = ycount + 1
GoTo nextline
End If
End If

If (ycode = 10) Then
Call ysix
ysizecount = ysizecount + 1
microdelay
If (ysizecount = ysize) Then
Call Delay(td)
Call Lockin(sign)
ycount = ycount + 1
GoTo nextline
End If
End If

If (ycode = 9) Then
Call yten
ysizecount = ysizecount + 1
microdelay
If (ysizecount = ysize) Then
```

```
Call Delay(td)
Call Lockin(sign)
ycount = ycount + 1
GoTo nextline
End If
End If

Loop 'Loop 5 ends

nextline:
If sign = -1 Then
GoTo xreverse
ElseIf sign = 1 Then
GoTo xforward
End If

'*************************************************
'Now the x motor is to be moved in reverse direction
xreverse:

xcount = 0
Do While (xcount < xstep)   'loop 4 begins

xsizecount = 0
Do While (xsizecount < xsize) 'loop 3 begins

If (xcode = 5) Then
Call xsix
xsizecount = xsizecount + 1
microdelay
If (xsizecount = xsize) Then
Call Delay(td)
Call Lockin(sign)
xcount = xcount + 1
Exit Do
End If
End If

If (xcode = 9) Then
Call xfive
xsizecount = xsizecount + 1
microdelay
If (xsizecount = xsize) Then
Call Delay(td)
Call Lockin(sign)
xcount = xcount + 1
Exit Do
End If
```

```
End If

If (xcode = 10) Then
Call xnine
xsizecount = xsizecount + 1
microdelay
If (xsizecount = xsize) Then
Call Delay(td)
Call Lockin(sign)
xcount = xcount + 1
Exit Do
End If
End If

If (xcode = 6) Then
Call xten
xsizecount = xsizecount + 1
microdelay
If (xsizecount = xsize) Then
Call Delay(td)
Call Lockin(sign)
xcount = xcount + 1
Exit Do
End If
End If
Loop 'loop 3 ends
Loop      'loop 4 ends
sign = 1

'*****************************************************
If (ycount = ystep) Then
Exit Do
Else: GoTo yincriment

End If

Loop     'loop 1 ends
'*****************************************************
Call Delay(td)
Call Lockin(sign)
Call reset

restart:
End Sub

Private Sub cmdstopscan_Click()
Call reset
End
```

End Sub

Private Sub cmdmanualreading_Click()

filename = "C:\Raghu\Readings\data.txt"
Call Lockin(sign)
End Sub
'***
Private Sub cmdreset_Click()
Rx = xcount * xsizecount
Rxcount = 0
Ry = ycount * ysizecount
Rycount = 0
Do Until (Rxcount = Rx)
If (xcode = 5) Then
Call xsix
Call microdelay
Rxcount = Rxcount + 1
GoTo redox
End If

If (xcode = 6) Then
Call xten
Call microdelay
Rxcount = Rxcount + 1
GoTo redox
End If

If (xcode = 10) Then
Call xnine
Call microdelay
Rxcount = Rxcount + 1
GoTo redox
End If

If (xcode = 9) Then
Call xfive
Call microdelay
Rxcount = Rxcount + 1
GoTo redox
End If
redox:
Loop
Do Until (Rycount = Ry)
If (ycode = 5) Then
Call ysix
Call microdelay
Rycount = Rycount + 1

78

```
GoTo redoy
End If

If (ycode = 6) Then
Call yten
Call microdelay
Rycount = Rycount + 1
GoTo redoy
End If

If (ycode = 10) Then
Call ynine
Call microdelay
Rycount = Rycount + 1
GoTo redoy
End If

If (ycode = 9) Then
Call yfive
Call microdelay
Rycount = Rycount + 1
GoTo redoy
End If
redoy:
Loop
End Sub
```
'**
'This procedure occurs when XFORWARD button is pressed for MANUAL MOVEMENT

```
Private Sub cmdxforward_Click()

xmanual = Val(txtxmanual.Text)
xmanualsize = xsize * xmanual
td = Val(txttimedelay.Text)

xmcount = 0

Do While (xmcount < xmanualsize)
If (xcode = 5) Then
Call xnine
Call Delay(td)
xmcount = xmcount + 1
If (xmcount = xmanualsize) Then
Exit Do
End If
End If
```

```
If (xcode = 6) Then
Call xfive
Call Delay(td)
xmcount = xmcount + 1
If (xmcount = xmanualsize) Then
Exit Do
End If
End If

If (xcode = 10) Then
Call xsix
Call Delay(td)
xmcount = xmcount + 1
If (xmcount = xmanualsize) Then
Exit Do
End If
End If

If (xcode = 9) Then
Call xten
Call Delay(td)
xmcount = xmcount + 1
If (xmcount = xmanualsize) Then
Exit Do
End If
End If
Loop
End Sub
```
'***
'This procedure occurs when XREVERSE button is pressed for MANUAL MOVEMENT
```
Private Sub cmdxreverse_Click()

xmanual = Val(txtxmanual.Text)
xmanualsize = xsize * xmanual
td = Val(txttimedelay.Text)

xmcount = 0

Do While (xmcount < xmanualsize)
If (xcode = 5) Then
Call xsix
Call Delay(td)
xmcount = xmcount + 1
If (xmcount = xmanualsize) Then
Exit Do
End If
End If
```

```
If (xcode = 6) Then
Call xten
Call Delay(td)
xmcount = xmcount + 1
If (xmcount = xmanualsize) Then
Exit Do
End If
End If

If (xcode = 10) Then
Call xnine
Call Delay(td)
xmcount = xmcount + 1
If (xmcount = xmanualsize) Then
Exit Do
End If
End If

If (xcode = 9) Then
Call xfive
Call Delay(td)
xmcount = xmcount + 1
If (xmcount = xmanualsize) Then
Exit Do
End If
End If
Loop
End Sub
```
'***
'This procedure occurs when YFORWARD button is pressed for MANUAL MOVEMENT
```
Private Sub cmdyforward_Click()

ymanual = Val(txtymanual.Text)
ymanualsize = ysize * ymanual
td = Val(txttimedelay.Text)

ymcount = 0

Do While (ymcount < ymanualsize)
If (ycode = 5) Then
Call ynine
Call Delay(td)
ymcount = ymcount + 1
If (ymcount = ymanualsize) Then
Exit Do
End If
```

```
End If

If (ycode = 6) Then
Call yfive
Call Delay(td)
ymcount = ymcount + 1
If (ymcount = ymanualsize) Then
Exit Do
End If
End If

If (ycode = 10) Then
Call ysix
Call Delay(td)
ymcount = ymcount + 1
If (ymcount = ymanualsize) Then
Exit Do
End If
End If

If (ycode = 9) Then
Call yten
Call Delay(td)
ymcount = ymcount + 1
If (ymcount = ymanualsize) Then
Exit Do
End If
End If
Loop
End Sub
'************************************************************
'This procedure occurs when YREVERSE button is pressed for MANUAL
MOVEMENT
Private Sub cmdyreverse_Click()
ymanual = Val(txtymanual.Text)
ymanualsize = ysize * ymanual
td = Val(txttimedelay.Text)
ymcount = 0

Do While (ymcount < ymanualsize)
If (ycode = 5) Then
Call ysix
Call Delay(td)
ymcount = ymcount + 1
If (ymcount = ymanualsize) Then
Exit Do
End If
End If
```

```
If (ycode = 6) Then
Call yten
Call Delay(td)
ymcount = ymcount + 1
If (ymcount = ymanualsize) Then
Exit Do
End If
End If

If (ycode = 10) Then
Call ynine
Call Delay(td)
ymcount = ymcount + 1
If (ymcount = ymanualsize) Then
Exit Do
End If
End If

If (ycode = 9) Then
Call yfive
Call Delay(td)
ymcount = ymcount + 1
If (ymcount = ymanualsize) Then
Exit Do
End If
End If
Loop

End Sub
'*******************************************************
Private Sub Form_Load()
xsize = Int(txtxsize.Text)
ysize = Int(txtysize.Text)

'*******************************************************
'This part returns the values of the current state of the steppers
Open "c:\Raghu\scanner\xcode.txt" For Input As #1
Input #1, xcode    'Variable xcode now contains the value saved in file xcode
Close #1

Open "c:\Raghu\scanner\ycode.txt" For Input As #2
Input #2, ycode    'Variable ycode now contains the value saved in file ycode
Close #2
'*******************************************************
End Sub

Private Sub txtxsize_Change()
```

83

```
xsize = Val(txtxsize.Text)
lblxsize.Caption = "= 0" + Str(xsize * 0.0025) + "mm"
End Sub

Private Sub txtysize_Change()
ysize = Val(txtysize.Text)
lblysize.Caption = "= 0" + Str(ysize * 0.0025) + "mm"
End Sub
'*******************************************************
Public Function Lockin(sign)

MSComm1.PortOpen = True

MSComm1.Output = "OUTX0" + Chr$(13)

MSComm1.Output = "SNAP?3,4" + Chr$(13)
tdelay = Timer
While ((Timer - tdelay) < 0.3)
Wend
Data = MSComm1.Input

MSComm1.Output = "OUTR?1" + Chr$(13)
tdelay = Timer
While ((Timer - tdelay) < 0.3)
Wend
Amplitude = MSComm1.Input
txtamplitude.Text = Amplitude
txtamplitude.Refresh
fAmplitude = Val(txtamplitude.Text)

MSComm1.Output = "OUTR?2" + Chr$(13)
tdelay = Timer
While ((Timer - tdelay) < 0.3)
Wend
phase = MSComm1.Input
txtphase.Text = phase
txtphase.Refresh
fphase = Val(txtphase.Text)

MSComm1.Output = "FREQ?" + Chr$(13)
tdelay = Timer
While ((Timer - tdelay) < 0.3)
Wend
frequency = MSComm1.Input
txtfrequency.Text = frequency
txtfrequency.Refresh
```

```
Open filename For Append As #11
Write #11, xcount, ycount, Data
Close #11

MSComm1.PortOpen = False

End Function
'*********************************************************************
Public Function xten()
        xcode = 10
        Out &H378, 10

        Open "c:\raghu\scanner\xcode.txt" For Output As #2 'changing the contents
        'of xcode file to store the current state of the stepper motor
        Print #2, 10
        Close #2
End Function

Public Function xsix()
        xcode = 6
        Out &H378, 6
        Open "c:\raghu\scanner\xcode.txt" For Output As #2 'changing the contents
        of xcode file to store the current state of the stepper motor
        Print #2, 6
        lose #2
End Function

Public Function xfive()
        xcode = 5
Out &H378, 5
        Open "c:\raghu\scanner\xcode.txt" For Output As #2 'changing the contents
        'of xcode file to store the current state of the stepper motor
        Print #2, 5
Close #2
End Function

Public Function xnine()
        xcode = 9
        Out &H378, 9
        Open "c:\raghu\scanner\xcode.txt" For Output As #2 'changing the contents
        'of xcode file to store the current state of the stepper motor
        Print #2, 9
        Close #2
End Function

Public Function yten()
        ycode = 10
        Out &H378, 160
```

```
        Open "c:\raghu\scanner\ycode.txt" For Output As #2 'changing the contents
        'of ycode file to store the current state of the stepper motor
        Print #2, 10
        Close #2
End Function

Public Function ysix()
        ycode = 6
        Out &H378, 96
        Open "c:\raghu\scanner\ycode.txt" For Output As #2 'changing the contents
        'of ycode file to store the current state of the stepper motor
        Print #2, 6
        Close #2
End Function

Public Function yfive()
        ycode = 5
        Out &H378, 80
        Open "c:\raghu\scanner\ycode.txt" For Output As #2 'changing the contents
        'of ycode file to store the current state of the stepper motor
        Print #2, 5
        Close #2
End Function

Public Function ynine()
        ycode = 9
        Out &H378, 144
        Open "c:\raghu\scanner\ycode.txt" For Output As #2 'changing the contents
        'of ycode file to store the current state of the stepper motor
        Print #2, 9
        Close #2
End Function

Public Function reset()
Out &H378, 0
End Function
'********************************************************************
Public Function Delay(td)
start = Timer
Do While (Timer <= start + td)
Loop
End Function
'********************************************************************
Public Function microdelay()
start = Timer
Do While (Timer <= start + 0.005)
Loop
End Function
```

CHAPTER 3

Photoacoustic imaging of selected solid sample configurations

3.1: Introduction

The last chapter discussed the design and construction details of the scanning photoacoustic microscope developed by us. Before such a system is used for industrial or commercial applications, it is necessary to put the system under a very rigorous test and calibration procedure. Such a process is very important because it will bring out clearly the advantages and limitations of the system. It is also useful for fixing the conditions under which the setup can give optimum performance and will serve to define the scope for future work and improvement.

The standard method to test an instrument of this sort is to use it to obtain the images of a variety of samples having a known profile of defects or samples in which defects are artificially introduced. A few workers have tried to use the technique for imaging applications. Wong et al used silicon nitride ceramic samples to study their surface features [1]. For subsurface imaging flaws were made hundreds of microns beneath the surface of Si_3N_4 and SiC ceramic materials[2]. Rosencwaig and Busse used electronic printed circuit boards and Aluminium discs with holes [3,4]. Busse and Ograbeck used an aluminium sample with steps cut on it [5]. Other types of samples/sample configurations used include integrated circuits, closed cracks in opaque solids, voids occurring at the interface of bonded silicon wafers etc [6-10].

In the following sections, we will discuss a number of sample configurations which we have used for testing the photoacoustic imaging setup fabricated by us. The important capabilities that are intended to test are 1) the ability to detect surface defects 2) the ability to detect change of material and 3) the ability to detect subsurface features. We have used samples, which are good thermal conductors as well as those which are thermal insulators.

3.2: Experimental details

In the experiments that follow this section, we have used a He-Ne laser of 20mW output power as the light source. As described in the second chapter, this light beam is intensity modulated using a mechanical chopper, focused and passed through an optical fiber. The light coming out of the fiber is allowed to fall on the sample kept inside the dual channel PA cell. The tip of the fiber from which light comes out is moved using translation stages driven by stepper motors so that the light beam scans the sample surface. The spot size of the beam falling on the sample is small (about 0.5mm). The step size and the area scanned are previously set in the computer program. This is different for different samples. The measured photoacoustic amplitude and phase values are recorded and stored as an ASCII file. This file is then used for plotting the amplitude and phase images of the sample.

3.3: Results on selected sample systems
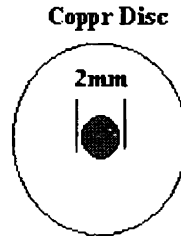
3.3.1: Surface defect on a copper disc

Coppr Disc

Fig 3.1

Fig 3.1 shows a copper disc of thickness 2 mm and diameter 1.7 cm. At the centre of the disc, a pit of diameter 2 mm and depth about 0.5 mm is drilled. This sample is given a very fine coating of carbon black by holding it over a benzene flame. This process is done very carefully to ensure that the coating is very thin and uniform. The surface of the copper disc is usually very reflecting. The photo acoustic signal strength depends on the amount of absorbed light. The thin carbon black coating increases the absorption of light. This is a standard practice adopted in photo acoustics which does not affect the results if the coating is sufficiently thin (thermally thin) and uniform [11].

This sample is kept inside the PA cell and scanning is performed. We selected a square area of size 8mm x 8mm around the pit for scanning. The lateral shift per step selected was 0.25mm in the X and Y directions. After reaching every point the beam is allowed to wait for a few seconds. After this time delay the PA amplitude and phase values are acquired by the lock in amplifier. The time delay is chosen in such a way so as to get a steady reading from a given spot. The

89

amplitude and phase values are stored as ASCII files. The readings are taken from the same sample many times by changing the time delay, changing the coating etc.

Figures 3.2 and 3.3 show the typical images obtained from such a scanning done on this sample. These are the amplitude and phase values obtained from different points on the sample. The images are the contour plots with the colours representing the PA amplitude/phase values from different positions as per the colour scale given along the side of the plot.

From the images it is immediately clear that the position of the pit is identifiable from the change in the values of amplitude and phase occurring in that region. The reason is that the optical absorption and thermal properties in the region of the pit are different from that in a normal region. The edge of the pit is not sharply demarcated in the images. The changes in amplitude and phase of the PA images extend somewhat outside the region of the pit also. The phase image is better in this aspect. Further, there are variations in the amplitude and phase values in the regions where we don't have visible defects. These may be due to the large noise signals occurring along with the PA signals. Thus even though the images are not perfect we can say that the instrument is capable of detecting the presence of surface defects with good resolution
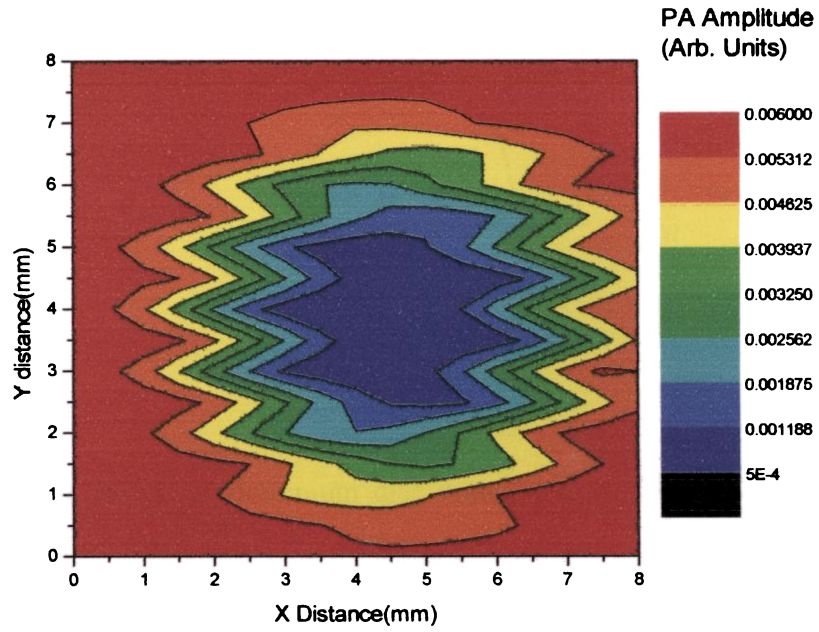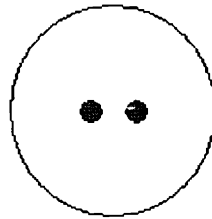
Fig 3.2: PA amplitude image of the sample shown in figure 3.1
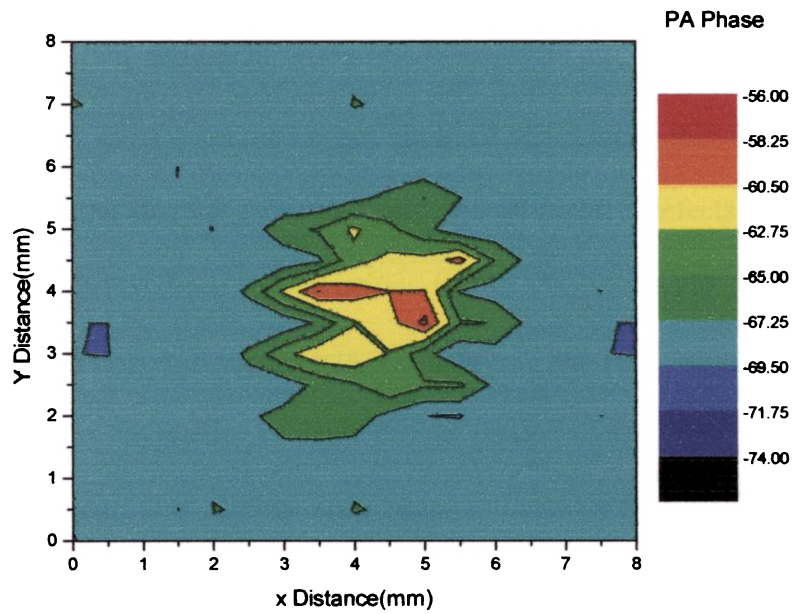
Fig 3.3: PA phase image of the sample shown in figure 3.1

### 3.3.2: Aluminium disc with surface defects

Aluminium Disc

Fig 3.4

Fig 3.4 shows an aluminium disc with 2 pits of diameter about 0.7 mm each drilled side by side along the same line. The disc is 2 mm thick and has a diameter of 1.7 cm. As in the case of the previous sample this disc is also given a fine and uniform coating of carbon black to reduce the optical reflection from the surface. We have selected an area of size 6 mm x 7.5 mm for scanning. The step size is 0.25 mm and the modulating frequency is 26 Hz. The time delay between consecutive steps is 3 seconds.

Figs 3.5 and 3.6 are the images obtained on scanning this sample. As in the previous case the images show the presence of surface defects on the sample. These are identified from the variations in the amplitude and phase of the PA signal from the region of the defects. The edges of the pits are not clearly defined as in the case of the previous sample but the images of the two pits show them as clearly separated. The patches seen around the region of the pits are due to spurious noise signals occurring due to the mechanical movement of the system. These are present in both the images but the phase image is much more vulnerable to such signals. Experimentally it is observed that it is much more difficult to get steady PA phase values from a position than PA amplitude values.
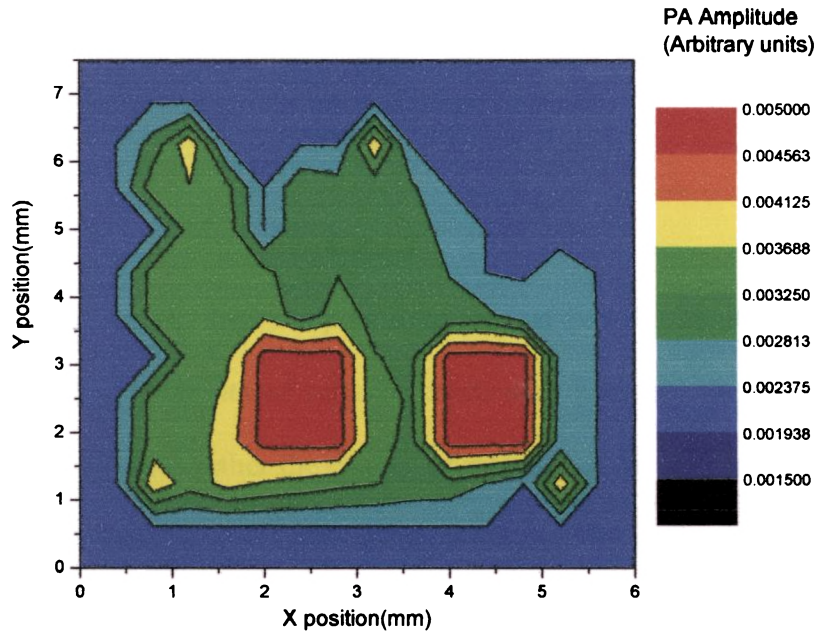
Fig 3.5: PA Amplitude image of the sample shown in figure 3.4
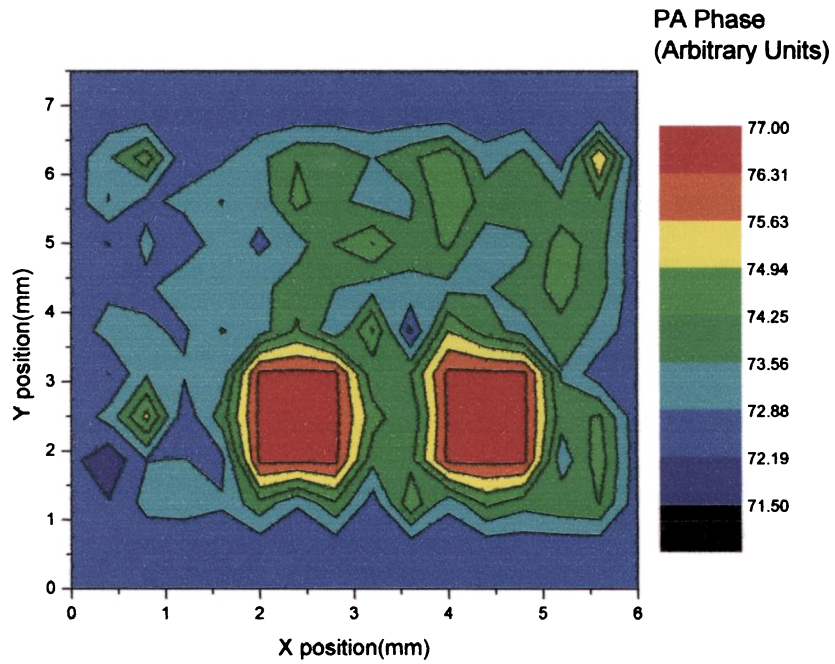
Fig 3.6: PA Phase image of the sample shown in figure 3.4

### 3.3.3: Brass disc inserted in a nylon disc

Fig 3.7

In the case of the two samples described above the capability of the technique to detect the presence of surface defects was discussed. In the next two examples we investigate whether the change of material in the region scanned get reflected in the PA images. A sample configuration used by us for this purpose is shown in Fig 3.7. We have a brass disc of radius 2 mm and thickness 2 mm inserted inside a nylon disc of radius 1.7 cm as shown in the figure. The top surfaces of the two discs are aligned at exactly the same horizontal level. Thus we have a thermal conductor surrounded by a thermal insulator.

The scanning is done on an area of size 8 mm x 7 mm on the sample. The step size selected is 0.25 mm and the time delay between two consecutive steps is 5 seconds. Here also we have given a very fine and uniform coating of carbon black on the sample for better absorption of the incident light. The frequency used for modulation is 20 Hz. The results of the scanning processes are shown in figures 3.8 and 3.9. The amplitude and phase values of the PA signal from the region of the two materials show marked difference. Had it been a uniform nylon disc we would have obtained a uniformly coloured image (assuming that there are no surface or subsurface flaws). These variations extend somewhat beyond the geometrical boundary separating the two materials.
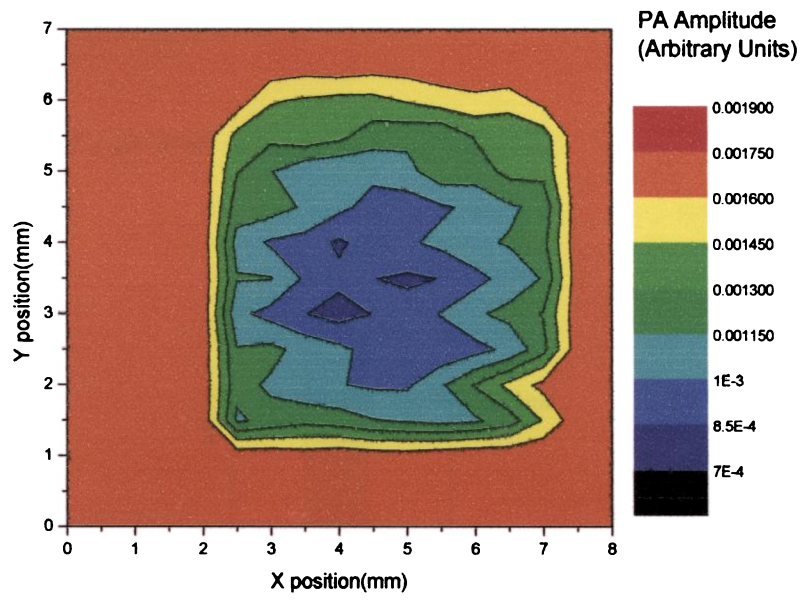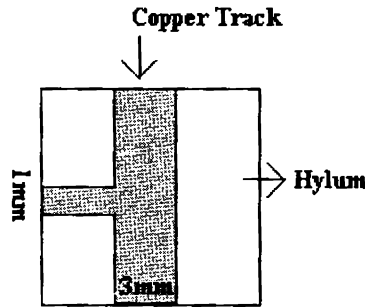
Fig 3.8: PA Amplitude image of the sample shown in Fig 3.7
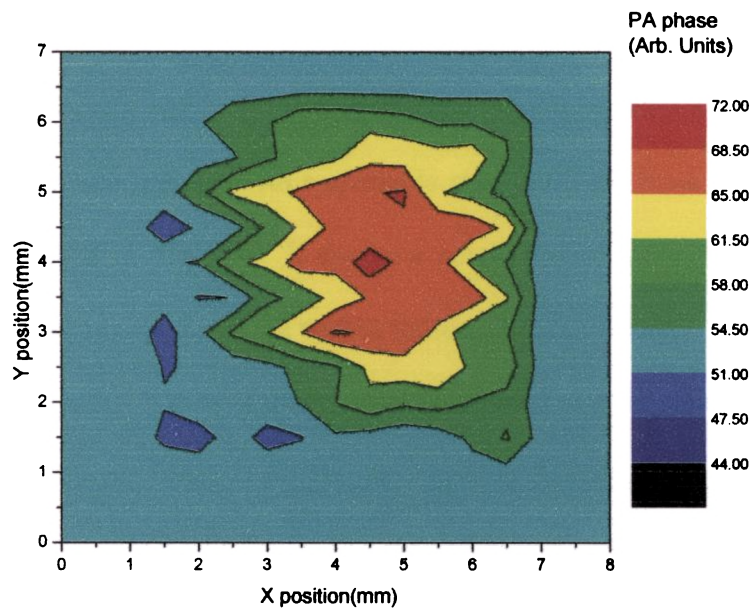
Fig 3.9: PA Phase image of the sample shown in Fig 3.7

Thus we can conclude that even though the resolution is limited, the instrument is capable of detecting the presence of different materials in different parts of the region scanned

3.3.4: A section of a printed circuit board (PCB)

Copper Track

1mm

Hylum

3 mm

Fig 3.10: A small section of a PCB

A printed circuit board has copper tracks separated by non conducting regions of hylum.The PA signal from these two regions should be different in the PA image of such a sample. This is of practical significance in the manufacture of PCBs, integrated circuit chips etc. In order to test whether our PAM is capable of differentiating the two regions with reasonable resolution we have used a sample configuration shown in Fig 3.10. It shows a small section of a PCB made of hylum with conducting tracks of the widths indicated in the figure.

An area 9 mm x 7 mm of this sample is scanned at a step size of 0.25 mm. The chopping frequency used is 62 Hz. A chopping frequency much lower than this can make the copper tracks thermally thin and we may not get these in the PA images. That is why we have used a chopping frequency higher than that in the previous cases. The time delay between consecutive steps of the scan is a few seconds.
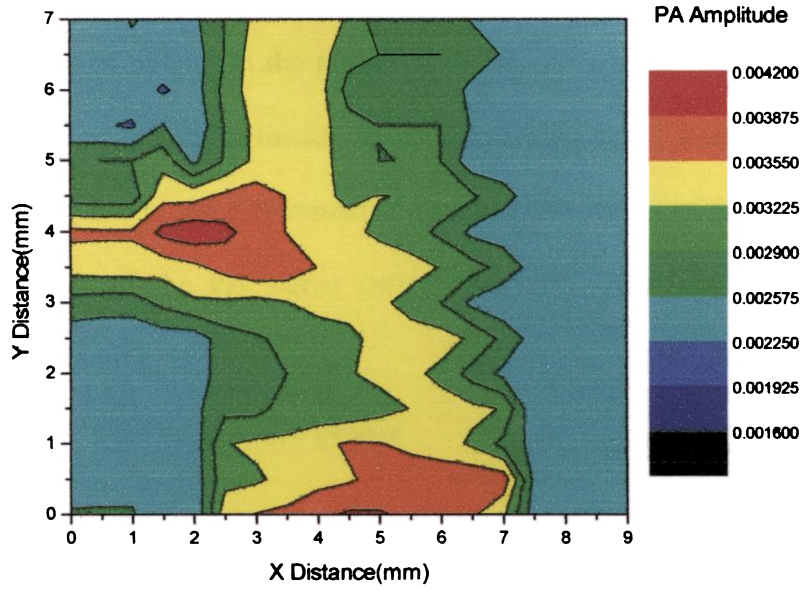
Fig 3.11: PA amplitude image of section of a PCB shown in Fig 3.10
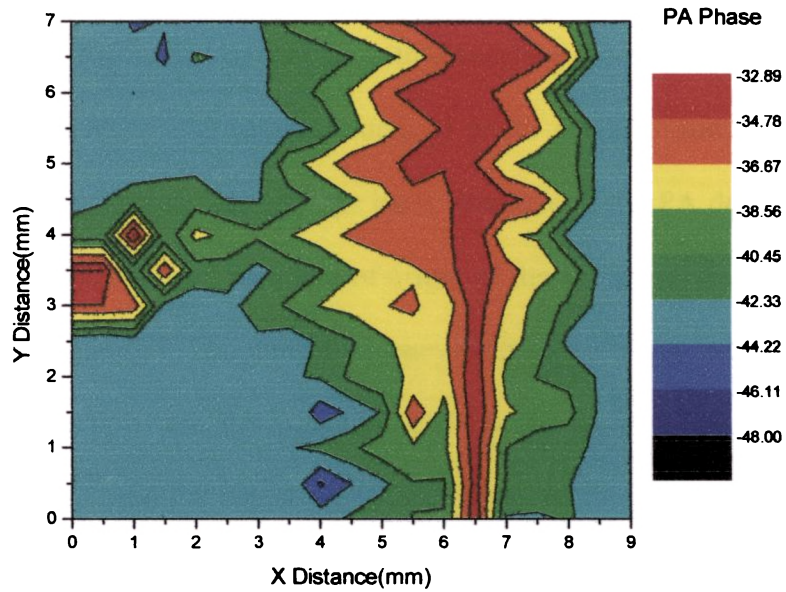
Fig 3.12: PA phase image of section of a PCB shown in Fig 3.10

Figures 3.11 and 3.12 are the PA amplitude and phase images of the PCB.
The images show demarcation between the conducting tracks and the non-
conducting regions of hylum. In the region of the copper tracks, the signal is not
uniform. This may be due to the thickness variation of the tracks from the edges to
the middle and /or due to the differences in optical absorption. As in all previous
cases, the variation of the PA signal extends slightly beyond the geometrical
boundaries of the region.

3.3.5: Copper disc with subsurface groove
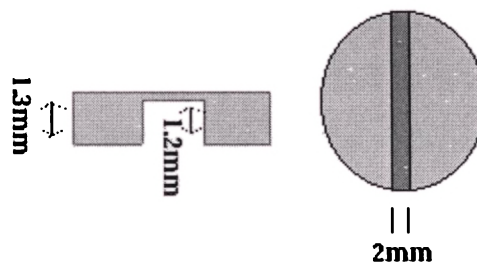
Fig 3.13: Copper disc with subsurface groove

One of the very interesting features of photo acoustic microscopy is its
ability to detect subsurface features. The basic principle of the PA depth profiling
technique is that the depth of the point of origin of the PA signal in a sample can
be varied by changing the chopping frequency of the irradiating light beam. The
amplitude and phase of the PA signal depend on the thermal properties of the
material from which the PA signal originates. Since the thermal diffusion length
decreases with increasing frequency, we can say that at lower frequencies the PA
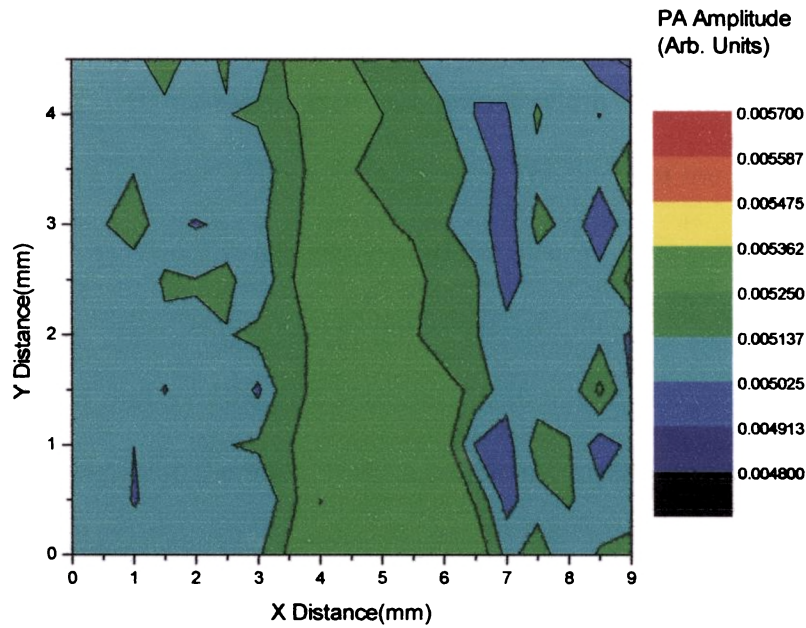amplitude and phase give information about the deeper layers of the sample.

Fig 3.14: PA Amplitude image of the subsurface defect shown in Fig 3.13
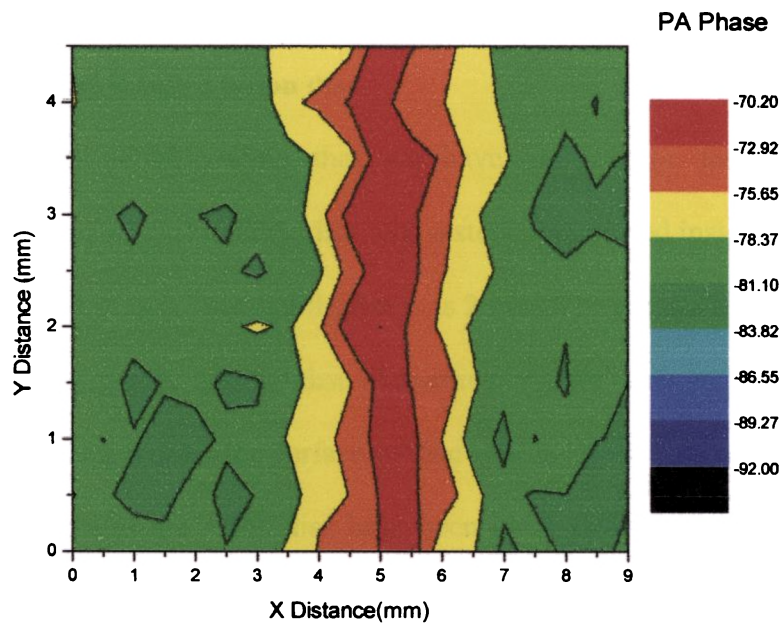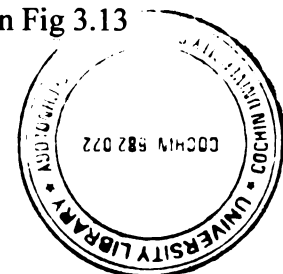

Fig 3.15: PA phase image of the subsurface defect shown in Fig 3.13

In order to study whether our instrument is capable of detecting the subsurface features of a sample we have selected a few sample configurations. Fig 3.13 depicts one of them. It is a copper disc with groove width 2 mm cut along a diameter as shown. The thickness of the disc is 1.3 mm. The depth of the groove is 1.2 mm. So when viewed from the opposite face of the disc we have a subsurface groove at a depth of 0.1 mm. The diameter of the disc is 1.7 cm.

An area 9 mm x 5 mm of the disc is scanned with a light beam modulated at 15 Hz. At this frequency, the thermal diffusion length of copper is more than 0.1 mm. The time delay between two consecutive steps is 5 seconds.

Figures 3.14 and 3.15 are the PA amplitude and phase images of the sample. The images show the presence of the subsurface groove. It is found that this is not detectable at higher frequencies where the thermal diffusion length is smaller than the depth at which the groove is situated.

3.3.6: Steel pin inserted inside a teflon disc.

Another sample configuration that we have studied for testing the subsurface imaging capability is a teflon disc with a steel pin inserted inside it. The diameter of the teflon disc is 1.7 cm and thickness is 2 mm. The pin has a diameter of 0.3 mm. The pin is inserted into the disc diametrically slant to its surface. The position of the pin is deeper from the surface of disc as it is inserted more into the disc. The opposite faces of the teflon disc have been made perfectly smooth and flat. Fig 3.16 shows the sample configuration.

The sample has been subjected to PA scanning by intensity modulated beam of the He-Ne laser modulated at 10 Hz. The laser beam scanned an area of the teflon disc of size 8 mm x 6 mm with a step size of 0.25 mm. The time delay

100

between successive steps was 5 seconds. To increase optical absorption the Teflon

sample is given a very thin uniform coating of carbon black
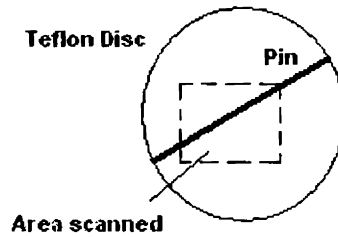
Fig 3.16

.A typical graph of PA amplitude obtained in one of the many trials is

shown in Fig 3.17. The image shows change of amplitude at the region of the pin.

The pin is not 'visible' up to its full length as because it is inserted in the Teflon

disc in such a way that as we move from left to right the depth of the pin from the

top surface of the disc increases. So the image of the pin is not visible when this

depth becomes more than the thermal diffusion length at the modulating frequency

used. When the experiment is repeated at higher frequencies, the image of the pin

is visible to an even lesser extent as is expected on the basis of RG theory [11].

The phase image shown in Fig 3.18 also indicates the presence of the pin to a

larger extent. It is found that both these images are affected by noise signals

significantly.

101
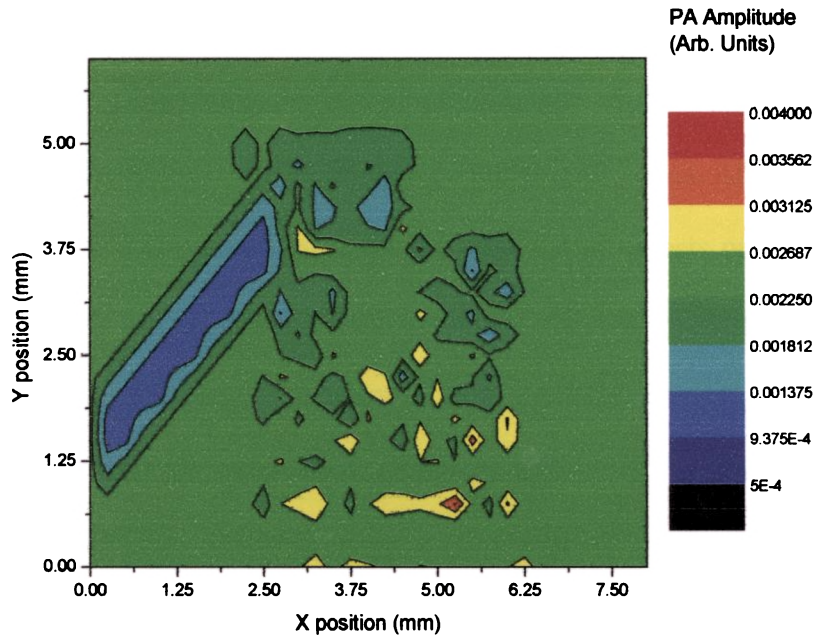
Fig 3.17: PA Amplitude image of the sample shown in Fig 3.16
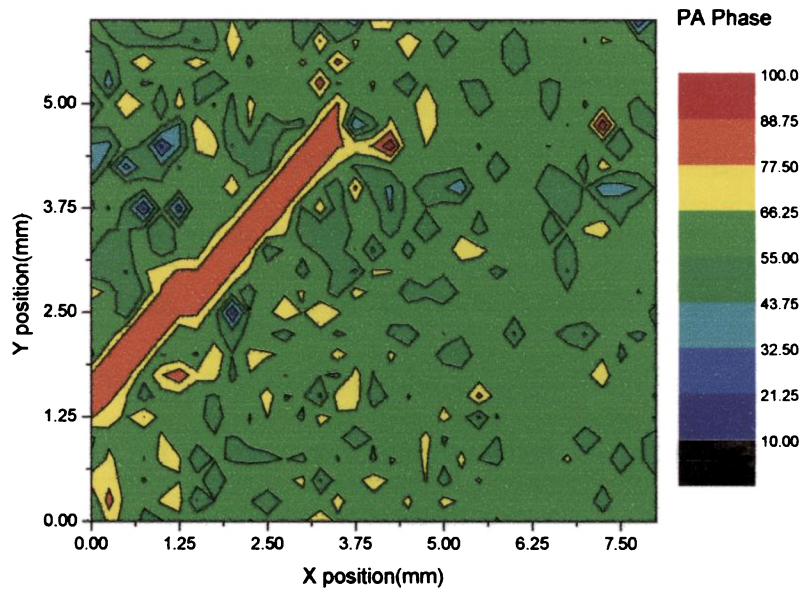
Fig 3.18: PA Phase image of the sample shown in Fig 3.16

3.4: Discussion of the results – performance of the photoacoustic microscope

The experimental results presented in this chapter confirm the capability of PA technique for surface as well as subsurface imaging of solids. As described in literature, the PAM can be used to detect the presence of defects on the surface, change of material, presence of subsurface defects etc. Our experiments clearly demonstrate this. The most important factor that determines whether the instrument can be used for practical industrial applications is the resolution of the images. Spatial resolution available using a PAM depends on many factors. The spot size of the modulated beam of light used for scanning the sample is one of them. It is clear that the spot size should be small to get better resolution. For this, the diameter of the core of the optical fiber should be small. The light coming out of the optical fiber has a Gaussian intensity profile with maximum intensity at the middle and decreasing radially outwards. This may be one of the reasons for the boundaries of the defects to be seen as 'blurred' in the images obtained by us. Another factor which affects spatial resolution is the spacing between two consecutive positions at which the beam comes to rest for illuminating the sample or step size of the scan. Larger is the step size, smaller will be the resolution. However, reduction of the step size to a value very much smaller than the diameter of the fiber tip does not increase the resolution. Further reduction in the step size of the movements of the stepper motor (microstepping) requires more complicated software and hardware. The coupling between the stepper motor and the translation stages also needs to be very carefully designed in that case because then

only the very small movements of the stepper motors will be transferred to the movement of the translation stages and hence that of the fiber tip.

Another very important factor which puts a limit on the available spatial resolution is the thermal wavelength. This in turn depends on the modulating frequency and the thermal properties of the sample being studied [8]. Smaller the modulation frequency larger is the thermal diffusion length and this in turn affects the resolution. One has to strike a compromise on this to get the optimum resolution.

Yet another problem encountered in our experimental setup is the noise signals arising from the mechanical movement of the scanning system. Although the amount of noise signals is much lower than that in the case of a PAM in which the PA cell is moved rather than the beam of light, they are still significant [12]. This is the reason for some of the image patches in the PA images obtained in our experiments. Isolating the mechanical scanning unit from the PA cell, to a large extent, will provide better images.

We have given a time delay of a few seconds between consecutive steps to ensure that the signal settles down to a steady value before the amplitude and phase values from a particular point on the sample are measured. However, this time delay increases the overall time required for obtaining the PA images. This is also true when we use smaller step size to increase the resolution. Generally, it takes 2 to 3 hours to get the images of the type we have obtained. Coufal et al have shown that PA imaging could also be performed by a spatial multiplexed technique eg via Hadamard transformations or Fourier transformations [13,14]. This method reduces the time required for data acquisition. Besides, it reduces the

104

power density at the sample, thus lowering the risk of sample damage and improves the signal to noise ratio.

In conclusion, we can say that the microscope developed by us is capable of providing the surface and subsurface images of a sample with reasonably good resolution. Eventhough some theoretical limitations exist for such an instrument we can obtain much better images by incorporating the points discussed above in future designs. The technique is particularly useful to image subsurface defects and flaws. The limitation is that the depth of the defect/flaw should be limited to the thermal diffusion length. The technique is definitely useful for specialized nondestructive testing applications.

References

1. Y.H.Wong, R.L.Thomas and G.F.Hawkins, *Appl.Phys.Lett.*(1978) **32(9)**, 538

2. Y.H.Wong, R.L.Thomas and J.J.Pouch, *Appl.Phys.Lett.* (1979) **35(5)**, 368

3. A.Rosencwaig and G.Busse, *Appl.Phys.Lett.* (1980) **36(9)**, 725

4. G.Busse and A.Rosencwaig, *Appl.Phys.Lett.* (1980) **36(10)**, 815

5. G.Busse and A.Ograbeck, *J.Appl.Phys.* (1980) **51(7)**, 3577

6. L.D.Favro, P.K.Kuo, J.J.Pouch and R.L.Thomas, *Appl.Phys.Lett.* (1980) **36**, 953

7. A.C.Gracias,C.Kuranga, J.R.Senna and M.D.Silva, *Rev.Sci. Instrum.* (2000)
   71(4), 1869

8. L.J.Inglehart, K.R.Grice, L.D.Favro, P.K.Kuo and R.L.Thomas, *Appl.Phys.Lett.*
   (1983) **43(5)**, 446

9. K.R.Grice, L.J.Inglehart, L.D.Favro, P.K.Kuo and R.L.Thomas, *J.Appl.Phys.*
   (1983) **54(11)**, 6245

10. P.K.Kuo, L.D.Favro, L.J.Inglehart, R.l.Thomas and .Srinivasan, *J.Appl.Phys.*
    (1982) **53(2)**, 1258

11. A.Rosencwaig, *Photoacoustics and Photoacoustic spectroscopy* Wiley,
    New York (1980)

12. A.A.Sudhakaran, *Ph.D Thesis,* Cochin University of Science and Technology,
    (1996)

13. H.Coufal, U.Moller and S.Schneider, *Appl.Opt.* (!982a) **21** , 116

14. H.Coufal, U.Moller and S.Schneider, *Appl.Opt.* (!982b) **21** , 2339

CHAPTER 4

Thermal properties of commercial paint coatings using scanning photoacoustic technique

---

4.1: Introduction

Thermo physical characterization of thin as well as thick coatings is of immense significance for different industrial applications. Thermal barrier coatings are increasingly being used to protect the base metal against chemical contamination at high operating temperatures in various systems such as gas turbines and diesel engine components. Non-destructive evaluation of their thermal properties is important to understand their effectiveness in providing the required protection. There are a number of nondestructive methods, which are based mainly on modulated laser beam or pulse heating techniques [1-8]. Modulated heating techniques are potentially appropriate for the characterization of coatings such as enamel paints.

For thin samples and coatings on a backing, the laser flash technique proposed by Parker et al is commonly used for diffusivity measurements [9]. The thermal transient response of a sample following a heating pulse, usually provided by a pulsed laser, can be used for diffusivity measurement. For an opaque sample, a surface heating pulse results in a rear face thermal transient which varies as

$$T(L,t) = T_0 \left[1 + 2\sum_{n=1}^{\infty} (-1)^n \exp\left(\frac{-n^2 \pi^2 \alpha t}{L^2} \right) \right] \qquad (4.1)$$

where T_0 is the maximum sample temperature rise and L is its thickness. Thermal diffusivity can be obtained from measurements of this rear face transient. This method has become an international standard for thermal diffusivity measurement techniques. Several algorithms have been presented in the literature for the evaluation of thermal diffusivity. The most commonly used method is to utilize $t_{1/2}$, the time at which the transient reaches half its peak value. The diffusivity is obtained from the expression:

$$\alpha = \frac{0.139L^2}{t_{1/2}} \qquad (4.2)$$

Ruby lasers or Nd doped glass lasers, which provide sufficient pulse energy to produce a temperature rise of over a degree in most materials, are used for the experiments. The sample is usually a disc with a thickness dependent on the diffusivity of the material concerned. A semiconductor infrared detector, e.g. InSb, is used to record the thermal transient at the unheated face of the sample.

The laser flash technique has been applied to a very wide range of materials with diffusivities ranging from 10^{-7} to 10^{-3} m^2s^{-1} at temperatures from 100 to 3300K. The accuracy of the method depends critically on the preparation of a homogeneous parallel sided sample with polished flat faces and on the measurement of the sample thickness. If the sample is a coating on a substrate, the thermal diffusivity of the coating material can still be obtained, but now both the heating and detection must take place at the sample surface. For an opaque coating heated by a plane pulsed heat source, the surface temperature decays as

$$T(0,t) = T_0 \left[1 + 2\sum_{n=1}^{\infty} R^n \exp(\frac{-n^2L^2}{\alpha t}) \right] \qquad (4.3)$$

where R is the coating-substrate thermal wave reflection coefficient. A data fitting procedure can be applied to determine the thermal diffusivity of the sample assuming that the coating thickness is known.

Imhof et al [10] introduced a single-access approach in their retro-geometry arrangement that was also used in the measurement of the thermal diffusivity of thermally conducting films on insulating substrates [11]. Moksin et al have measured the thermal diffusivity of black paint coatings using this single-access pulsed laser technique [12]. Moksin and Almond have also measured the thermal diffusivity of paint coatings using a thermal wave interference approach employing infrared detection [13]. Coelho et al have recently determined the thermal properties of thin acrylic paints using thermal wave interferometry [14]

In this chapter we describe a scanning photoacoustic (PA) method based on thermal wave interference theory applicable tp opaque thin coatings such as paints spread on a suitable backing. The method can determine the thermal transport properties - diffusivity, effusivity, conductivity and specific heat capacity - of paints coated on a backing, whose thermal properties are known. The thermal diffusivity and effusivity of four different black paint coatings on a copper backing are determined and reported in this work. From these, the thermal conductivity and heat capacity are also determined and presented in this chapter.

When it comes to thermal transport in thin/thick films such as paint coatings, one has to realize that we are dealing with two - dimensional heat flow and the thermal properties of the backing material can significantly influence the thermal properties of the film. Nobody seems to have seriously investigated the influence of the thermal properties of the backing on the thermal transport in

thin/thick coatings. In this work we have also measured the thermal properties of the same paint coating on five different backings, three of which are good thermal conductors and the other two are poor conductors. The theoretical background, experimental details and the results are presented and discussed in details in the following sections.

4.2: Theoretical background

The well established theory of photoacoustic effect in solids by Rosencwaig and Gersho gives exact expressions for the photoacoustic amplitude and phase [15]. However, this theory does not explain why the particular solution is chosen for the wave equation or how it can be modified for other situations. Subsequent to Rosencwaig's work, Bennett and patty published an alternative approach based on the concept of thermal waves [16]. It is seen that this more recent approach leads to the equations of Rosencwaig and Gersho more quickly. Bennett and Patty's use of the modulus and phase of their expression as well as the concept of ratioing the measurements on coated and uncoated substrates (backings) are helpful in practice in determining coating thickness and thermal properties of coatings.

In their development of an expression for the thermal wave amplitude of the photoacostic signal obtained from a gas cell configuration, Bennett and Patty used the same assumptions as Rosencwaig and Gersho viz the backing material (henceforth called the substrate) and the gas above the sample are thermally thick (the sample is henceforth referred to as coating), no light is absorbed in the gas or the substrate and hence no thermal waves are generated in them and transmitted into the coating. However, the thermal waves within the coating itself will

repeatedly reflect between the coating-gas boundary and the coating-backing boundary. The reflection and transmission coefficients at the boundaries are given respectively by the following general expressions

$$R_{12} = \frac{1 - \xi_{12}}{1 + \xi_{12}} \qquad (4.4)$$

$$T_{12} = \frac{2}{1 + \xi_{12}} \qquad (4.5)$$

where $\xi_{12} = \dfrac{e_2}{e_1}$ is the ratio of thermal effusivities of region 2 and region 1. Now, for the sample, backing and gas, let us use the subscripts s, b and g respectively instead of numbers 1 and 2. Then the amplitude of the thermal waves generated by the light absorbed between x and $x + dx$ is given by

$$K = \frac{\beta I_0 \exp(\beta x)dx}{4k_s \sigma_s} \qquad (4.6)$$

where β is the optical absorption coefficient, I_0 is the maximum intensity of the incident light beam, wave k_s is the thermal conductivity of the sample, and σ_s = $(1+i)a_s$ where a_s is the thermal diffusion coefficient in the sample.
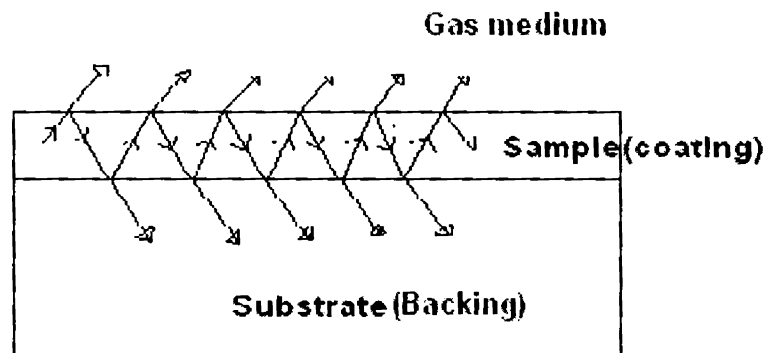
Fig 4.1(a): Multiple reflections and transmissions of the thermal wave initially traveling towards the gas

111
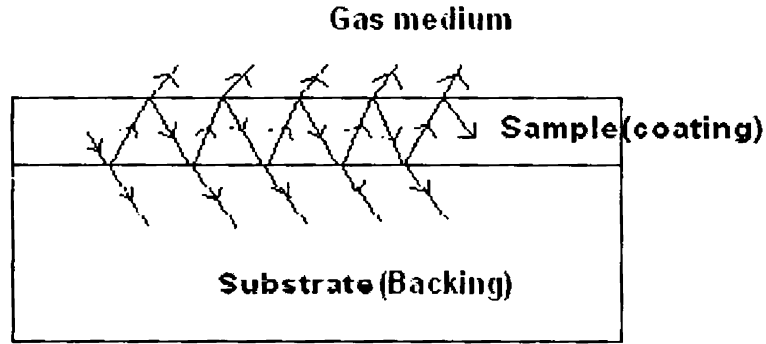
Fig 4.1(b): Multiple reflections and transmissions of the thermal wave initially traveling towards the substrate.

Fig 4.1(a) schematically depicts the path taken by the thermal wave generated at a depth x in the sample (coating) that initially travels towards the gas. When it reaches the gas region its amplitude and phase would have changed by $\exp(\sigma_s x)$. (We choose the coordinate system taken by Rosencwaig in his theory in which the sample gas boundary is at $x = 0$, and in the sample region $-l_s \leq x \leq 0$). The wave transmitted to the gas medium is the incident amplitude multiplied by the transmission coefficient

$$K \exp(\sigma_s x) \, T_{sg} = \frac{\beta I_0 \exp(\beta x) T_{sg}}{4k_s \sigma_s} \exp(\sigma_s x) dx \qquad (4.7)$$

The part of the thermal wave that is not transmitted into the gets reflected at the sample-gas boundary and travels to the sample-backing boundary where a part of the energy is lost by transmission into the backing and the rest is again reflected and travels back to the sample-gas boundary, where part of the wave is transmitted into the gas. The amplitude of the wave transmitted this second time is the product of the original amplitude, the thermal wave reflection coefficient at the sample-gas boundary, the reflection coefficient at the sample-backing boundary and the

corresponding attenuation coefficients in the sample. As the thermal wave continues to reflect back and forth between the two boundaries as described above, a fraction of it is transmitted each time it arrives at the sample-gas boundary. These transmissions are summed to get the temperature at the sample-gas boundary It can be shown that they form an infinite geometric series whose sum is given by

$$\frac{\beta I_0 \exp(\beta x) T_{sg} \exp(\sigma_s x)}{4k_s \sigma_s}\left[\frac{1}{1 - R_{sb} R_{sg} \exp(-2a_s l_s)}\right]dx \qquad (4.8)$$

Similarly, the thermal wave that originally travels towards the backing material will contribute a series of transmitted terms at $x = 0$ (Fig 4.1(b)). The sum of these terms is given by

$$\frac{\beta I_0 \exp(\beta x) T_{sg}}{4k_s \sigma_s} R_{sb} \exp(-\sigma_s(2l_s + x))\left[\frac{1}{1 - R_{sb} R_{sg} \exp(-2\sigma_s l_s)}\right]dx \qquad (4.9)$$

Adding the two contributions, we get

$$\frac{\beta I_0 \exp(\beta x) T_{sg}}{4k_s \sigma_s (1 - R_{sb} R_{sg} \exp(-2\sigma_s l_s))}\left[\exp(\sigma_s x) + R_{sb} \exp(-\sigma_s(2l_s + x))\right]dx \qquad (4.10)$$

The above expression is the result from one thin slice extending from x to $x + dx$. The signal measured is the sum of the thermal waves from all such slices. In order to get the total contribution we integrate the above expression from $x = -l_s$ to $x = 0$. Then we get

$$U_0 = \frac{\beta I_0 T_{sg}}{4k_s \sigma_s}\left[\frac{\left(\frac{1}{\beta + \sigma_s}\right)\left(1 - e^{-(\beta + \sigma_s)l_s}\right) + R_{sb} e^{-2\sigma_s l_s}\left(\frac{1}{\beta - \sigma_s}\right)\left(1 - e^{-(\beta - \sigma_s)l_s}\right)}{1 - R_{sb} R_{sg} e^{-\sigma_s l_s}}\right] \qquad (4.11)$$

113

If we make the substitutions

$$R_{sb} = \frac{1-b}{1+b}$$ (4.12)

$$R_{sg} = \frac{1-g}{1+g}$$ (4.13)

$$T_{sb} = \frac{2}{1+b}$$ (4.14)

$$T_{sg} = \frac{2}{1+g}$$ (4.15)

and $$\frac{\beta}{\sigma_s} = r$$ (4.16)

the above expression will be exactly the same as the one obtained by Rosencwaig

and Gersho following an entirely different approach.

4.2.1: Application of the theory to opaque coatings

The analysis of the PA signal generated from thin / thick opaque coatings

such as paints on a thermally thick backing is understood better with the thermal

wave interference approach proposed by Bennett and Patty. It has some

advantages over the thermal piston model of Rosencwaig and Gersho. As in the

latter model, Bennet and Patty assume that the sample, which is a coating on a

substrate, is contained in a gas-filled cell, which is illuminated uniformly by an

intensity-modulated beam of light. The energy absorbed at a given depth will

initiate a thermal wave that travels through the sample and repeatedly get reflected

between the sample-backing and sample-gas boundaries. At each boundary a

fraction of the thermal wave will be transmitted into the other medium. This wave

delivers a part of its energy into the gas every time part of it is transmitted at the

sample-gas boundary. The sum of these transmissions from the waves generated at

114

all the depths at which the incident light is absorbed makes up the periodic thermal flux into the gas, which generates the acoustic signal. Unlike the Rosencwaig and Gersho theory, this approach gives explicit expressions for the modulus as well as phase of the normalized PA signal.

In a photoacoustic gas cell, the photoacoustic signal depends on cell resonances, frequency response of the microphone, phase shifts and gain variations of the amplifiers as well as the pressure variations within the cell caused by thermal waves transmitted into the gas medium. The response of the measurement set up is normalized selecting an appropriate reference sample, and comparing the signal generated from that with the experimental sample. A thermally thick coating of the same material can provide such a reference. The thermally thick coating is assumed to be optically opaque enough so that all of the light is absorbed inside the sample. If U_0 and U_r represent respectively the signal from the sample and that from the reference at a given modulation frequency ω, then their ratio as a function of ω is given by

$$R(\omega) = \frac{U_0}{U_r} \qquad (4.17)$$

In this expression, the quotient depends only on the thermal and absorptive properties of the coating under investigation; specifically it does not depend on the particular gas cell or the equipment used for the measurement. The expression for $R(\omega)$ is obtained from equation (4.11) as [13]

$$R(\omega) = \frac{\left(1 - e^{-\beta l_s} e^{-\sigma_s l_s}\right) + R_{sb} e^{-2\sigma_s l_s} \left(\frac{\beta + \sigma_s}{\beta - \sigma_s}\right)\left(1 - e^{-\beta l_s} e^{\sigma_s l_s}\right)}{1 - R_{sb} R_{sg} e^{-2\sigma_s l_s}} \qquad (4.18)$$

Here, β = optical absorption coefficient of the sample,

115

$\sigma_s = (1+ i\ )\ a_s$, where a_s is the thermal diffusion coefficient of the sample at the modulating frequency used,

l_s = thickness of sample (coating),

R_{sb} = reflection coefficient of the thermal wave in the sample at the sample-backing boundary, and

R_{sg} = reflection coefficient of the thermal wave in the sample at the sample-gas boundary

In many situations, such as in our case, the coating is quite opaque so that the optical absorption length is much shorter than the thermal diffusion length for the modulation frequencies used. Therefore, $\beta >> a_s$; then exp $(-\beta\ l_s) \cong 0$ and the above equation (equation (4.18)) reduces to

$$R_o(\omega) = \frac{1 + R_{sb}e^{-2\sigma_s l_s}}{1 - R_{sb}R_{sg}e^{-2\sigma_s l_s}} \qquad (4.19)$$

The subscript o refers to the opaque coating. The modulus and phase of the signal can be separated as

$$|R_o(\omega)| = \sqrt{\frac{\left(1 + R_{sb}e^{-2a_s l_s}\right)^2 - 4R_{sb}e^{-2a_s l_s}\sin^2 a_s l_s}{(1 - R_{sb}R_{sg}e^{-2a_s l_s})^2 + 4R_{sb}R_{sg}e^{-2a_s l_s}\sin^2 a_s l_s}} \qquad (4.20)$$

$$\Delta\phi = \arctan\left(\frac{-R_{sb}(1 + R_{sg})e^{-2a_s l_s}\sin(2a_s l_s)}{1 - R_{sg}(R_{sb}e^{-2a_s l_s})^2 + R_{sb}(1 - R_{sg})e^{-2a_s l_s}\cos 2a_s l_s}\right) \qquad (4.21)$$

4.2.2: Analysis of magnitude ratio and phase difference equations
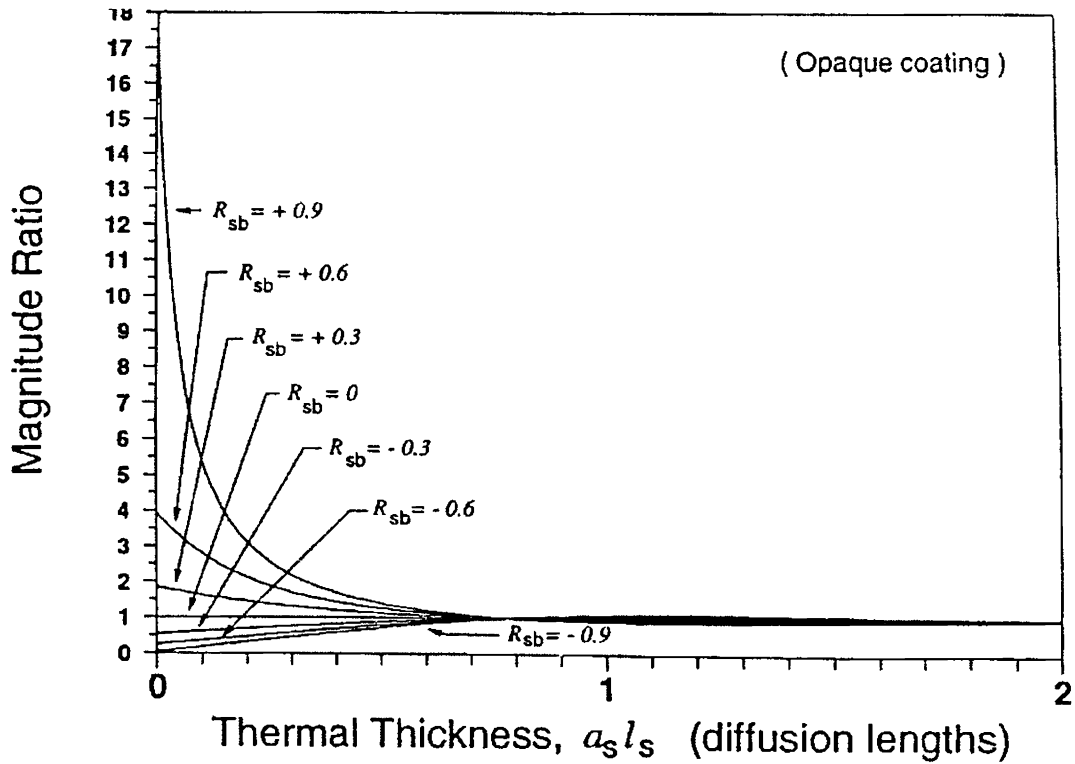
Fig 4.2: Variation of magnitude ratio with thermal thickness

Fig 4.2 shows the variation of $R_0(\omega)$ as a function of thermal thickness $a_s l_s$ or l_s/μ_s (where a_s is the thermal diffusion coefficient) of the coating. From the figure it is clear that as l_s/μ_s becomes large i.e., the coating becomes thermally thick as $|R_0(\omega)|$ becomes 1. This result is self evident as the ratio of signal from a thermally thick coating to that from a thermally thick backing of the same material should be unity.

When $l_s/\mu_s \to 0$ i.e. for thermally thin coatings assuming that $R_{sg} \geq 0.99$, we will get

$$|R_0(\omega)|_{\frac{l_s}{\mu_s} \to 0} = \frac{1}{b} = \frac{e_s}{e_b} \qquad (4.22)$$

For backings with the same thermal properties as the coating, $R_{sb} = 0$, and the curve is simply a straight line with $|R_o(\omega)| = 1$. Since there is no thermal difference between the coating and the backing, the whole coating-backing assembly acts as a single thick coating and hence the ratio should be 1. All of Rosencwaig and Gersho's special cases are in this category as the backing is assumed to have thermal properties similar to the sample.

For backings that have a higher effusivity than the coating, $b>1$, and at $l_s/\mu_s = 0$, $|R_o(\omega)| < 1$. The signal is lower on a conducting specimen as the temperature swings are not as great as in the previous case.

Similarly, for backings that are more insulating than the coating or sample, $b<1$ and $|R_o(\omega)| > 1$ as l_s/μ_s tends to zero. This is very reasonable since the insulating backing dominates in this case and the heat cannot escape as easily so that the temperature swings and hence the signal are greater for the same irradiation intensity.

Fig 4.2 also shows that although oscillations continue indefinitely, $|R_o(\omega)|$ drops rapidly towards 1 as l_s/μ_s increases.

Fig 4.3 shows the variation of phase difference with thermal thickness (l_s/μ_s) for different values of R_{sb} reflection coefficients of the thermal wave traveling from the sample to the backing (for $R_{sg} \approx 0.99$). The phase difference oscillations do not die out as quickly as the amplitude ratio oscillations. Thus, the phase is better suited for experimental use than the corresponding magnitude ratio. This is consistent with the experimental observation that one can see about twice as deeply using the phase as using the magnitude in photoacoustic imaging [17]. The phase difference becomes zero as the coating becomes very thick compared to

the thermal diffusion length. It becomes zero for very thin coatings also. The extrema of phase difference curves depend more strongly on R_{sb} than in the case of magnitude ratio.
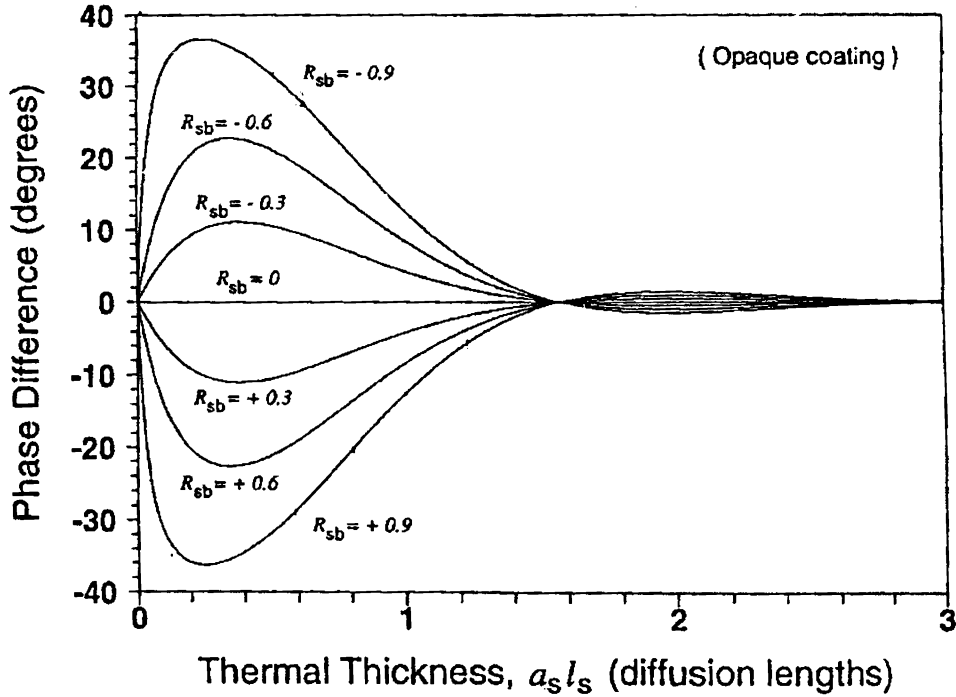
Fig 4.3: Variation of phase difference with thermal thickness

4.2.3: Determination of thermal properties of coatings

We have used the phase difference in our experimental method. In equation (4.21) we assume $R_{sg} \approx 0.99$ which is a good approximation for all the cases studied by us. If the thickness of the coating is known, the thermal diffusivity can be obtained from the fitted values obtained for a_s from $a_s l_s$, because

$$a_s = \sqrt{\frac{\omega}{2\alpha_s}} \qquad (4.23)$$

where α_s is the thermal diffusivity of the coating. We can also obtain R_{sb} from curve fitting. It is related to thermal effusivity as

119

$$R_{sb} = \frac{1 - \dfrac{e_s}{e_b}}{1 + \dfrac{e_s}{e_b}} \qquad (4.24)$$

where e_s and e_b are the thermal effusivities of the sample and backing respectively. If the effusivity of the backing is known, the effusivity of the coating can be obtained as

$$e_s = \left(\frac{1 - R_{sb}}{1 + R_{sb}}\right) e_b \qquad (4.25)$$

Knowing the thermal diffusivity and effusivity, we can calculate the thermal conductivity and heat capacity of the coating, following the relations

$$k_s = e_s \sqrt{\alpha_s} \qquad (4.26)$$

$$c_s = \frac{e_s}{\rho \sqrt{\alpha_s}} \qquad (4.27)$$

where ρ is the density of the coating.

4.3: Experimental Details

4.3.1: Sample preparation

The coatings are prepared by applying commercially available spray paint (Matt black) on cleaned copper substrates of thickness 1.5 mm. The paint is coated in a step like manner. Six steps of width 2.5 mm each have been coated one by one carefully. The height of the steps (thickness of the paint coating) varied from 15μm to 70μm in our experiments. The paint is coated at one stretch with no drying time in between, which reduces the chances for development of multilayer structures. After drying, the average thickness of each of the regions is measured

with a micrometer (Mitutoyo 193-111), with 1μm resolution. The mass densities of the paint coatings are determined by measuring the mass and volume of the coatings of definite thickness. For this a glass plate of known thickness and mass is coated with the paint sample on one side. The coating is done very carefully to make it as uniform as possible. The length, breadth and thickness of the coating are measured using a micrometer. Hence, volume of the coating is determined. Mass of the coating is determined from the difference in masses of the coated and uncoated glass plates measured using an electronic balance.

4.3.2: PA scanning setup

We have used the photoacoustic set up with provision for scanning the sample with the incident beam of light. It has already been described in detail in chapter 2. The light source used is a 20mW He-Ne laser. The laser beam is intensity modulated with a mechanical chopper and focused further with a lens. The modulation frequencies used in our experiments are 10-20Hz, which ensures that the physical thickness of the coating is much smaller than the thermal thickness of the coating. The focused beam is launched into a multimode optical fiber. The output light from the fiber is made to fall on the sample kept inside the photoacoustic (PA) cell. The spot size of the laser beam falling on the sample is small (less than a mm in diameter). We have used the dual channel PA cell described in chapter 2 for high signal to noise ratio [18]. The electrical signals from the two microphones (Knowles Model BT 1759) mounted inside the cell are added and the resultant signal is fed in to a lock-in amplifier (Stanford Research Systems Model SR 830) for measurement. The tip of the optical fiber from which light emerges and falls on the sample surface is fixed to X-Y translation stages.

Stepper motors under computer control drive the translation stage in such a way that the laser beam can scan the sample surface in a step-by-step manner. In the present case, the scanning is done along a line so that the paint coatings of varying thickness are covered by the scanning light beam. The phase of the PA signal from the paint coatings of varying thickness are measured with the lock-in amplifier interfaced to a PC. The phase data are stored in to the PC as the scanning progresses. The scanning is done many times along different parallel lines in forward as well as reverse directions. The phase value corresponding to a particular coating thickness is an average of several readings obtained from the same region during the scan. The phase values are normalized with respect to the readings obtained from a very thick coating of the same paint that is prepared side by side with the coatings of varying thickness. The whole set up is automated using software developed in Visual Basic.

4.4 : Results and Discussion

Figures 4.4, 4.5, 4.6 and 4.7 show the variation of the normalized photoacoustic phase with the thickness of the paint samples of four different brands of locally available commercial Matt Black paint. A nonlinear least squares curve fitting is performed with the theoretical expression for normalized phase (equation 4.21) on this data. We have assumed $R_{sg} = 0.99$ which is a realistic approximation in this case. The values of thermal diffusivity and effusivity obtained, along with the parameter χ^2 used for curve fitting, are tabulated in Table 4.1. The lower the value of χ^2, the better is the fitting of the experimental data with the theoretical value. The diffusivity value of Sample III is higher than those of the

122

other three samples. This sample (sample III) is a metallic paint. Generally metallic paints diffuse and radiate heat more efficiently than non-metallic paints. This is getting reflected in its thermal diffusivity value. The thermal diffusivity values obtained for these samples lie in the same range of some similar paints studied by a few other groups using different techniques [12-14]. A similar comparison of the values of thermal effusivity could not be done, as such values could not be found in literature. The corresponding thermal conductivity and heat capacity values are also given in the same table. Again, a comparison of the obtained values of thermal conductivity and heat capacity with reported values could not be done, because such values for paint samples are not available in literature.

In order to compare the values of possible thermal parameters of the paints on which the measurements have been done, we have measured the thermal diffusivity of these paint samples by the well-established photo acoustic technique [19]. The values obtained are also reported in Table 4.1. It can be noted that the thermal diffusivity values obtained by the scanning technique (column 5, Table4.1) agrees very well with the values obtained by the conventional photo acoustic technique (column 6, Table 4.1).

The indicated uncertainties in the values of the various parameters shown in Table 4.1 take in to account the possible errors in the values of the various assumed and measured parameters used to determine them.
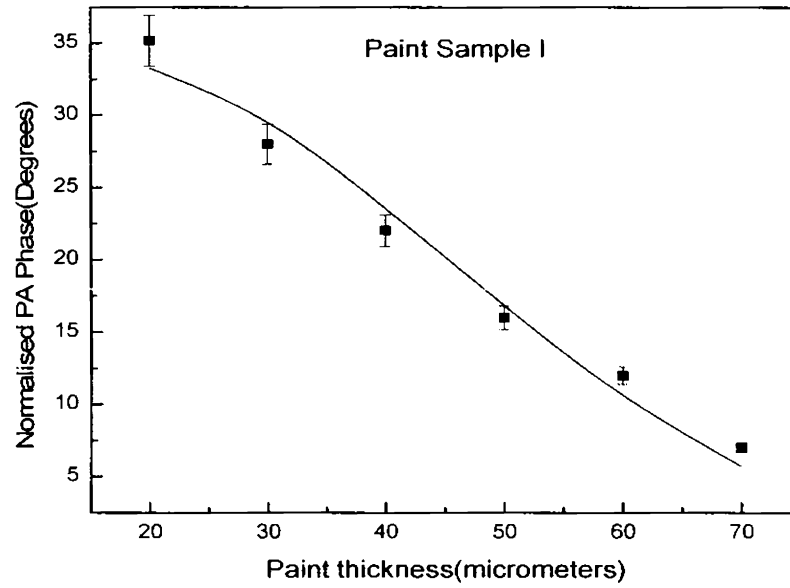
Fig 4.4: Variation of the normalized PA phase with thickness of the paint coating (sample 1)
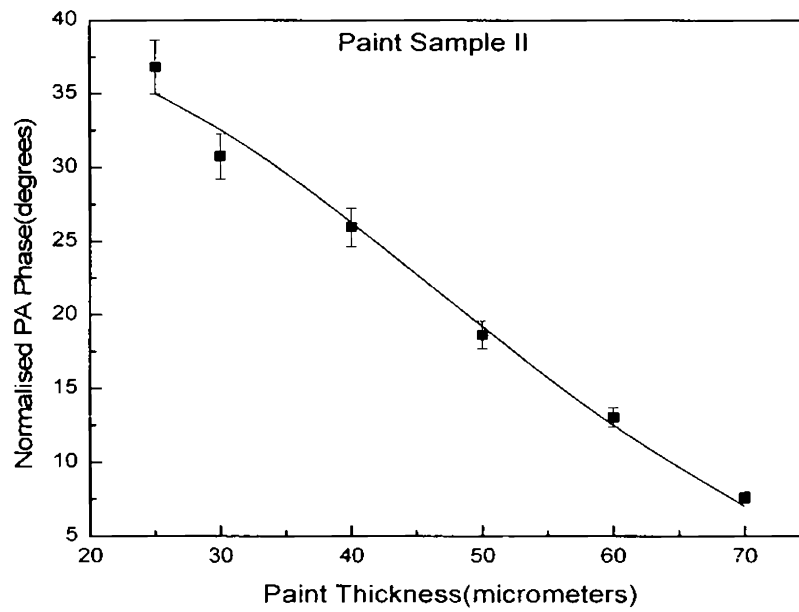
Fig 4.5: Variation of the normalized PA phase with thickness of the paint coating (sample II)

Fig 4.6: Variation of the normalized PA phase with thickness of the paint coating (sample III)

Fig 4.7: Variation of the normalized PA phase with thickness of the paint coating (sample IV)
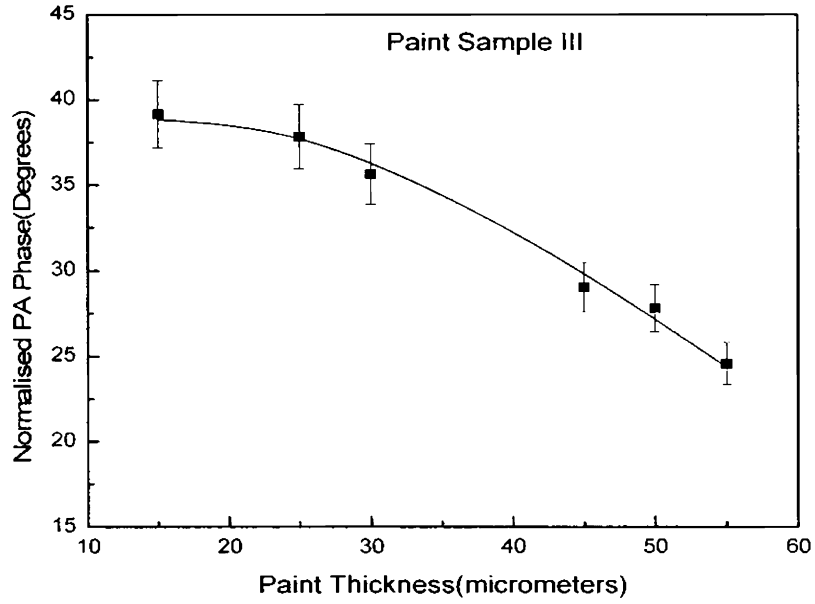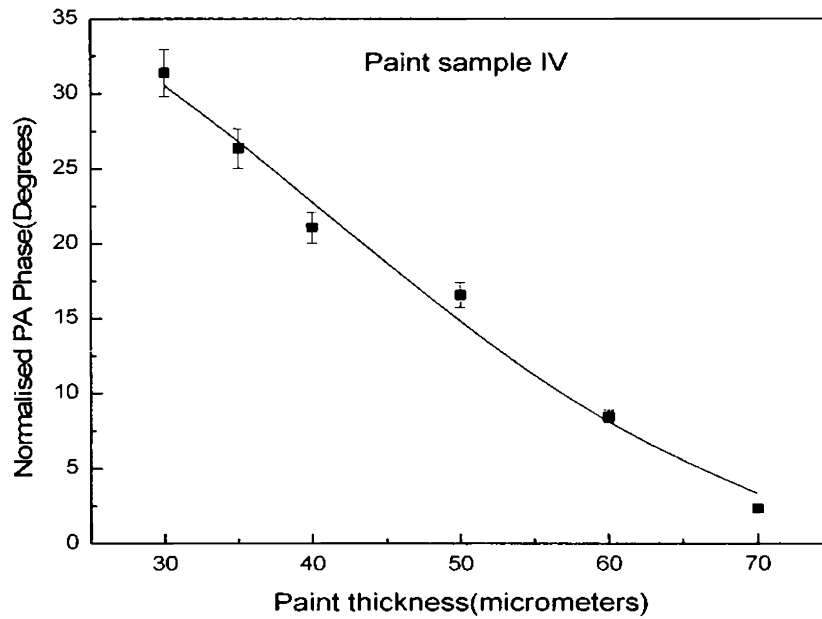
125

Table 4.1. Thermal properties of paint samples measured using PA scanning technique

| Paint sample	Density kg/m^3	Parameter χ^2	Thermal effusivity (Ws$^{1/2}$m^{-2}K^{-1})	Thermal diffusivity (x 10^{-7} m^2/s)	Thermal diffusivity by photo acoustic technique (x 10^{-7} m^2/s)	Thermal conductivity (Wm^{-1}K^{-1})	Heat capacity (J/kg K)
(1)	(2)	(3)	(4)	(5)	(6)	(7)	(8)
I	1331±39	3.14	3163±126	2.10±0.15	1.98±0.10	1.45±0.11	5184±518
II	1303±39	1.88	1567±51	2.21±0.12	2.20±0.11	0.74±0.04	2557±230
III	1251±37	0.39	1247±12	3.56±0.11	3.59±0.17	0.74±0.02	1670±100
IV	1162±34	1.98	1366±71	1.72±0.11	1.71±0.09	0.57±0.05	2835±283

[a] Value of the thermal effusivity of copper (backing) used for calculations is 37136 Ws$^{1/2}$m^{-2}K^{-1}

We have performed the measurements on the same paint sample (Sample I of Table 4.1) coated on backings other than copper. These include thermally insulating backings such as teflon and nylon as well as backings that are thermally less conducting than copper, such as aluminum, stainless steel and brass. Figures 4.8, 4.9, 4.10, 4.11 and 4.12 show the variation of the normalized PA phase values obtained along with the best fits for equation 4.21 for this sample on different backings. Table 4.2 gives the thermal parameters of paint Sample I when coated on different backings. The table also reports the calculated values of the thermal wave reflection coefficients (R_{sb}) corresponding to the coating – backing interface. A negative value for R_{sb} indicates a phase lead (thermal diffusivity of backing is higher that of the coating) and a positive value for R_{sb} indicates a phase lag (thermal diffusivity of the backing is lower than that of the coating). The thermal parameter values obtained for the same paint sample on conducting and non-conducting backings are comparable, with values lying more or less in the same range. As a matter of fact, they lie within the experimental uncertainties. This leads to an important conclusion that the thermal parameters of paint coatings are more or less independent of the nature of the backing on which they are coated. Experiments have been repeated with other paint samples on different backings and the results are comparable and reproducible, with deviations lying within experimental uncertainties.

It may be noted that the shape of the phase curves in Figures 4.8 to 4.12 depend on the thermal properties of the backing. It shows downward slope for conducting backing and upward slope for non-conducting backing. The slope of the curve is determined by the relative thermal properties of the coating and the

backing, which in turn determine the thermal wave reflection coefficients. The expression for the phase difference in the theory (equation 4.21) involves the reflection coefficients explicitly, and depend on the thermal properties of the coating only implicitly. It is the reflection coefficient that controls the shape of the phase curves, and not the thermal properties of the coating. The complex dependence of the thermal wave reflection coefficients and the coating thickness on the photo acoustic phase eliminates any dependence for the slope of the phase curves on the values of thermal effusivity and/or diffusivity of the coating
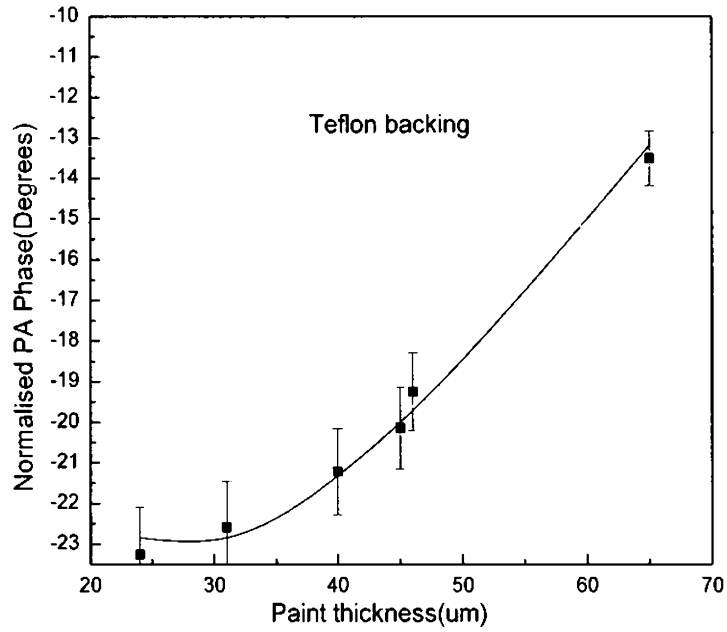
Fig 4.8: Variation of the normalized phase with thickness of paint coating (Sample I of Table 4.1) on teflon backing
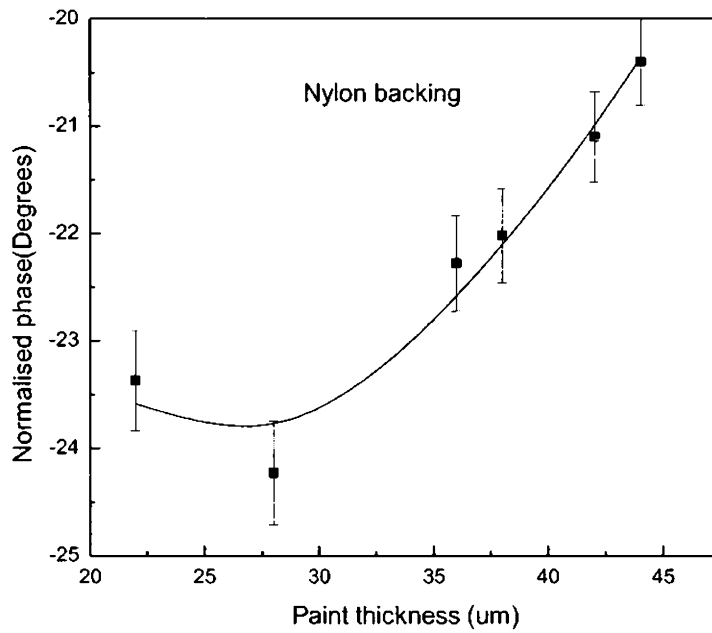
Fig 4.9: Variation of the normalized phase with thickness of paint coating (Sample 1 of Table 4.1) on nylon backing
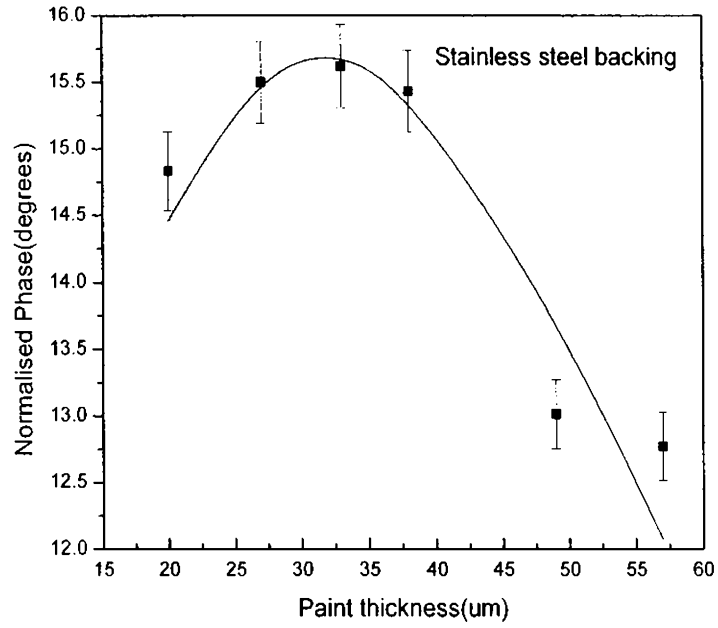
Fig 4.10: Variation of the normalized phase with thickness of paint coating (Sample I of Table 4.1) on stainless steel backing
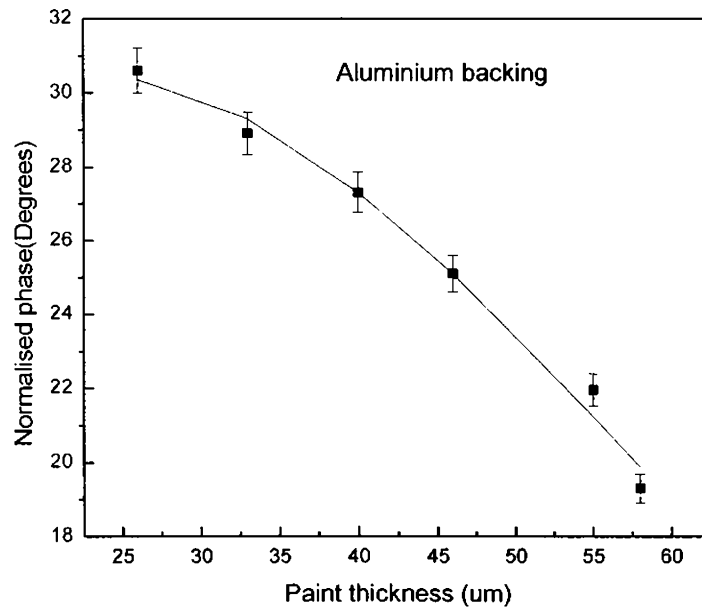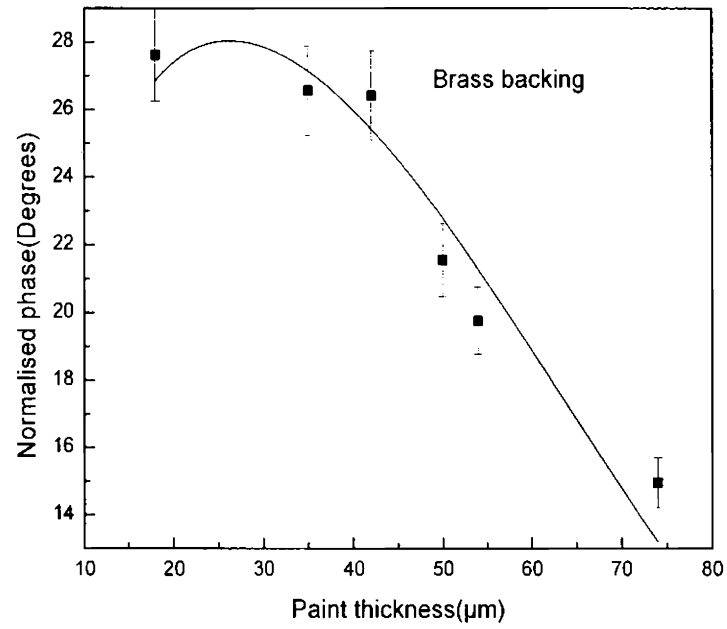

Fig 4.11: Variation of the normalized phase with thickness of paint coating (Sample I of Table 4.1) on aluminium backing

130

Fig 4.12: Variation of the normalized phase with thickness of paint coating

(Sample I of Table 4.1) on brass backing

Table 4.2. Thermal properties of the same paint coating (Sample 1 of Table1) on different backings. (The results with copper backing are the same as in Table 4.1)

Backing material	Thermal effusivity of backing(Literature value) $(Ws^{1/2}m^{-2}K^{-1})$ e_b	Thermal wave reflection coefficient R_{sb}	Thermal effusivity of paint coating $(Ws^{1/2}m^{-2}K^{-1})$	Thermal diffusivity of paint coating $(x\ 10^{-7}m^2/s)$	Thermal conductivity of paint coating $(Wm^{-1}K^{-1})$
Teflon	756	0.604	3062±122	2.34±0.09	1.48±0.11
Nylon	714	0.624	3084±123	2.14±0.08	1.43±0.11
Aluminum	24642	-0.776	3108±124	1.92±0.08	1.36±0.11
Stainless Steel	7224	-0.421	2943±117	2.20±0.09	1.38±0.11
Brass	18600	-0.723	2990±126	2.11±0.09	1.37±0.11
Copper	37136	-0.844	3163±126	2.10±0.15	1.45±0.11

4.5 : Conclusions

Our investigations show that the thermal parameters of opaque coatings like paints on a backing can conveniently be determined by this scanning photoacoustic technique. Even though the sample preparation is somewhat involved, this technique offers a good method to determine most of the important thermal transport parameters simultaneously. The method is comparatively simple and fast. With suitable modifications the technique can be extended to determine thermal properties of semiconductor thin/thick film coatings; for that matter any absorbing coating. The only condition is that the thermal effusivity of the backing as well as the thickness of the coating should be known previously.

The thermal parameters discussed in this work can form another set of parameters that determine the quality of paint coatings. The method described in this work can be perfected and standardized to measure these parameters for quality testing.

References

[1] Almond D P, Patel P M, 1996 *Photothermal Science and Techniques*,

Chapmann & Hall, London 209-219

[2] Garcia J A, Mandelis A, Farajbakhsh B, Lebowitz C and Harris I,

Int. J. Thermophys. (1999) **20**, 1587

[3] Almond D P, Patel P M and Reiter H, *Mater. Evaluation* (1987) **45**, 471

[4] Lau S K, Almond D P and Patel P M, *J. Phys. D: Appl. Phys.* (1991) **24**, 428

[5] Taylor R E, *Mater. Sci. Eng.* A (1998) **245**, 160

[6] Almond D P, Patel P M, Pickup I M and Reiter H, *NDT Int.* (1985) **18**, 17

[7] Cielo P and Dallaire S, *J. Mater. Eng.* (1987) **9**, 71

[8] Bendada A, *Meas. Sci. Technol.* (2002) **13**, 1946

[9] Parker W J, Jenkins R J, Butler C P and Abbott G L,

J. Appl. Phys. (1961) **32**, 1679

[10] Imhof R.E., Thornley F.R., Gilchrist J.R.and Birtch D.J.S.,

J.Phys D:Appl.Phys. (1986) **19**, 1829

[11] Imhof R.E, Whitters C.J. and Birtch D.J.S, *Mater.Sci.Eng.* (1990) **B5**, 113

[12] Moksin M M, Grozescu I V, Wahab Z A and Yunus W M M,

Meas.Sci.Technol. (1999) **10**, 7

[13] Moksin M M and Almond D P, *J. Mater. Sci.* (1995) **30**, 2251

[14] Coelho T.M., Nogueira E.S., Pereira J.R.D., Baesso M.L. and Bento A.C.,

J.Phys.IV France (2005) **125**, 519

[15] Rosencwaig A and Gersho A, *J. Appl. Phys.* (1976) **47**, 64

[16] Bennett C A and Patty R R, *Appl. Optics* (1982) **21**, 49

[17] Busse G, *Appl. Phys. Lett.* (1979) **35(10)**, 759

[18] Raghu O and Philip J, *J. Instrum. Soc. of India* (2003) **33**, 155

[19] Madhusoodanan K.N, Thomas M.R. and Philip J, J.Appl.Phys.(1987) **62**, 1162

CHAPTER 5

Determination of thermal effusivity of selected solid samples by scanning photoacoustic technique


5.1: Introduction

Thermal characterization of materials is one of the most important applications of photoacoustic(PA) effect [1]. Thermal characterization involves measurement of the thermal parameters such as thermal diffusivity, thermal effusivity, thermal conductivity and heat capacity. A few different techniques employing the PA effect have been developed for the measurement of these quantities [2-3]. The most accepted one among these measures the variation of PA amplitude or phase as a function of chopping frequency f, and determination of the characteristic frequency f_0 at which the sample goes from a thermally thin to a thermally thick regime [4-6]. If l_s is the thickness of the sample, the thermal diffusivity can be determined using the relation $\alpha = f_0 l_s^2$. Measurements as a function of sample thickness enables one to determine thermal effusivity as well, and hence the thermal conductivity and heat capacity of the sample [3]. Another technique to measure thermal diffusivity of a solid sample involves determination of the amplitude ratio or phase lag of the PA signal between the front and rear surface illuminations at a single chopping frequency [7-8].

All the methods described above suffer from the limitation that the measurement accuracy is dependant on PA cell calibration. Measurements

136

involving variations in sample thickness or chopping frequency can cause errors in the measurements. Accuracy of the measurement of amplitude ratio or phase lag between front and rear surfaces of the sample also depend on the experimental conditions.

A scanning photoacoustic technique to determine the thermal effusivity of solids has been developed by Philip [9]. This technique has the advantage that the measurement is more or less free of PA cell parameters and experimental conditions. In the next section, we give a brief outline of the theory and the principle of this technique.

5.2: Principle and Theory of PA Scanning Technique

Modulated light beam

$\longrightarrow$ Scan

$\longrightarrow$ Absorber layer(C)

$\longrightarrow$ Experimental sample(S)
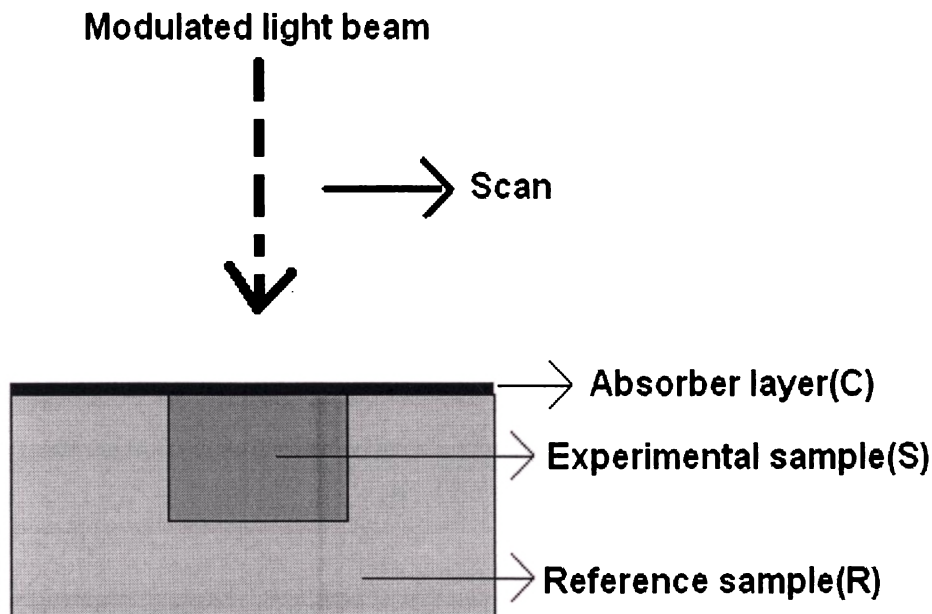
$\longrightarrow$ Reference sample(R)

Fig 5.1: Experimental configuration

The theory is developed for an experimental configuration of the type shown in Fig 5.1. Here the experimental sample S whose thermal effusivity is to be

137

determined, is inserted in the reference sample R whose thermal effusivity is known. The experimental sample is inserted into the reference sample in such a way that the top of both the samples are flat and are at the same level. A thin layer of a highly light absorbing material such as carbon black is coated over the entire top surface of the sample configuration (C). The use of carbon black as an absorber layer for photothermal conversion has been reported earlier [10]. This absorber layer can be considered as an optically opaque and thermally thin photoacoustic sample with two different backings S and R at the same horizontal level. The absorber layer surface is scanned with an intensity modulated beam of light in a step by step fashion. The above sample configuration is kept in a PA cell and the PA amplitude as well as the phase are measured as the sample surface is scanned in a one dimensional manner (along a line). The backing medium is changed from the reference sample R to the experimental sample S and again to the reference sample as the absorber layer is scanned with the chopped beam of light.

According to the Rosencwaig-Gersho Theory of PA effect in condensed media, the complex envelope of the sinusoidal PA signal is given by

$$U_0 = \frac{\beta I_0 P_0 \mu_g}{2\sqrt{2} T_0 k_s l_g (\beta^2 - o_s^2)} \left[\frac{(b+1)(r-1)e^{\sigma_s l_s} - (r+1)(b-1)e^{-\sigma_s l_s} + 2(b-r)e^{-\beta_s}}{(g+1)(b+1)e^{\sigma_s l_s} - (g-1)(b-1)e^{-\sigma_s l_s}} \right] \quad (5.1)$$

where k : thermal conductivity

ρ : density

c : specific heat capacity

138

$\alpha = \dfrac{k}{\rho c}$: thermal diffusivity

$a = \left(\dfrac{\omega}{2\alpha} \right)^{1/2}$: thermal diffusion coefficient

$\omega = 2\pi\upsilon$, where υ is the frequency of modulation of the light beam

$\mu = \dfrac{1}{a}$: thermal diffusion length

β : optical absorption coefficient of the sample

$l_\beta = 1/\beta$: optical absorption length

The subscripts b, s and g used with the above symbols represent these parameters in

the backing, sample and gas region respectively. Also

$\sigma = (1 + i)a$

$b = \dfrac{k_b \sigma_b}{k_s \sigma_s} = \dfrac{e_b}{e_s}$

$g = \dfrac{k_g \sigma_g}{k_s \sigma_s} = \dfrac{e_g}{e_s}$

γ is the ratio of specific heats of the gas, P_0 is the ambient pressure in the

cell, and T_0 is the ambient temperature and I_0 is the intensity of the light beam.

For a sample configuration of the kind shown in Fig 5.1, the PA signal is

generated from the absorber sample with samples S and R acting as the backing

media. For a good absorber such as carbon black, the optical absorption coefficient

is very high, and at modulation frequencies less than 100Hz the absorber layer can

be considered as thermally thin. Under these realistic assumptions, the PA

amplitude ratio from the absorber sample with backings S and R works out to be

[11]

139

$$\frac{A_S}{A_R} = \left[\frac{e_S^2(e_C + e_S)^2 \left[(e_C^2 + e_R^2)^2 + 4e_C e_R \left[(e_C + e_R)^2 - e_C e_R\right]\right]}{e_R^2(e_C + e_R)^2 \left[(e_C^2 + e_S^2)^2 + 4e_C e_S \left[(e_C + e_S)^2 - e_C e_S\right]\right]} \right]^{\frac{1}{2}}$$

$$(5.2)$$

where e_C, e_S and e_R are the thermal effusivities of the absorber sample, backing S

and backing R, respectively. Thermal effusivity is defined by $e = \sqrt{\rho k C}$ where ρ, k

and C represent the density, thermal conductivity and specific heat respectively.

Depending upon whether the thermal wave reflection coefficients at the absorber-

backing boundaries are positive or negative we can considerably simplify equation

5.2 and several special cases can be deduced [11].

The phase difference as the backing is changed from S to R works out to be

$$\phi_S - \phi_R = \tan^{-1}\left(1 + \frac{e_S}{e_C}\right) - \tan^{-1}\left(1 + \frac{e_R}{e_C}\right)$$

$$(5.3)$$

φ_S and φ_R in this equation cannot be separated as the absolute phases are not known.

We can estimate the value of e_C by using samples of known effusivities as the

backing samples. Measurement of the phase difference, rather than individual

phases separately, nullifies cell parameter effects and other static components.

5.3 : Work presented in this chapter

The thermal effusivity of selected samples such as a few pure ceramics as

well as composite polymer ceramics have been determined by the scanning PA

technique. The same PA setup described in chapter 2 has been used for the

measurements. The measurement procedure is also the same as the one outlined in

chapter. The PA scanning is done along a line covering the reference sample and the experimental sample. The reference sample is one whose thermal effusivity is already known. The principle of the PA scanning technique described above has been followed to determine the thermal effusivity of the experimental sample by measuring the amplitude ratio and phase difference of PA signal from the carbon black sample with the backing changed from the reference sample to the experimental sample.

The work done and the results obtained on selected composite polymer ceramic samples are described below.

5.4 : Work on Ceramic Samples

Ceramics are solid compounds, which are formed by the application of heat and pressure, comprising of two or more elements, metals or non-metals. The family of ceramics is large and varied including such materials as refractories, glasses, bricks, cements and plasters, abrasives, art wares, porcelain enamels, ferrites, ferroelectrics and dielectric insulators etc [12-17].

The main features of ceramic materials are the following.

(i)   The presence of strong covalent character of chemical bonding. The high strength of the covalent bond is responsible for the general high melting point of ceramics, their brittleness, good corrosion resistance, low thermal conductivity and high compressive strength. The enormous range of electronic and diamagnetic properties of ceramics is the manifestation of slight variations in chemical bonding.

141

(ii)   Microstructure comprising of inorganic crystalline compounds and / or amorphous glass in varying proportions.

(iii)   Processed at high temperatures. High temperature processing in ceramics is important as chemical reactions are accelerated and many constituents of the raw material decompose at high temperature and form more stable compounds. High temperatures are also necessary to produce new crystal compounds and form homogeneous solid solutions. Thermal processing also increases the density of ceramic objects, as the porosity is gradually eliminated and inter-granular bonds are strengthened.

5.4.1 : Preparation of ceramics

The basic steps involved in the preparation of ceramic materials are : (i) preparation of the ingredients for the formation of the ceramic (ii) shaping or forming the part (iii) drying and (iv) sintering.

(i)Preparation of raw materials

The raw materials are weighed, mixed and blended either wet or dry. In dry processing, the required plasticity for shaping is obtained by grinding and blending plastics with finely pulverized non-plastic ingredients and adding alkalies, acids and salts.

(ii)Forming methods

Ceramics can be formed by a large number of methods, either in a dry semiliquid or liquid state or in either a cold or hot condition. The different methods include slip casting, jiggering, pressing, extrusion, molding etc.

The dielectric ceramics for the present measurements are formed by pressing. This method can be done with dry, plastic, or wet raw materials. In dry processing, ceramic mixtures with liquid level up to 5% by weight are pressed into shape under high pressure in a metal dye. This method is widely used for manufacturing ceramics like electric insulators, electronic ceramic parts etc, since it produces small uniform parts to close tolerance. Powder pressing produces bodies with the lowest porosity and highest strength because of the high pressure and small amount of binder required.

(iii) Drying and sintering

The purpose of drying is to remove any water if present. The function of sintering is to convert the shaped dry ceramic part into a permanent product. The sintering process and temperatures used depend on the ceramic composition and desired properties. The maximum temperature at which the ceramic is sintered is called the maturing temperature. In the first stage of firing, any moisture still present after drying is removed. In the next stage, chemical reactions cause the material to lose it's plasticity. In the last stage, vitrification of the ceramic begins and continues up to the maturing temperature. During vitrification , a liquid glassy phase forms and fills the pore spaces. Up on cooling, the liquid solidifies to form a vitreous or glass matrix that bonds the inert unmelted particles together. Electronic ceramics are often fired at high temperatures, sometimes above 3000°C, to obtain the desired vitrification or ceramic bond.

143

5.4.2: Applications of ceramics

Ceramics are vital for a whole spectrum of applications in areas such as electronics, communication, medical electronics, environmental engineering, research etc. There are ceramics used as capacitor dielectrics, piezoelectric and ferroelectrics ceramics, ceramic substrate materials, ferroelectrics films, superconductors, NTC and varistors, microwave dielectrics, ferrites and piezoelectric ceramics. They form the basis of thermal imaging systems, gas sensors, circuit protection device for computers, precision control devices in cameras and automobile suspension systems.

With the technological advances in using dielectric ceramics as microwave resonators, the progress in microwave telecommunication and satellite broadcasting has risen rapidly. In microwave applications, dielectric resonators are used to manufacture microwave integrated circuits, pass-band filters, oscillators etc. High quality dielectric ceramics with high dielectric constant, low dielectric loss and low temperature coefficient of resonant frequency are extensively used in mobile communications for the purpose of miniaturization of dimensions of resonator. By the use of new generation of ceramic resonators, the filter/combiner units of cellular base stations process the messages and send them out again. Today, the ceramic resonators look a bit like doughnut in shape, about 5-10 cm in diameter, depending on the working frequency. Much smaller filters are used in handsets. Resonant frequency of a band-pass filter may be adjusted by using a tunneling metallic element. Dielectric ceramics monoblock microwave band-pass filters are compact, high Q, surface mountable filters with excellent temperature and time stability. Dielectric ceramic resonators are also used for impedance converters, discriminators

144

and matching circuits. Combiners are used to transmit multiple frequencies on a single antenna.

Coaxial resonators made with modern, high performance ceramic dielectric materials are very useful as compact frequency standards and distributed inductive or capacitive circuit elements. The high Q obtained in the UHF and microwave frequency range makes resonators ideal for many applications. When cost, size and stability are important, these resonators are the best choice. High dielectric ceramic materials assure antennas with compact-small size, wide band and high gain. Low loss and high gain antenna switch modules suitable for SMD mounting in portable wireless designs can be constructed using ceramic materials. Ceramic components help to reduce the near field of the antenna, which in turn reduces the specific absorption rate (SAR).

Commercial wireless communication applications emerged in the late 1970's, evolved in the 1980's and have exploded through 1990's. Numerous systems are rapidly filling the 400MHz – 20GHz band. Cellular telephones (400MHz – 1GHz), Television Receivers (TVRO, 2 –5 GHz), Direct broadcasting (DBS, 11 – 13 GHz) and specialty satellite communications are now deployed worldwide. Wireless cables, high definition and interactive TV, collision avoidance, global positioning, cellular satellite and personal communications (PCS) of many types loom in the near future for consumers.

Among several factors, industrial growth has been spurred by the development of special ceramics and their commercialization as high volume, low cost products. These materials are easily integrated into rf/microwave circuits using glues, epoxies, screws or solder. They function as frequency filters, capacitors,

inductors and signal distributing elements. Electrical requirements for the materials used are, low loss (high Q), high dielectric constant (ε_r) and very low temperature coefficient of resonant frequency (τ_f). High Q not only minimizes circuit insertion losses, but for some filter applications, also allows more channels, within a given frequency allocation. In addition, electrical noise is suppressed in oscillator devices.

One of the first materials utilized for this application was TiO_2, which was inexpensive, displayed excellent Q ($\approx$ 15,000 at 3 GHz) and high ε_r ($\approx$ 100), but it possesses a large τ_f of about 400 ppm/$^\circ$C. The binary Strontium Titanates have practical applications in modern microwave resonators. Strontium Titanate based ceramics were used as filters for the base stations of the infant cellular industry and for conventional telephone microwave relays.

There are a number of research works for developing new ceramics and also for improving the properties through substitution and addition of additives. Several series of microwave dielectric ceramics have been developed like $Sr-R_2O_3-TiO_2$ (R=Ce,Nd...) system. Dielectric ceramics in TiO_2 –rich region of the $SrO - Ce_2O_3-TiO_2$ ternary system have excellent dielectric constants, low dielectric losses and low temperature coefficients of capacitance.

Strontium Cerium Titanate (SCT) is an important microwave dielectric ceramic, which received much scientific and commercial interest as the key material for microwave dielectric resonators and filters. To get dense ceramics with homogenous microstructure SCT ceramics has to be sintered at temperature of about 1300-1400°C. When the materials are sintered at such temperatures, the bottom electrode or inner electrode must be a noble metal such as Pt, and which increases manufacturing costs. Therefore, studies of dielectric ceramics have

146

focused on decreasing the sintering temperature and improving the dielectric properties by controlling the sintering conditions and microstructure by adding sintering aids like glasses that have low melting points.

5.4.3: Preparation of the composite polymer ceramic PTFE+$Sr_2Ce_2Ti_5O_{16}$

The pure SCT ceramics are prepared by accurately weighing high purity (99.9%) $SrCO_3$, Ce_2O_3 and TiO_2 in the stoichiometric proportions and wet mixed with distilled water and ball-milled with ZrO_2 balls for 24 hrs. The dried powders are calcined in a platinum crucible at 1150°C for 4 hrs. The calcined powder is again ground well in agate mortar and PVA (5%) is added and mixed well. After drying, the mixture is again ground well for half an hour. This fine powder is pressed into cylindrical compacts of suitable dimensions under a pressure in the range of 100 to 150 MPa. The pellets so obtained are then sintered at a temperature of 1350°C for about 4 hrs.

For PTFE (poly tetra fluro ethylene) added samples, the chemicals $SrCO_3$, Ce_2O_3 and TiO_2 are weighed in stoichiometric ratios. The powders are mixed well and calcined as described above. The calcined powder was then divided into parts of different wt% and fixed wt% of PTFE are added to different parts. Dielectric ceramics are prepared from the powders by the conventional method as described above and the samples are then sintered at appropriate optimized temperatures.

Polytetrafluoroethylene (PTFE) is a fluorocarbon-based polymer. Commercially, the material is best known as Teflon. It is made by free radical polymerization of tetrafluoroethylene and has a carbon backbone chain where each carbon has two fluorine atoms attached to it.
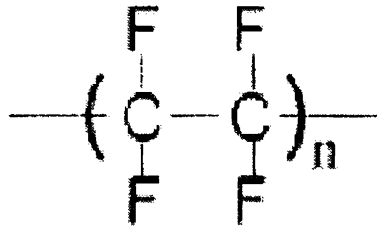
Fig 5.2 : Polytetrafluoroethylene repeat unit. The degree of polymerization is very high(>1000)

This polymer is hydrophobic (water hating), biologically inert, non-biodegradable, and also has low friction characteristics and excellent "slipperiness." The chemical inertness (stability) of PTFE is related to the strength of the fluorine-carbon bond. This is why nothing sticks to this polymer. When stretched, PTFE forms a strong porous material called expanded PTFE (ePTFE). A commercial name for this form of Teflon in Goretex.

Many popular products take advantage of the characteristics of PTFE polymer. It has applications in medical, industrial, electronic, and performance fabric fields. As a medical material, PTFE has many uses, including arterial grafts, catheters, sutures, and uses in reconstructive and cosmetic facial surgery.

The samples selected for study in this work are pure PTFE, PTFE with 0.1, 0.2, 0.3, 0.4, 0.5 wt% of SCT added to it as well as pure SCT.

5.5: Experimental method

For measuring the thermal effusivity of a sample by the PA scanning technique the experimental sample and a suitable reference sample should be attached together as a single sample configuration as shown in figure 5.1. This sample configuration consists of a reference sample (copper in our case) in the form of a disc in which the experimental sample is inserted by drilling a pit in the

148

reference sample. The copper disc is 1.7 cm in diameter and 2.5mm thick. A circular pit is drilled at its centre with a diameter of 4 mm.The experimental sample is made in the form a cylindrical piece of diameter 4 mm and height 2.5 mm. This is then inserted tightly into the circular pit drilled in the reference sample disc. The top surface of this sample combination is hand lapped and made perfectly flat so that it has a single uniform surface. The thickness of the experimental and reference samples should be more than the thermal diffusion length of the thermal wave, which is generated as the sample configuration is subjected to PA scanning process. This condition can be met by choosing the light modulation frequency appropriately.

A thin layer of a highly light absorbing material such as carbon black is coated over the entire top surface of the sample configuration. The carbon black layer is applied by holding the sample above a benzene flame for a few seconds. It is estimated to have a few tens of microns thickness and is uniform within 10 %. This absorber layer can very well be considered as an optically opaque and thermally thin layer at modulation frequencies less than 100 Hz.. The absorber layer coating is made on the sample combination with extreme care so that its thickness does not exceed a few microns. Under these circumstances, this absorber layer is optically opaque and thermally thin

The sample thus prepared is placed inside the PA cell and subjected to PA scanning by using the setup already described in chapter 2. The PA scanning setup is programmed to move horizontally in a step by step manner along a diametric line on the sample. Each step provides a lateral shift of 0.5 mm. As the light beam scans the absorber surface changing the backing from one to the other (reference sample

149

to the experimental sample and vice versa), the PA amplitude and phase from each point are recorded after ensuring that the readings are stabilized. We have used a modulation frequency of 30Hz in our experiments. Besides the ceramic samples, we have measured the thermal effusivities of some standard samples such as brass, stainless steel and nylon to ensure that this experimental method provides accurate results.

5.6: Results and Discussion

Figures 5.3 to 5.12 depict the variation of the amplitude and phase of the PA signals as a function of scanning distance along a line for different sample configurations. All graphs show sharp changes in amplitude and phase of the PA signals at two specific points as the distance is varied. These correspond to the boundaries between reference and experimental samples. The middle region of all the plots presented in the amplitude and phase of PA signals are from the experimental sample whereas the side regions of the graphs are from the reference sample. It has been verified that there is no variation in amplitude or phase, except for variations at the boundaries when the same material is used as the experimental and reference samples, leading to a value zero for the phase difference and unity for the amplitude ratio. The thermal effusivity of carbon black layer used as the absorber is estimated by measuring the amplitude ratio and phase difference in one experiment in which both the backings used have known thermal effusivities. It is found to be 739.2 $Jm^{-2}K^{-1}s^{-1/2}$. The effusivity of copper reference is taken as 37136 $Jm^{-2}K^{-1}s^{-1/2}$ from literature.

Using the amplitude ratio and phase difference values obtained from the experiment, we have determined the thermal effusivities of all the experimental

samples. These are tabulated in Table 5.1. The thermal effusivities of these composite polymer ceramic samples determined using an independent photo pyroelectric technique are also shown for comparison [25]. The two values show good agreement within experimental error limits.

From Table 5.1 it can be seen that the thermal effusivity of the polymer PTFE decreases with the addition of the ceramic SCT. The thermal effusivity decreases with the increase in the concentration of the ceramic. This can be attributed to the fact that the thermal conductivity and heat capacity of the composite decreases with the addition of the ceramic SCT.

This work demonstrates that the PA scanning technique can be used for determining the thermal effusivity of solids without much difficulty. The precautions to be taken care of in the experiment are 1) we have to ensure a thin uniform coating of carbon black layer over the sample configuration. 2) The top surfaces of the experimental and reference samples should be at the same level and they should be flat. Besides, the thermal effusivity of the reference sample should be known. This measurement does not involve any variations in frequency or sample thickness as in conventional PA experiments the technique is quite straightforward and fast. This method could be developed into a standard experimental technique to determine the thermal effusivity of bulk solid samples.
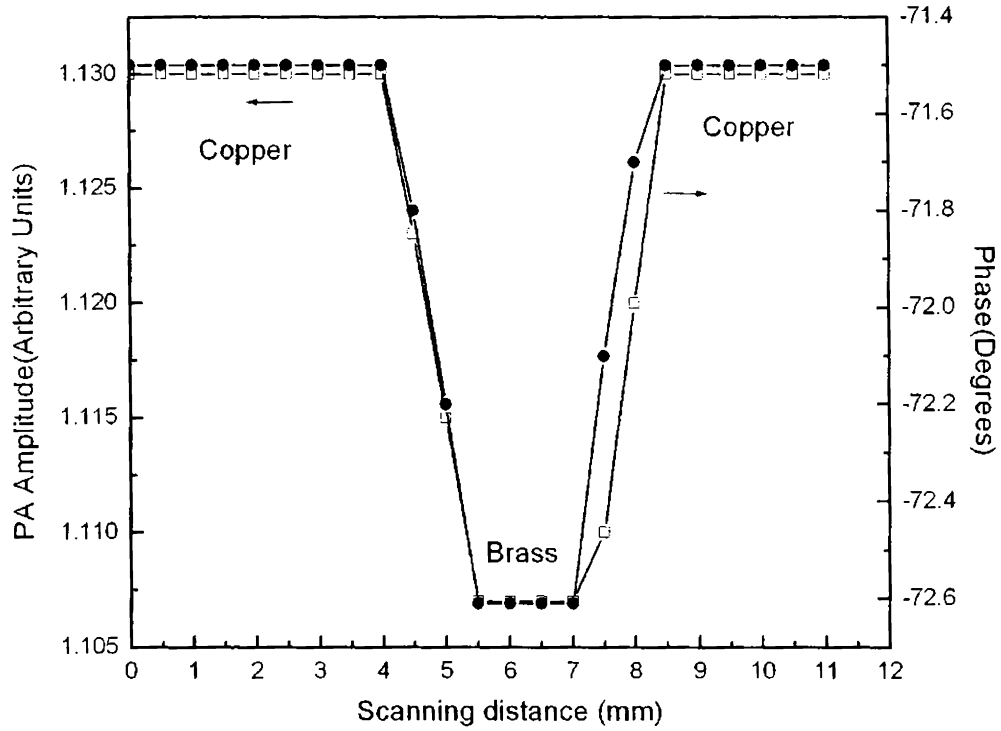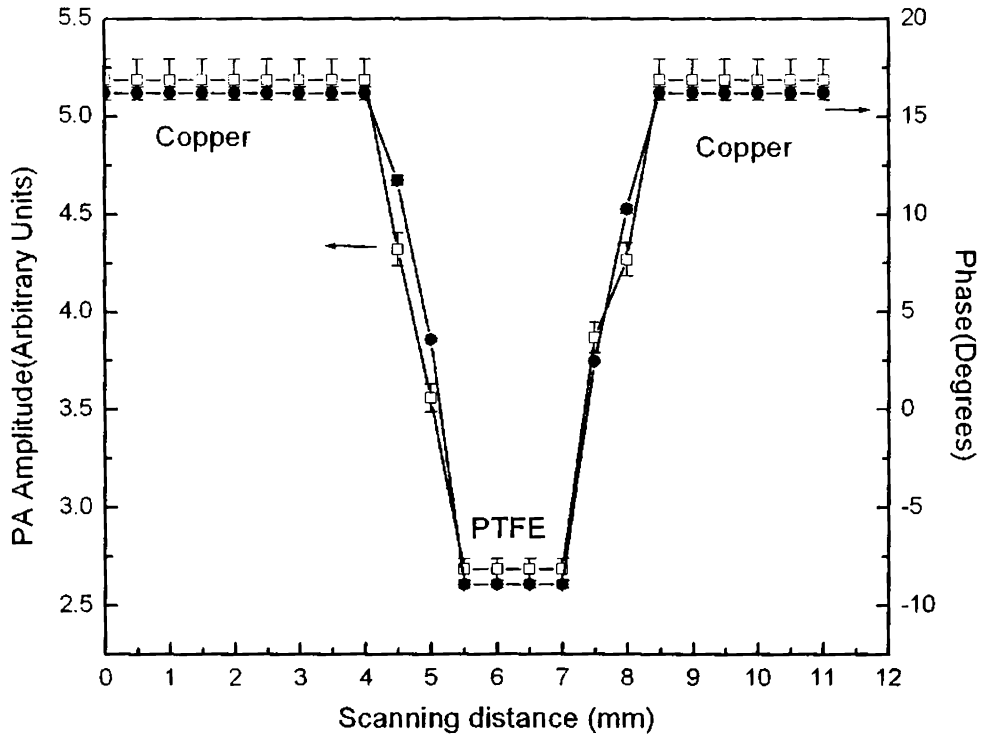
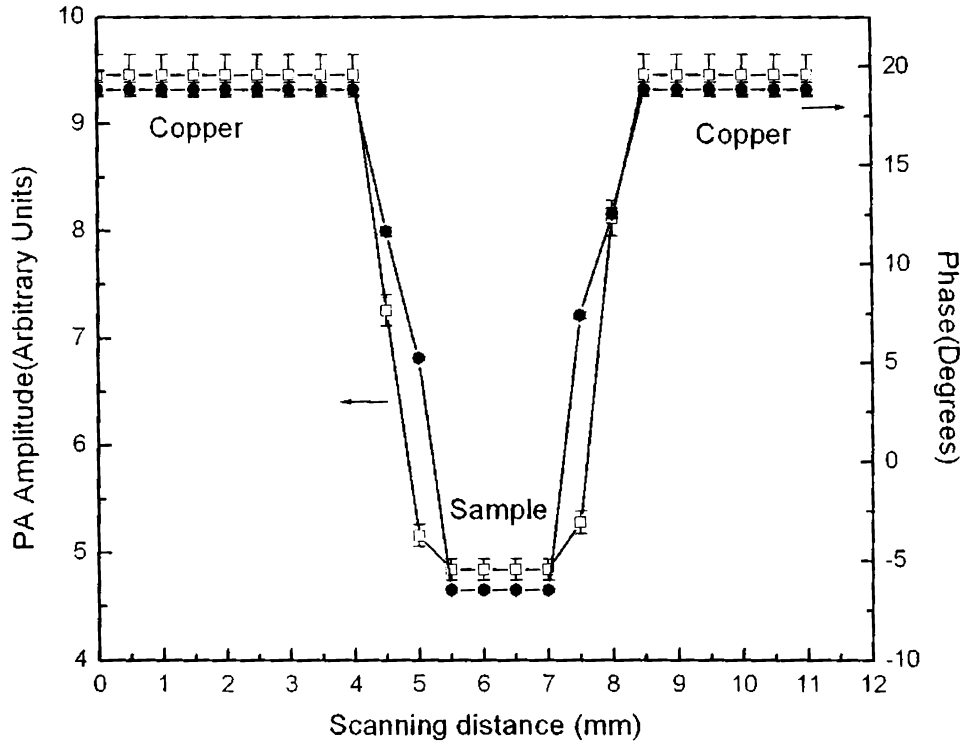**Fig 5.3:** Variation of PA amplitude and phase with scanning distance in the copper –brass sample pair
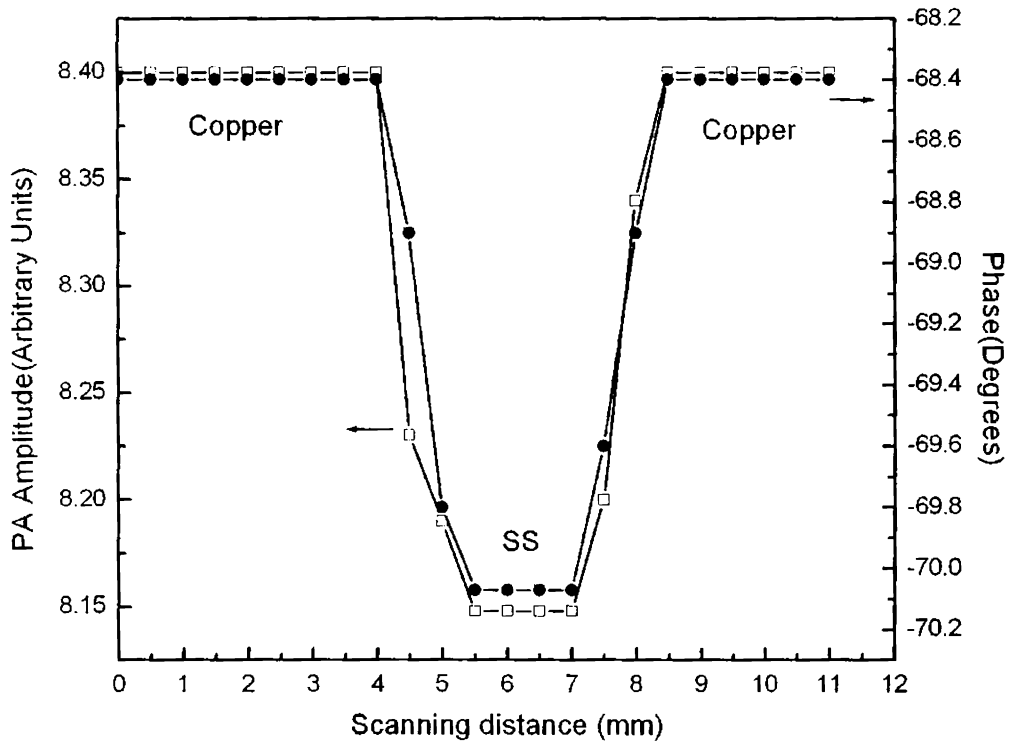
Fig 5.4: Variation of PA amplitude and phase with scanning distance in the Copper –Stainless Steel sample pair
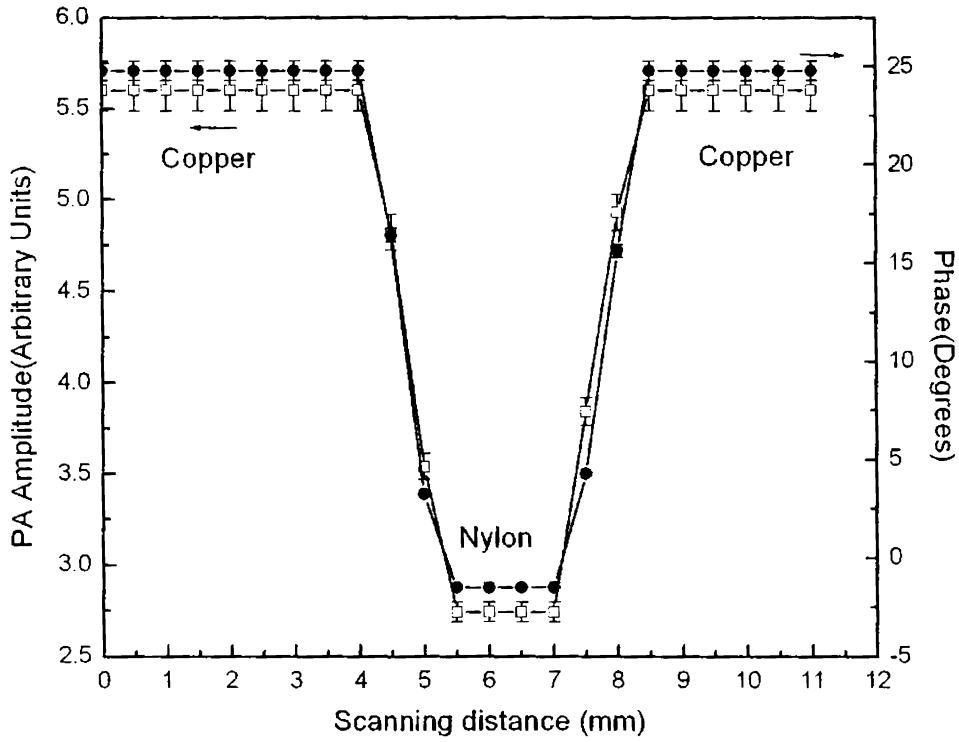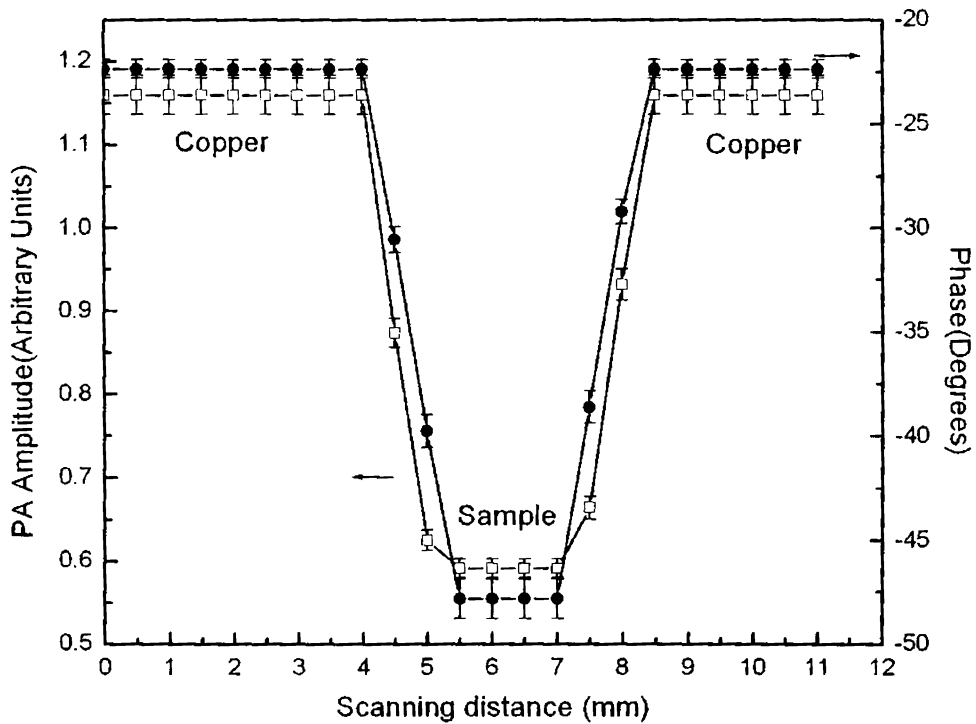
Fig 5.5: Variation of PA amplitude and phase with scanning distance in the Copper –Nylon sample pair
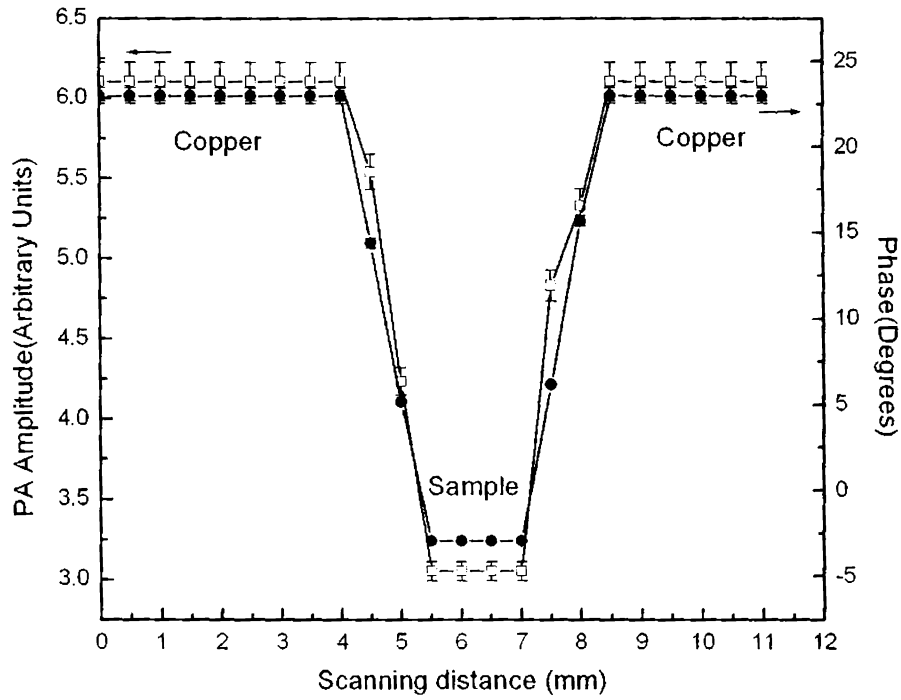

Fig 5.6: Variation of PA amplitude and phase with scanning distance in the Copper –PTFE sample pair

153

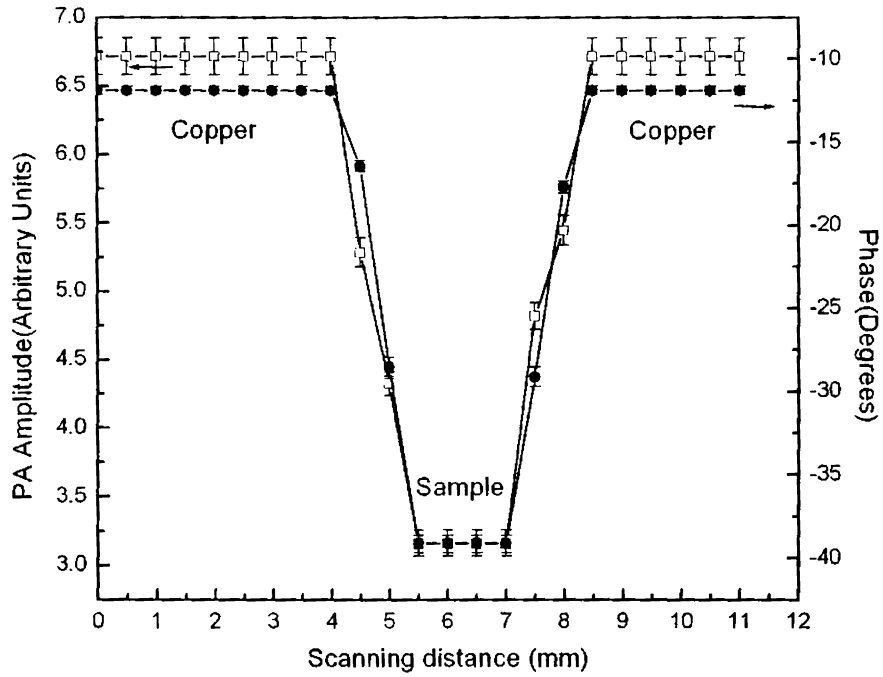**Fig 5.7:** Variation of PA amplitude and phase with scanning distance in the Copper –PTFE+0.1 wt% of $Sr_2Ce_2Ti_5O_{16}$ sample pair

Fig 5.8: Variation of PA amplitude and phase with scanning distance in the Copper –PTFE+ 0.2 wt% of $Sr_2Ce_2Ti_5O_{16}$ sample pair

Fig 5.9: Variation of PA amplitude and phase with scanning distance in the Copper –PTFE+ 0.3 wt% of $Sr_2Ce_2Ti_5O_{16}$ sample pair

Fig 5.10: Variation of PA amplitude and phase with scanning distance in the Copper –PTFE+ 0.4 wt% of $Sr_2Ce_2Ti_5O_{16}$ sample pair

Fig 5.11: Variation of PA amplitude and phase with scanning distance in the Copper –PTFE+ 0.5 wt% of $Sr_2Ce_2Ti_5O_{16}$ sample pair
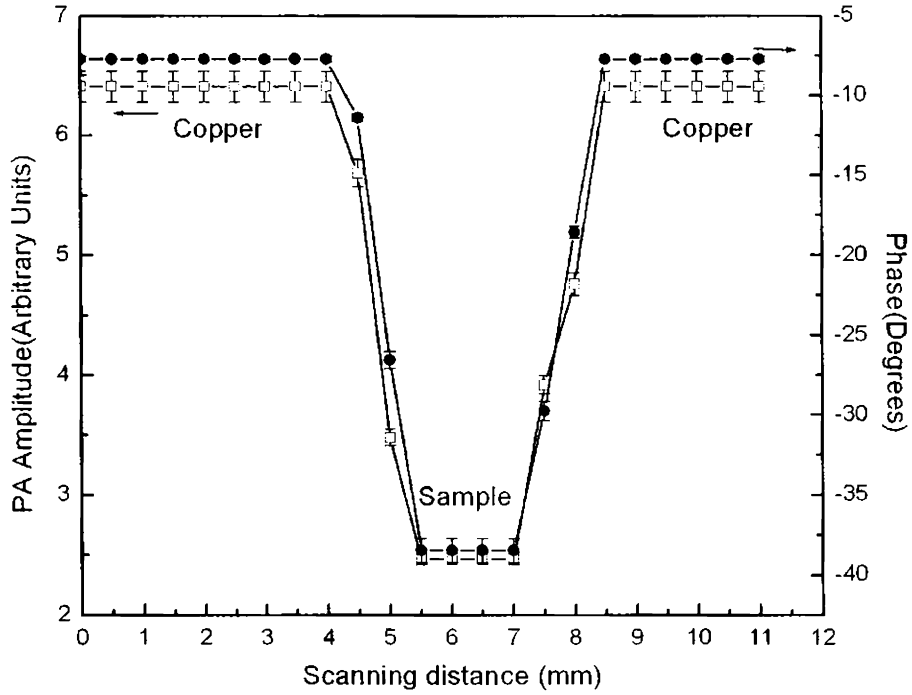

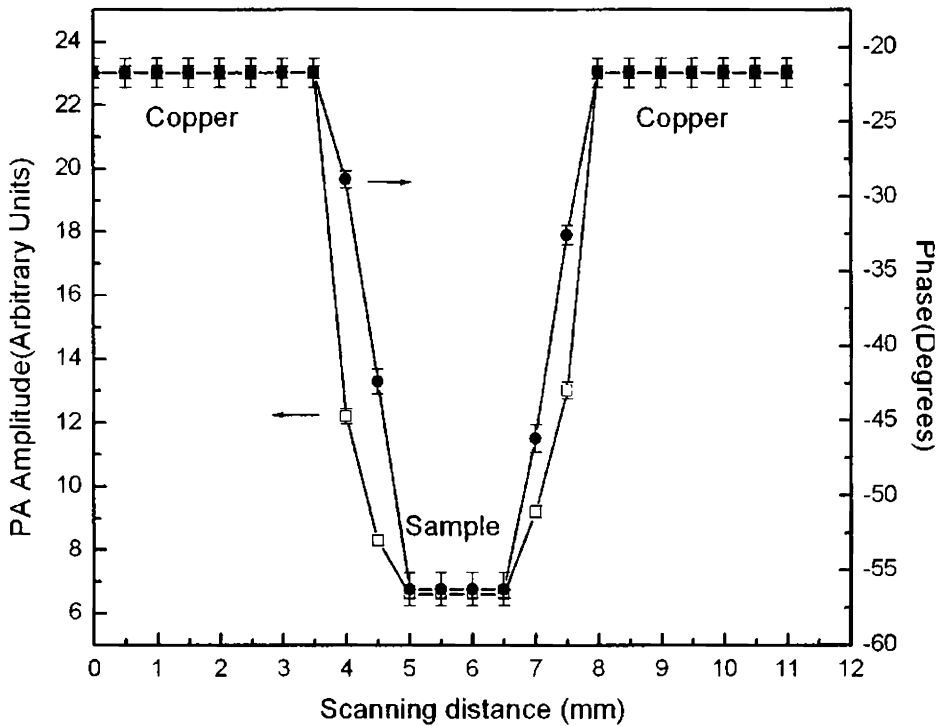**Fig 5.12:** Variation of PA amplitude and phase with scanning distance in the Copper – $Sr_2Ce_2Ti_5O_{16}$ sample pair

Table 5.1: Thermal effusivities of some known samples and the polymer - ceramic samples measured by the PA scanning technique

Sample	Reference	Amplitude ratio	Phase Difference (Degrees)	Effusivity of sample $J/m^2K^{-1}s^{-1/2}$	Literature value/Value obtained by PPE method $J/m^2K^{-1}s^{-1/2}$
Brass	Copper	0.98	-1.11	18241± 912	18606
Stainless Steel	Copper	0.97	-1.67	14456 ± 723	14738
Nylon	Copper	0.49	-26.3	686 ± 34	714
PTFE	Copper	0.5173	-25.1	761 ± 38	770
PTFE + 0.1 wt% of $Sr_2Ce_2Ti_5O_{16}$	Copper	0.512	-25.3	746 ± 37	765
PTFE + 0.2 wt% of $Sr_2Ce_2Ti_5O_{16}$	Copper	0.5099	-25.45	739 ± 37	761
PTFE + 0.3wt% of $Sr_2Ce_2Ti_5O_{16}$	Copper	0.4997	-25.907	710 ± 36	724
PTFE + 0.4wt% of $Sr_2Ce_2Ti_5O_{16}$	Copper	0.4701	-27.211	632 ± 32	644
PTFE + 0.5wt% of $Sr_2Ce_2Ti_5O_{16}$	Copper	0.3854	-30.768	449 ± 23	457
Pure $Sr_2Ce_2Ti_5O_{16}$	Copper	0.2874	-34.569	290 ± 15	299

References

1.A.C.Tam, *Rev.Mod.Phys.* (1986) **58(2)**, 381

2.B.K.Bein, S.Krueger and J. Pelzel, *Can J.Phys.* (1986) **64**, 1208

3.A.Lachaine, *J.Appl.Phys.* (1985) **57**, 5075

4.P.Charpentier, F.Lepoutre and L.Bertrand, *J.Appl.Phys.* (1982) **53**, 608

5. A.Lachaine and P.Poulet, *Appl.Phys.Lett.* (1984) **45**, 953

6. K.N.Madhusoodanan, M.R.Thomas and J.Philip, *J.Appl.Phys.* (1987) **62**, 1162

7.O.Pessoa Jr., C.L.Ceasar, N.A.Patel,H.Vargas, C.C.Ghizoni and L.C.M.Miranda,

   J.Appl.Phys. (1986) **59**, 1316

8. S.Thomas , J.Issac and J.Philip, *Rev.Sci.Instrum.* (1995) **66**, 3907

9. J.Philip, *Rev.Sci.Instrum.*(1996) **67(10)**, 3621

10.C.A.Bennett and R.R.Patty, *Appl.Opt.* (1982) **21**, 49

11.A.A.Sudhakaran, Ph.D.Thesis Cochin University of Science and Technology

   (1996)

12.M.W.Barsoum, Fundamentals of Ceramics, McGraw-Hill, New York (1997).

13.W.D.Kingerry, H.K.Bowen, D.R.Uhlmann, Introduction to Ceramics,

   John Wiley & Sons (1975).

14.J.F.Yang, Z.Y.Deng and T.Ohji, *J.Euro.Ceram.Soc.* (2003) **23**, 371.

15.K.Suzuki and M.Sasaki, *J.Euro.Ceram.Soc.* (2005) **25**, 1611.

16.W.Li, Z.Liu, M.Gu and Y, Jin, *Ceram. Internat.* (2005) **31**, 159.

17.J.M.Mota, M.A.Martinez, F.Velasco and A.J.Criado, *Ceram.Internat.* (2004)

   30, 30

18. Sheela K. Ramasesha, Science and Technology of Ceramics, *Resonance*, Aug (1999) 16.

19. M.Singh and J.A.Salem, *J.Euro.Ceram. Soc.* (2002) **25**, 2709.

20. H.J. Choi and Y.W. Kim, *J.Euro. Ceram.Soc.* (2004) **24**, 3795.

21. N.Ichinose, H.Amada, *J.Eurp. Ceram.Soc.* (1974) **57**, 450.

22. Wu, H.W.Wang, *J.Am.Ceram.Soc.* (1999) **82**, 1207.

23. M..A.Akbar, P.K.Davies, *J.Am.Ceram.Soc.* (1998) **81**, 670.

24. R.Ubie, I.M.Reancy, W.E.Lee, *J.Am.Ceram.Soc* (1996) **82(5)**, 13361.

25. C.Preethy Menon and J.Philip, *Meas. Sci.& Technol.* (2000) **11**, 1744

CHAPTER 6

Summary and conclusions

Photoacoustic and photothermal phenomena have come to be regarded as an effective tool for the measurement of thermal, optical and structural properties of materials, especially solids. The absorption of a portion of the intensity modulated radiation falling on a sample kept inside a cell and the consequent pressure change occurring in the medium surrounding it, leading to the production of an acoustic signal is referred to as photoacoustic effect. There are well established theories such as the one by Rosencwaig and Gersho which give expressions for the acoustic signal amplitude and phase produced in terms of the optical and thermal properties of the sample, the backing on which the sample is placed and the surrounding medium. Side by side with the advances in the theoretical understanding of the phenomena, development of the instrumentation for using the effect for various practical applications has also been an active area of research. The most important requirement for any PA setup are the excitation light source, modulation mechanism, PA cell, detector and signal processing instruments.

Among the various applications of PA effect, PA imaging has an important place. Many groups working in the area of photoacoustic microscopy (PAM) and photoacoustic depth profiling have revealed a number of advantages of this form of imaging. Among them non-destructive evaluation (NDE) of solids for defects is an important application. It gives visual information on a microscopic scale. It can

provide details of optical absorption as well as thermal and elastic properties on a microscopic scale. It gives information about de-excitation processes occurring on a microscopic scale and is capable of depth profiling as well.

In this work, we have developed a photoacoustic microscope for non destructive evaluation (NDE) of solid samples. To improve the signal to noise ratio of the PA signal we have designed a dual channel PA cell for the PAM. Its characterization has been done. The signals from the two channels of the PA cell are added using a summing amplifier. The modulated light beam coming out of an optical fiber is made to scan the sample in the PA cell with the help of a scanning unit. It has translation stages driven by stepper motors for X and Y motions. The whole setup is automated using a software developed in VB which controls the movement of translation stages, time delay and data acquisition. The instrument has been tested on different sample configurations. It is found to be capable of detecting the presence of surface and subsurface defects, change of material etc. The samples studied by us include copper discs with surface and subsurface defects, a section of a printed circuit board, a Teflon disc with a steel pin inserted inside etc.

It is seen that the instrument is capable of providing good quality images of the samples with reasonably good resolution. It is found that the spatial resolution depends on the spot size of the light beam and step size of the scanning besides the thermal diffusion length in the sample at the given modulation frequency. It is expected that if smaller beam size and and finer movements of the translation stages are used in future designs a better resolution can be achieved. Another feature observed is the noise signals occurring along with the PA signals. Even though

noise elimination techniques are required in all PA experiments, it is found that it is even more important in the case of PAM.

Another important application of PA effect is the determination of thermal properties of various materials. Thermal diffusivity and effusivity are very important parameters in heat transport problems. From these properties one can determine thermal conductivity and heat capacity of the material. There are only very few methods which can determine all these properties simultaneously, especially in the case of samples in the film form. We have devised a scanning photoacoustic technique for this purpose and measured the thermal properties of commercially available paints using the technique. The method involves coating different thicknesses of the paint on a substrate in a step like manner and scanning this sample along a line with the intensity modulated laser beam. The phase values of the PA signal are noted from regions of different thicknesses of the paint and normalized using the phase values obtained from a thermally thick coating of the same material. These normalized phase values are then given a least squares curve fit using the theoretical expression for phase. If we know the effusivity of the substrate material on which the paint is coated and the density of the paint coating we can determine all the four desired thermal properties(thermal diffusivity, effusivity, conductivity and heat capacity) of the paint following this method.

This method can very well be adapted for the determination of thermal properties of semiconducting thin films as well as composites, which have important practical applications. If the thermal diffusivity is known the method can also be used to determine the thickness of opaque films for which hardly any

method exist at present. A fully automated set up can be a very useful instrument for industrial applications.

We have used our scanning photoacoustic set up for the determination of thermal effusivity of some ceramic samples, following the technique developed and used by our research group earlier in the case of thermally conducting and insulating standard samples. The method involves using the experimental sample as a backing along with a reference sample whose thermal effusivity is known. A very thin uniform layer of carbon black is coated over both the sample and the reference whose top surfaces are flat and kept at the same horizontal level. Scanning this sample configuration along a line with intensity modulated laser beam, the amplitude and phase of the PA signal from the regions of both the backing are measured. The amplitude ratio and phase difference of the PA signal from the two regions are calculated. From these values, we can determine the thermal effusivity of the experimental sample, knowing the thermal effusivity of the reference and that of the coating.

To conclude, the scanning photoacoustic set up developed by us can be used as a measuring instrument to measure thermal transport properties of films, with a number of industrial and research applications. There is scope for improving and remodeling the design to suit various types of samples and experimental conditions.

Eventhough the area of photoacoustics has got matured over the past three decades, there still remains a lot way to go to exploit the full capabilities of the technique for industrial and commercial applications. The prototype PA imaging unit developed by us can very well be perfected to be made as a commercial instrument. In general, there are lots of possibilities for applying PA technique in

material characterization applications, particularly for thermal characterization of materials in different forms. To the best of our knowledge, photoacoustics is the only method that enables one to determine thermal diffusivity/conductivity of film samples. There is lot of scope to do instrumentation development in this area.

Photoacoustic spectroscopy in the infrared regime is still an unexploited area of research. Details of the subband levels in materials, particularly semiconductors, can be revealed by this technique. Again PA technique is not used much to study the influence of particle size on the properties of nanomaterials. There is plenty of scope for doing good work in this area.